AN ABSTRACT OF THE THESIS OF

THOMAS WILLIAM HODLER for the DOCTOR OF PHILOSOPHY

in GEOGRAPHY presented on 26 May 1977

Title: REMOTE SENSING APPLICATIONS IN HYDRO-GEOTHERMAL EXPLORATION OF THE NORTHERN BASIN AND RANGE PROVINCE

Abstract Approved: Redacted for Privacy

Charles L. Rosenfeld

A program of remote sensing overflights with ground truth teams was initiated in order to evaluate the effectiveness of remote sensing applications to geothermal resource reconnaissance in the northern section of the Basin and Range physiographic province. This area included parts of south central Oregon and northeastern California. It is composed of land both privately owned and publically administered by many branches of government. The government's involvement in this area, specifically the Fremont National Forest, was the impetus for seeking such the evaluation of the existing geothermal potential. Such an evaluation was conducted utilizing side-looking-airborne-radar (SLAR) and thermal infrared (TIR) detectors in a complementary fashion flown by the Oregon Army National Guard.

The program consisted of preliminary overflights of SLAR for the detection of fault lineaments along which surface expressions of

hydro-geothermal activity are localized. Interpretation of the SLAR imagery was used to generate TIR flightlines corresponding to the major lineaments. Subsequent flights incorporated TIR line scanners utilizing the mercury-cadmium-telluride (HgCdTe, 8-14 μm), indium antimonide (InSb, 1-6 μm), and indium arsenide (InAs, 1-3.4 μm) detectors. A map was produced depicting the interpreted data. The map graphically portrays the structural relationship between the interpreted surface hydro-geothermal sites and the fracture traces, at a scale of 1:500,000.

From the SLAR imagery two classes of lineaments were distinguished, those greater than 500 meters vertical displacement and those smaller scarplets of lesser relief. The two fault trends, of NW-SE and NE-SW are easily seen on the map. The lineaments of greater displacement have a tendency to run NE-SW and are relatively few in number. The lesser displacement lineaments are quite numerous and trend NW-SE.

Analysis of the TIR imagery located one new potential hydro-geothermal site and determined a more accurate designation of geographic coordinates for five other sites than were provided in previous studies. Location was more easily accomplished through the use of a dual channel system. The HgCdTe detector provided detailed terrain imagery and is best suited for actual geographic location, while the InAs detector senses only the hotter targets (greater than

50° C.). The InSb detector exhibits partial traits of both the HgCdTe and the InAs sensors, resulting from their wavelength characteristics. As a result of several technical difficulties, this research was not conclusive in determining which sensor or sensor combination was best suited for locating hydro-geothermal sources.

During overflight the following temperatures were measured by ground teams: air, soil, water, and radiometer. These parameters were used as site-specific indicators of the physical attributes depicted on the imagery.

The map product graphically depicts the relationship of the hydro-geothermal sites to the geologic structure. The hydro-geothermal sites located were found to exist along the major lineaments. A clustering of hot springs was found to exist at three locations in the study area. Lineaments and hydro-geothermal locations were interpreted from the imagery while all surface temperatures were derived by on-site measurements.

Utilizing a temperature decay function (0.27° C/km), isothermal rings were established utilizing each of the hot spring clusters, plus one singly occurring hot spring as the centroids. The area within each isotherm can theoretically be supplied with the equivalent temperature water from the relative centroid. The majority of the study area can be supplied with 70° C temperature water or hotter. This research suggests the principle use of the hydro-geothermal resource

in the study area is for space heating of homes and other structures.

Although the remote sensing survey of surface hydro-geothermal sites failed to show heat potential for near surface direct electrical production, the thermo-structural relationship mapped may serve along with other geophysical techniques to direct subsurface exploration of the resource. Structural lineaments and hydro-geothermal source locations can be determined through the complementary use of SLAR and TIR. Once potential locations are determined, limited ground truthing would be required to verify the remotely sensed data. Such a reconnaissance tool may be of greatest value in a less developed area with similar geologic structure and geothermal promise.

Remote Sensing Applications in Hydro-Geothermal Exploration of the Northern Basin and Range Province

by

Thomas William Hodler

A THESIS

submitted to

Oregon State University

in partial fulfillment of
the requirements for the
degree of

Doctor of Philosophy

Commencement June 1978

APPROVED:

Redacted for Privacy

Assistant Professor of Geography
in charge of major

Redacted for Privacy

Chairman of Department of Geography

Redacted for Privacy

Dean of Graduate School

Date thesis is presented 26 May 1977

Typed by Illa W. Atwood for Thomas William Hodler

ACKNOWLEDGEMENTS

I would like to express my sincere appreciation to the Fremont National Forest for providing both financial support and unrestricted access to the Forest area. I am especially indebted to Mr. Marvin Crocker for his assistance in narrowing the scope of this research. I also appreciate the long hours he spent with me while conducting field observations and measurements.

Dr. Charles L. Rosenfeld is gratefully acknowledged for his coordination effort between this research and the 1042 Military Intelligence Company (Aerial Surveillance) of the Oregon Army National Guard. The SLAR and thermal infrared imagery necessary for this thesis was acquired by the Oregon Army National Guard. For such imagery, I am extremely grateful.

The Oregon Department of Energy provided the needed financial assistance in support of the field work, data collection, and printing of the final map.

The help provided by Mr. and Mrs. Steve Walsh in the final stages of this thesis is also appreciated.

To those people not specifically mentioned who contributed to this research, I also extend my sincere thanks.

Mostly, I want to express my deepest appreciation to my wife Mary Kay, for the months of encouragement that brought this thesis

to its final conclusion. Not only did she work to keep the bills paid but also spent many hours in an editorial effort which greatly contributed to the legibility of this manuscript. So that her efforts might not go unrewarded, I offer this thesis as a tribute to her contributions. Mary Kay, thank you.

TABLE OF CONTENTS

TABLE OF CONTENTS (cont.)

TABLE OF CONTENTS (cont.)

LIST OF TABLES

LIST OF FIGURES

LIST OF FIGURES (cont.)

LIST OF FIGURES (cont.)

REMOTE SENSING APPLICATIONS IN HYDRO-GEOTHERMAL EXPLORATION OF THE NORTHERN BASIN AND RANGE PROVINCE

I. INTRODUCTION

Origin of the Problem

The need for developing alternate energy sources is a political, economic, and social concern of many nations. The American people were surprised and shaken by the oil embargo of 1973. The petroleum dominated economy of the United States began to weaken as the petroleum resource became scarce.

The energy crunch brought about three developments in the United States. The first development was society's awakening to the need to conserve the available energy. More efficient use of petroleum products was encouraged by the Federal Government. Carpooling, more mass transit, lower speed limits, and lower home temperatures were suggested as ways to conserve all fossil fuels (oil, coal, and natural gas).

The second development was higher prices to the consumer. Suppliers of oil and natural gas raised their prices. Further exploration and development of new reserves required larger capital investments. As demand for the scarce resource continued, prices escalated.

Finally, a new dedication to the development of alternate energy sources resulted from the energy crisis of 1973. Geothermal energy could provide one such source. Restricted by its geographic location, this energy resource must be developed and utilized relatively close to its origin. In reaction to the renewed interest in developing new energy sources, this research was undertaken.

Objectives

The objectives of this proposed research are fourfold. First, the research intends to examine and to explore the potential for using thermal infrared (TIR) and side-looking-airborne-radar (SLAR) imagery in a complementary fashion. This combination of sensors may have great potential for locating hydro-geothermal surface expressions (i.e., water-related surface manifestations that occur in conjunction with subsurface geothermal reservoirs) in the areas of structural lineations or lineaments (surface expressions of geologic structure). The northern portion of the Great Basin section of the Basin and Range physiographic division serves as an ideal study area for achieving this research goal.

The second objective is to examine the use of a single versus a combination of thermal infrared sensors for detecting surface heat anomalies. Three detectors will be examined as potential sensors for locating and analyzing surface hydro-geothermal expressions.

These detectors are: mercury-cadmium-telluride; indium arsenide; and, indium antimonide. The third objective of this research is to examine the predictability of surface hydro-geothermal temperatures, utilizing the different TIR sensor combinations. From this objective, an estimate as to the degree of ground truthing required for accurate temperature determination will also be ascertained.

Finally, a map was to be created depicting the lineaments and surface hydro-geothermal locations identified from the imagery. The map will indicate the spatial distribution of the analyzed data. Potential economic and/or social uses of the geothermal resource in the study area will be inferred from the proposed map.

Geothermal Energy

World energy consumption reached a high of 65.2×10^{15} kilocalories (kcal) in 1971 (Cook, 1976). Nearly seventy-eight percent of this total was composed of energy produced by the three largest nonrenewable energy resources: crude oil; coal and lignite; and, natural gas. These three resources, along with the two other nonrenewable resources of uranium and geothermal water, play an important role in the production of electrical energy. Table 1 indicates that nearly three-fourths of the world's electricity production results from the consumption of fossil fuels. Hydroelectric power is the second most important, while nuclear and geothermal production play relatively

Table 1. Electrical Production, 1971.

Source	Percent of World Production	Percent of USA Production
Fossil-fueled power	74.4	75.50
Hydroelectric power	23.5	22.30
Nuclear power	2.0	2.20
Geothermal power	0.1	0.03

Source: Adapted from Cook, 1976

minor roles. However, as demand for energy increases, the roles of nuclear and geothermal power increase, because hydroelectric power production has nearly reached its maximum and the fossil fuel resources are limited.

In 1971, the production of electrical energy in the United States by geothermal methods was approximately 0.03 percent. Thus, out of a total of 8,455 kilowatt hours of per capita consumption in the U.S., less than three kilowatt hours were produced from geothermal sources. The production and utilization of geothermal-powered electrical energy is still in its infancy in the United States. The major restriction in the development of geothermal energy lies in the fact that it can be obtained only in zones of active vulcanism throughout the world (Figure 1).

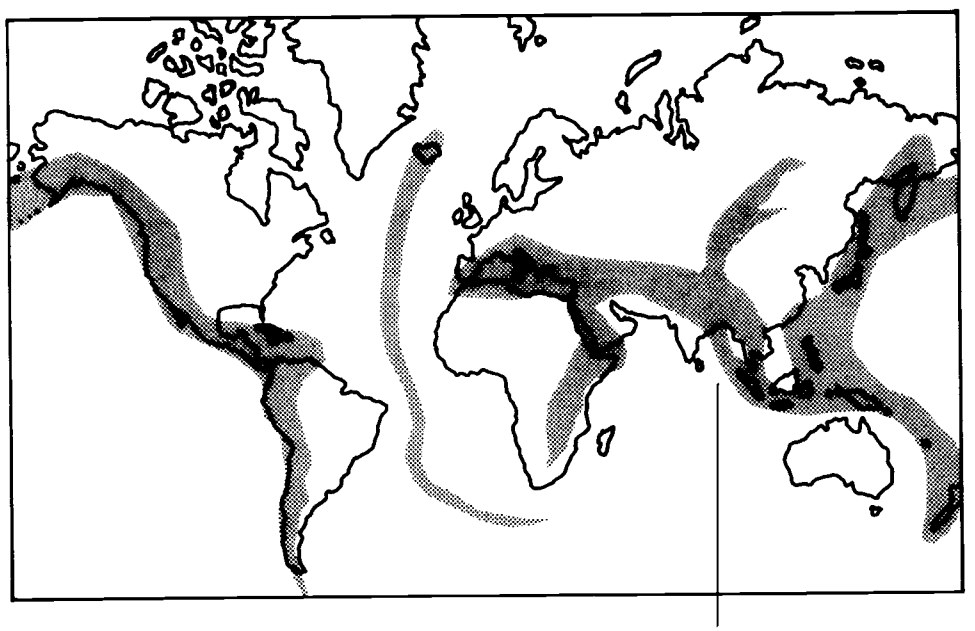

Figure 1. Geothermal zones of the world (after Kruger and Otte, 1973).

Historical Geothermal Development

Kruger and Otte (1973) extensively discussed the historical development of the world's geothermal resources and their information serves as the basis for this presentation. According to them, the history of the utilization of geothermal heat originates with very primitive people. They used the heat from fumaroles for cooking food. The steam condensation was used for drinking water in the more arid lands. Sulfur, kaolinitic clays, mercury, and alum deposited by or around the fumaroles have been utilized for centuries. The modern geothermal development began with the recovery of boric acid from the fumaroles at Larderello, Italy. This development, which began in 1812, continued to expand through the late 1820's. The first well as a source of steam and boric acid was drilled around 1930. In 1904 the first experimental production of electricity by natural steam was undertaken. A 250 kilowatt (kw) generating station began production of continuous geothermal electrical generation at Larderello in 1913.

Both of the World Wars served as catalysts for geothermal development. Post-World War I activities included the installation of a one kilowatt generator at Beppu, Japan in 1924. The 1920's were a period in which the United States first began experimental pursuit of its geothermal resources. Test borings were drilled at The Geysers and Niland, California, as well as in the fumarole area of Yellowstone

National Park. These projects were abandoned either because there was no market for the potential electrical generation or in order to preserve the aesthetics of the location. In the 1930's, hot-water wells were drilled for heating purposes in Reykjavik and Reykir, Iceland and in Rotorua, New Zealand. After World War II, renewed interest in the production of electrical energy by geothermal sources was aroused in Italy, Japan, and New Zealand. This interest resulted from a shortage of fossil fuels and from the destruction of generating plants and transmission facilities during the war.

Italy. Presently, the Larderello field has thirteen plants producing a total capacity of 365 megawatts (Mw). The four smaller plants at Monte Amiata produce a total capacity of 25 Mw, for an annual capacity for the Larderello region of 390 megawatts. In 1971, there were approximately two hundred wells in production within this 250 km^2 region. The reservoir fluid is composed of steam with a maximum reservoir temperature approaching 250 degrees Celsius. As can be seen on Table 2, the three major uses for the geothermal energy in Italy are power generation, chemical production, and ore processing.

New Zealand. The Taupo volcanic depression in the North Island of New Zealand contains the major area for geothermal development. Power stations producing 160 Mw of electricity at Wairakei and 10 Mw at Kawerau, as well as hot-water wells, are mainly used

Table 2. Applications of Geothermal Energy Outside the U.S.

Country	Uses
Italy	1. Power generation 2. Chemical production 3. Ore processing
New Zealand	1. Process heat for newsprint, pulp and lumber mills 2. Space heating 3. Power generation 4. Space cooling 5. Biodegradation of wastes from pigsties 6. Washing and drying of wool 7. Soil and bulb sterilization 8. Tree seedling nurseries 9. Cooking and sterilizing garbage feed 10. Alfalfa drying
Iceland	1. Space heating 2. Hot houses for flowers and vegetables 3. Industrial utilization 4. Power generation 5. Drying of seaweeds 6. Curing cement building slabs 7. Mining of diatomaceous earth 8. Fish breeding (salmon)
Japan	1. Space heating 2. Melting road snow 3. Sewer heat treating 4. Livestock barn heating 5. Egg hatching and poultry 6. Power generation 7. Tropical animal breeding 8. Tropical and food fish breeding 9. Greenhouses 10. Sapling growing 11. Soil disinfection 12. Heating irrigation water 13. Cooking 14. Bathing

Table 2 continued

Country	Uses
Japan (continued)	15. Heating swimming pools
	16. Desalting sea water
	17. Tropical gardens
Mexico	1. Power generation
USSR	1. Domestic hot water
	2. Space heating
	3. Greenhouses
	4. Soil heating
	5. Industrial uses
	6. Mining uses
	7. Dairy farming
	8. Power generation (experimental)
	9. Iodine recovery

Source: Raschen and Cook, 1976

in the area's timber industry. Steam is used for boiler operations, timber drying, equipment power, and other uses (Table 2). Over 1,000 wells supply hot-water heat to homes, schools, hospitals, and commercial establishments in the city of Rotorua. As a result of the discovery of natural gas in New Zealand, no new development of geothermal power is planned through 1980. However, local hot-water usage is encouraged by the New Zealand government.

Iceland. The most notable fact concerning the geothermal energy in Iceland is that it is used as a heating source by nearly sixty percent of the nation's inhabitants. Ninety percent of the homes in Reykjavik are heated by hot-water geothermal energy, distributed by a city municipal service. This hot water is distributed a distance of 18 km in concrete insulated steel pipelines, with a temperature loss of approximately five degrees Celsius. The temperature of the water when used at its destination is about eighty degrees Celsius. Space heating is the dominant use of the energy, however, electricity is generated on the island near Namafjall. Additional uses are listed in Table 2.

Japan. Japan has perhaps utilized geothermal waters longer than any other nation. The use of hot springs for therapeutic spas, baths, and resorts has been practiced for centuries. Greenhouses, commonly used for growing vegetables and fruits, are heated by the geothermal waters. Other more specialized uses for these waters

include rice processing at Beppu and salt extraction from seawater through evaporation at Shikabe. As can be seen from Table 2, Japan has utilized geothermal energy in more ways than any other country.

The first geothermal generating unit was installed at Beppu in 1919 with a generating capacity of one kilowatt. In 1951, that capacity was expanded to 30 kw annually. Two other small generating plants are located at Yunosawa (8 kw) and Hakone (30 kw). The two largest generating plants are located at Otake and Matsukawa; 13,000 kw of electricity have been produced annually since the power plant was constructed at Otake in 1953. Since 1961, 9,000 kw have been produced at Matsukawa. Plans presently call for an increase in power generation to 27,000 kw in the late 1970's and eventually up to 60 Mw. Matsukawa has the hottest reservoir temperatures (240-250^{o} C) of any of the Japanese geothermal sites. Other future power plants are under consideration; 10,000 kw at Hachimantai, and 7,000 kw to be produced in the larger salt extraction plant planned at Shikabe.

Other Countries. Certain other countries of the world are either already utilizing geothermal energy or are planning for its development. Several of these countries include Turkey, Taiwan, Guadaloupe, Chile, Indonesia, The Phillippines, Ethopia, Kenya, El Salvador, Mexico, Hungary, and the Soviet Union. Through the help of scientific teams from UNESCO, several of these countries

are creating specific uses for their geothermal resources.

United States. In 1960, the first turbine generator was installed at The Geysers steam field in California. At first the generator produced 12,500 kw per year and later, generation was increased to 302,000 kw annually. In 1973, another generator was installed to produce 110,000 kw. By 1980 plans call for a 1,190 Mw capacity. Estimates of The Geysers' maximum sustained yield were reported by the California Geothermal Resources Board to the State Senate, as nearly 4,800 Mw annually. The Geysers have a reservoir temperature approaching 250° C, similar to that of Matsukawa, Japan and Larderello, Italy.

In the early 1960's, a 3,000 kw generator was installed at Niland, California near the Salton Sea. Presently, this generator is inactive as a result of high saline brine content of the water. Unlike The Geysers, this plant utilizes higher temperature water instead of steam. Bowen (1971) indicates that environmental restrictions concerning the disposal of the hot saline water are so severe that the production of electricity has not been feasible. However, some chemicals were extracted and natural gas was produced from the many wells in the Niland field. Other areas in California, where experimental drilling found temperatures of up to 175° C, include Clear Lake, Long Valley, and Surprise Valley in northeastern California.

Thirteen shallow test holes were drilled in the geyser area of Yellowstone National Park. The deepest hole was 300 meters. A maximum temperature of 240° C was recorded. Although the indicators of a potential resource existed, no development occurred because the area was designated a National Park with the preservation of the aesthetics of the area a prime requisite.

Boise, Idaho has been utilizing its hot-water resources for years as a means of space heating for both private and municipal buildings. Exploration and development of geothermal resources are continuing in California, Nevada, and Oregon. Presently, new emphasis is being directed toward the geothermal potential in Arizona, Idaho, New Mexico, and Utah (Table 3).

Other than power generation, the most common use of geothermal energy in the United States is space heating. Of the states cited in Table 3, space heating ranks first or second on each list. However, based on the number of people served by space heating, the United States ranks fifth in the world behind Iceland, USSR, Japan, and Hungary (Karr, 1976).

Oregon. Groh (1966) states that Oregon had the greatest amount of vulcanism of all the western states throughout the Tertiary and Quaternary periods. Therefore, Oregon has an excellent geothermal energy potential. Presently, the principal area of geothermal application is within the city of Klamath Falls in south central Oregon

Table 3. Applications of Geothermal Energy in the U. S.

State	Uses
California	1. Power generation 2. Space heating 3. Heating water for domestic uses 4. Greenhouses 5. Spas and recreation 6. Lumber mill drying kilns
Idaho	1. Space heating 2. Domestic hot water 3. Greenhouses 4. Swimming pools, resort use 5. Fish propagation 6. Animal husbandry 7. Irrigation 8. Forest campgrounds
Nevada	1. Source for domestic water 2. Space heating 3. Safe heat source for processing explosives 4. Spas and recreation 5. Greenhouses
Oregon	1. Space heating 2. Heating water for domestic use 3. Pasteurization 4. Industrial cleaning 5. Refrigeration 6. Coils under pavement to melt snow and ice 7. Greenhouses 8. Tree seedling nurseries 9. Spas with saunas

Source: Raschen and Cook, 1976

(Peterson, 1967). Some 350 wells supply hot water which has been used to heat private and municipal buildings since 1900. The geothermal water is used in conjunction with heat-exchangers and with the pure municipal water.

In other Oregon locations greenhouses, resorts, baths, farm buildings, and schools are heated by geothermal resources. In Lakeview, Oregon the Oregon Dairy Farms' greenhouse is used to produce tomatoes the year round. Hot geothermal water is pumped into heat exchangers. The air is then forced through a series of plastic conduits and is distributed throughout the greenhouse. Several private homes are also heated by the hot water.

The most recent exploration of geothermal energy in Oregon started at Timberline Lodge in the summer of 1976. A borehole was drilled to see if the geothermal heat beneath the surface of Mt. Hood could be utilized in heating the Lodge. The results are presently being reviewed.

Types of Geothermal Energy

The increase in temperature with increasing depth within the earth's crust is well known. The world average temperature gradient, i.e., the change in temperature with depth, is approximately 25° C/km with a range between eight and 50° C/km. Thus the normal temperature at a depth of one kilometer is 25° C warmer than the

surface temperature. The temperature gradient indicates that the earth is losing heat from within at a rate of 1.5 $\mu cal/cm^2 sec$ or 1.5 hfu (heat flow units). The 1.5 microcalories per square centimeter is roughly equivalent to 60 kilowatts per square kilometer. The loss of energy over surface area is roughly equivalent to 1/2000 of the solar energy received by that same surface area (Kruger and Otte, 1973; Bodvarrson, 1966).

The movement of heat from within the earth to its surface occurs through either conduction or convection systems. Thermal conduction results either by heat flow through solid rock materials; by flow in circulating fluids; or by mass transfer in magma. Convection will cause the temperature to redistribute and will stabilize the internal temperature regime. Hydrothermal convective systems are the dominant form of heat transfer in geothermal resources. Cellular movement of water, liquid or vapor, transports heat from the depths in the earth's crust up to a relatively shallow depth; shallow in the sense that it is within the reach of drilling.

Experience gained from geothermal exploration and drilling indicates that pressure within the earth's crust is controlled by fluids in fractures and in rock pore space. As drilling continues, head pressure increases with depth. Normally, 70 to 90 percent of the mixture reaching the wellhead is liquid water and the rest is steam. In a very few instances, the wells emit only saturated vapor and

superheated steam. This dry-steam has no liquid water and thus the pressure within the system is vapor dominated.

Vapor-Dominated Systems. The vapor-dominated systems are rare in occurrence. The three commercial fields that belong to this system type are found at: Larderello, Italy; The Geysers, California; and, Matsukawa, Japan. White, Muffler, and Truesdell (1971) suggest that these systems developed originally from reservoirs of hot-water in association with very high temperatures. Water evaporated at a faster rate than recharge, so that eventually these reservoirs were depleted of water. Moisture retained in micropore space slowly descends to lower level saturated rocks. The internal pressures are maintained and vapor is continually emitted. Minor amounts of gases other than water vapor are found in the steam, and the steam can be fed directly to the turbines.

Several factors characterize the vapor-dominated systems. Kruger and Otte (1971) cite the characteristics, which are summarized here:

1. Reservoirs, which are located deeper than 350 meters, tend to have internal temperatures at or above 250^{o} C and pressure approaching 35 kg/cm^{2};

2. Relatively uniform temperatures and pressures increase as the percentage of other gases increase in the vapor;

3. Reservoir pressure is well below hydrostatic pressure and

the difference becomes larger with increasing depth;

4. Fumaroles, mud pots, turbid pools, and highly acid springs characterize the surface area where these vapor-dominated systems are located; and,

5. Superheated steam is obtained from the production wells, however, liquid water can be extracted from non-productive wells at the periphery of the reservoir.

Hot-Water Systems. The hot-water systems are characterized by circulating fluids which are thermally driven convective systems transferring heat from an igneous source at great depth to a geothermal reservoir at shallow depths. These reservoirs are located within the earth's crust at shallow enough depths to be reached by drill holes. Renner, White, and Williams (1975) described the system as having surface expressions or manifestations that serve as indicators of their existence.

Hot springs and geysers are surface indicators of the hot-water system at depth. Their existence is a clue as to the probable subsurface temperatures, volumes, and heat content. Hot springs do not form in areas where the reservoir is covered by an impermeable rock layer. However, the fluid can penetrate such impermeable layers if fracturing or faulting of the rock layer has occurred, or if an intrusion such as a dike has reached the surface through the rock layer. Such fractures, faults, fissures, or intrusions serve as

transport routes for the hot-water to reach the surface (Figure 2).

It is generally accepted that the hot-water system is separated into three divisions based upon their temperature ranges (Denton, 1972; Renner, White, and Williams, 1975). Surface temperatures rarely exceed the boiling temperature, which varies with altitude (100° C at sea level and 93° C at 2,200 meters). Although the actual temperature extremes for each division vary slightly, the following description typifies the temperature regimes:

1. Above 150° C. This category applies to high temperature hot-water systems which can be considered for the generation of electricity. The water is brought to the surface and flashed to steam. The liquid and steam are separated and the vapor is directed to the turbines. Usually, the water is reinjected into the reservoir through a separate drill hole;

2. From 90° C to 150° C. This division applies to intermediate temperature hot-water systems. This system is useful in space heating and heat processing. The fluid is brought to the surface and passed through a heat exchanger. The heat is then passed to a second fluid in a closed system. Some heating systems utilize the geothermal waters directly, allowing the fluid to pass through piping in the flooring (i.e., a form of radiant heat). This is usually less acceptable because the chemical content and heat content of the fluid can cause the fixtures to deteriorate;

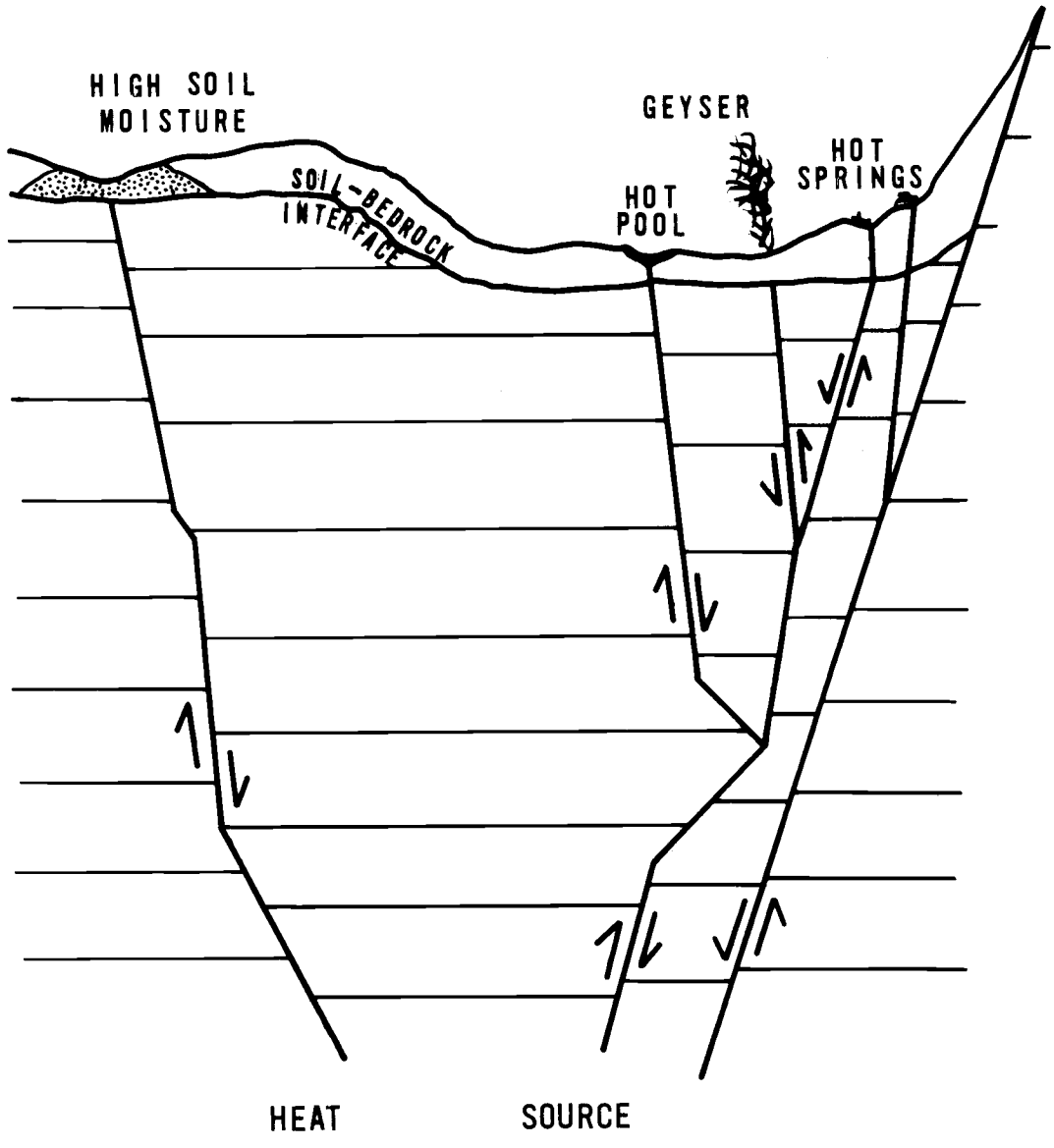

Figure 2. Cross sectional diagram: subsurface structure and hydrogeothermal sources.

3. Less than 90° C. This category applies to low temperature water systems. This sytem is utilized for process heating under certain favorable circumstances. The fluid is piped through another medium and the heat is then dispersed by that second medium. This form of processing heat can be applied to commercial and residential buildings, paper and pulp manufacturing, and other related industries. The restriction on this division is that it can not be transported any great distances, i.e., it must be utilized on a local basis.

II. BASIN AND RANGE: THE STUDY AREA

Study Area Description

Location

The study area is located in the northern portion of the Basin and Range Physiographic Province of North America, referred to as the Great Basin (Figure 3). Included in this area are portions of south central Oregon and northeastern California. The Oregon portion of the study area is bounded on the east by the Warner Valley, the Coleman Valley, and the Hart Mountain National Wildlife Refuge; on the west by the westernmost part of the Klamath-Lake County line; and on the north by Bald Mountain, Fort Rock, and Christmas Valley. In California, the study area is bounded on the east by the Surprise Valley; on the west by the 121st meridian; and on the south by the Warm Springs Valley through which the Pit River flows. The entire study area is comprised of approximately 27,630 square kilometers.

Basin and Range Geology and Structure

The Great Basin has been geologically active since the Miocene epoch. Late Miocene and early Pliocene basalt flows several hundred meters thick are predominant throughout the study area. Such flows are easily seen along the Abert Rim escarpment. Vulcanism continued through the latter part of the Pliocene. Tertiary rhyolite

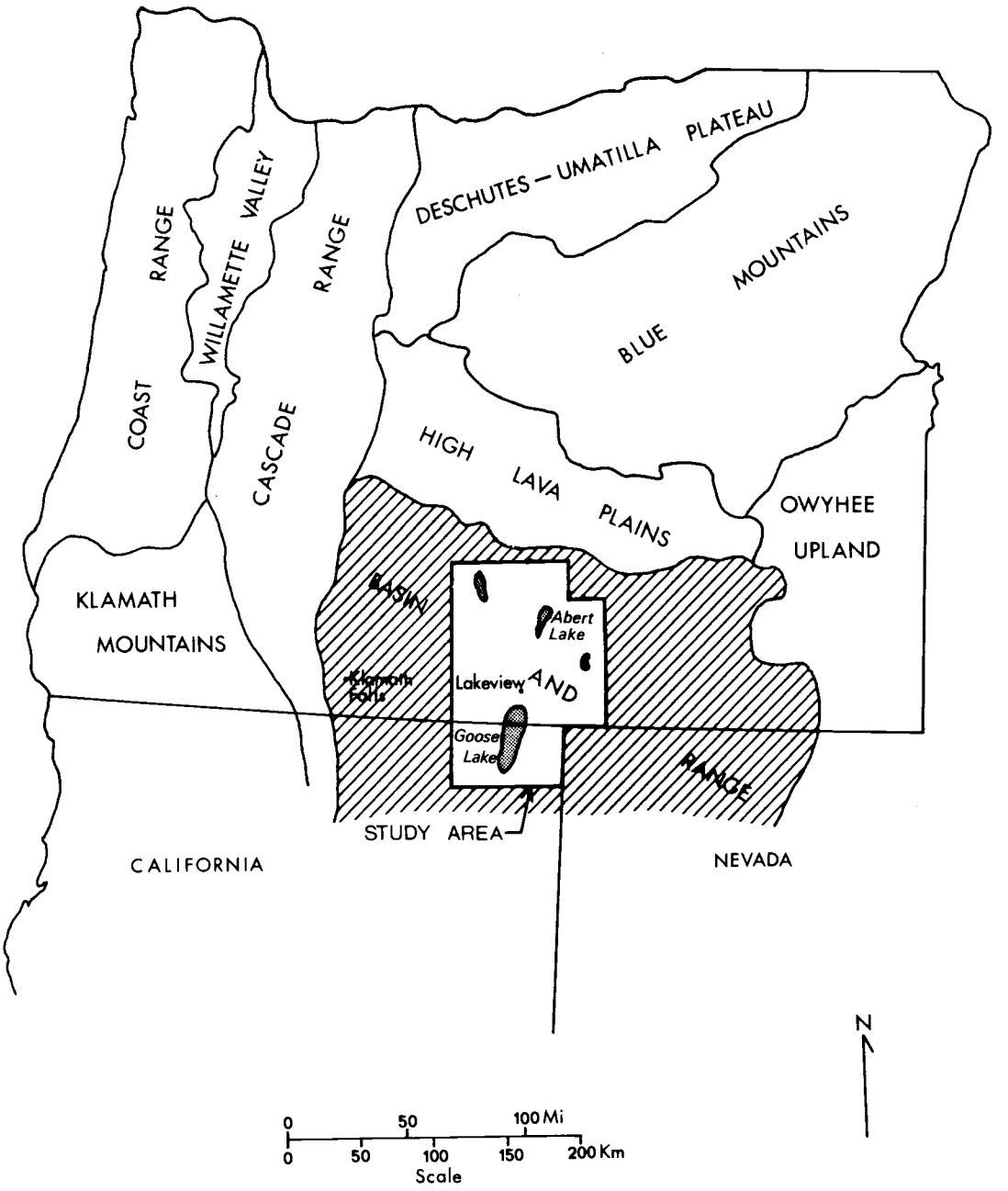

Figure 3. Physiographic provinces (from Thornbury, 1965).

intrusives and volcanic pyroclastic rocks are found to exist in conjunction with the fault structure of the Basin and Range. Tuffaceous sedimentary rocks are intermixed with andesite and basalt flows. Alluvium, deposited during the Pleistocene and Holocene epochs, is the second most frequently found material in the study area. Internally drained basins of the Pleistocene have created valleys filled with alluvial material several hundreds of meters thick. The above-mentioned geologic materials are continually being altered through structural realignment (Walker and Repenning, 1965; Jenkins, 1968; and Peterson and McIntyre, 1970).

The Great Basin section is believed by many geologists to be the leading edge of the Basin and Range province extending itself north and westward into the Columbia Plateau. The fault structure mechanics exhibited in the Great Basin is still undergoing debate in the scientific community. Stewart (1971) summarized the current theories pertaining to the causal creation of the Basin and Range structure. Stewart's use of clay and dry mortar models, to create scaled versions of the faulted structure, supported the theory that the Basin and Range structure is related to the fragmentation of a brittle crustal slab overlying a plastically extending substratum. As the substratum is extended, the base of the crustal slab is pulled apart along a series of narrow zones which cause depressions in the surface of the slab. Such an extension of the substratum creates the surface structure exhibited

in the Great Basin, i.e., tilted fault blocks, horsts and grabens, and internally drained basins (Stewart, 1971).

Lawrence's (1976) analysis of Landsat imagery yielded four strike-slip fault zones extending west-northwest across much of Oregon. Two of these fault zones, the Eugene-Denio zone and the Mount McLoughlin zone, extend across a portion of the study area. Lawrence reported the Eugene-Denio zone to trend N. 50° West. Such a zone is comprised of many individual faults; most less than 10 km long. The zone was mapped through the High Cascades as a series of lineaments that produced a 10-20 km right lateral offset across the zone. The Summer Lake and Abert Lake basins and associated faults (Winter Rim and Abert Rim escarpments respectively) terminate against this zone. Lawrence reported that the Warner Lakes basin was slightly constricted and offset by the Eugene-Denio zone.

The Mount McLoughlin zone is comprised of many lineaments trending N. 45° W. (Lawrence, 1976). The projection of this zone from Oregon passes through the northeastern portion of California, specifically the Surprise Valley.

Donath (1962) provided a detailed study of the structure of the area surrounding Summer Lake, Oregon. He identified two major fault trends, one N. 20° E. and the other N. 35° West. He observed the northeast trending faults to be normal faults possessing large

vertical displacement. These faults were found to dip nearly vertical, greater than 85 degrees in most instances. The fault traces that possessed a northwesterly trend were of much lesser relief and of shorter linear extent. The interlocking nature of the two fault traces was noted by Donath to form a rhombic pattern. Donath concluded that all recent motion along the fault traces was in the nature of dip-slip movement.

Donath (1962) also noted that the fault traces produced a very angular and irregular interlocking pattern. No one trend consistently offset the other. Thus, movement along each set of faults was concurrent and that the fault trends were contemporaneous in origin (Donath, 1962).

Fuller and Waters (1929) were one of the first to use aerial photography in geologic interpretation. Their investigation suggested that this portion of the Great Basin is comprised of seven great north-south trending tectonic depressions or grabens, bounded on either side by fault scarps. The seven major fault depressions are: the Klamath graben; the Summer Lake-Chewaucan Marsh-Goose Lake depression; the Warner-Surprise graben; and, the Guano graben; the Catlow Valley; the Alvord graben; and, the McDermitt Valley depression (Figure 4) (Fuller and Waters, 1929). Only the Summer Lake-Chewaucan Marsh-Goose Lake depression is a valley system of nearly fifty kilometers in length, which lies in the center portion of the study

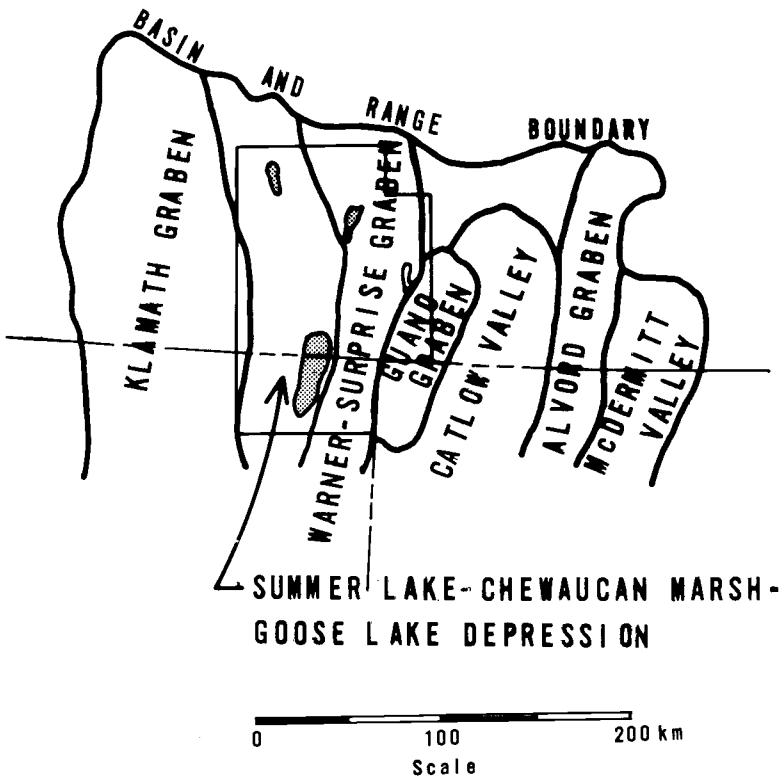

Figure 4. Depressions and grabens in the Northern Basin and Range (from Fuller and Waters, 1929).

area. Along its eastern boundary is Abert Rim, a scarp of nearly 800 meters relief, which extends southward into California where it dies out below the Goose Lake Valley. The scarp itself exhibits a linear trend with minor jagged appearance and with directional variations.

The western boundary of this depression is Winter Rim, which overlooks Summer Lake. Winter Rim and Abert Rim are quite similar. Both rise equally high above the valley floor and both are vertical fault scarps. However, unlike Abert Rim, Winter Rim exhibits a curved non-linear structure which bends around the southern tip of Summer Lake in an easterly direction. A few kilometers east of the lake, the fault bends southward again, trending roughly S. 65^{o} E. (Fuller and Waters, 1929).

Waring (1909) indicates that there is a feature worth noting in the Summer Lake depression. To the northeast of Summer Lake lies Diablo Mountain. Through this mountain is a fault with a northwest-southeast trend. North of Diablo Mountain, the scarp is downthrown toward the lake, while south of the mountain the scarp is downthrown away from the lake. Below Diablo Mountain the fault dies out, and approximately four kilometers to the south a fault begins which defines the eastern edge of the Chewaucan Marsh and maintains the same linear trend as the Diablo Mountain fault. This structure appears to be a pivotal rotational fault which Donath (1962) described

as existing in the south-central portion of Oregon (Figure 5).

Chewaucan Marsh and Goose Lake lie in depressions that are grabens. The Chewaucan Marsh is bounded on the northeast and southwest by tilted fault blocks. The Goose Lake depression is also bounded by two fault blocks, the eastern fault being Abert Rim.

The second major fault depression in the study area is the Warner-Surprise graben. In Oregon, Crump, Hart, Flagstaff, Campbell, and Bluejoint Lakes lie in this true graben, which is bounded by walls nearly 900 meters high. Fuller and Waters (1929) note that the western escarpment of this valley fades out a few kilometers north of Plush, so that the northern end of the graben lies between Abert Rim, to the west, and the high eastern scarp of Poker Jim Ridge.

Hart Mountain, an undissected horst only a few kilometers in width, comprises the eastern boundary of the graben. Hart Mountain appears as a table-top structure rising nearly 1,000 meters above the valley. To the north, the graben is bounded by the Poker Jim Ridge escarpment, which extends some eighteen kilometers beyond Hart Mountain.

Fuller and Waters (1929) indicate that in the northern section of this graben several smaller fault scarps are located. These scarps are closely spaced, have only a hundred meters of relief, and extend for nearly six kilometers to the northeast. Allison (1949) also

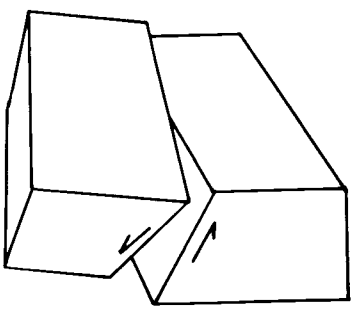

Figure 5. Pivotal Rotational Fault (from Donath, 1962).

indicated that these smaller fault scarps of relatively little relief were quite numerous locally. He concurred with Fuller and Waters concerning the trend, extent, and quantity of these smaller scarps. However, he implied a much smaller relief existed and that they may be easily overlooked on the ground. As a result of their smaller size, many of these faults have not been previously mapped. Field surveying of such features have proved to be both difficult and laborious. The frequency and pattern of these faults are surface indicators of the highly fractured structure in this part of the Great Basin.

The continuous trend of the east-facing escarpment south of Plush and the west-facing scarps of Hart Mountain and Poker Jim Ridge appear to have structural characteristics similar to the pivotal rotational fault type discussed by Donath (1962). However, the investigation by Lawrence (1976) suggests that this offset is created by the Eugene-Denio fault zone intersecting the structures possessing a northeasterly trend. Such displacement of a few tens of kilometers is common along the Eugene-Denio zone (Lawrence, 1976).

The Surprise Valley graben lies to the west of the fault system extending southward into California from the Warner Valley graben. Three alkali lakes are located in the depression. The valley consists of lacustrine and fluvial sediments as well as talus and landslide debris. Three smaller intrusive bodies found in the center of the

valley southeast of the Upper Alkali Lake are related to the fault pattern in that part of the depression.

Climate

The climatic changes which have occurred in the study area are quite diverse. Climatological data are collected at various weather stations and are used in generating the following climatic description. It should be noted however, that topographic variation within the area creates havoc in trying to describe or classify the entire study area into a climatic regime. The weather stations, from which the data was acquired, are located in the valleys at the lower elevations. Climatic zonation occurs with increasing elevation and aspect. Keeping this in mind, the climatic description and characteristics are given below.

Temperature. The average number of frost-free days vary from 90 to 119 across the study area. The summer average temperature is 18.8° C [65.8° F] with a maximum summer temperature of 37.8° C [100° F] occurring in August. The mean winter temperature is 0.4° C [32.8° F] with a winter minimum of -26.1° C [-15° F] being measured in December. The diurnal temperature variation is approximately 18° C [32° F] in the summer and 9° C [17° F] in the winter.

Estimates for the highland areas include a summer average of 15.5° C [60° F] and a winter average of -2.8° C [27° F]. The

summer temperature extreme is around 32.2° C [90° F] and the winter minimum is -31.7° C [-25° F] with diurnal variations of approximately 4.4° C [40° F]. Typical of highland areas, the temperature regime is much cooler than the lower valleys.

Water. The annual precipitation received at stations throughout the study area ranges from 26.1 cm/year [10.29 inches/year] for the low to 37.4 cm/year [14.71 inches/year] for the high. There is a winter maximum period of precipitation with the greater amounts occurring in the months of December and January. In the higher elevations, the precipitation largely occurs in the form of snow, which becomes the source for spring runoff into the existing lakes. In the valleys, the precipitation occurs as rain or snow, depending on the ambient air temperature.

The evaporation rates are practically reversed when compared to the amount of precipitation. High summer temperatures occur in conjunction with very sparse cloud cover, which creates high evaporation rates in the summer when precipitation is at its lowest. At the Summer Lake station the average summer precipitation (May-October) is 9.3 cm [3.64 inches] while the mean evaporation rate for the same period is 124.1 cm [48.85 inches]. The moisture deficiency for the Summer Lake area in the summer is 114.8 cm [45.20 inches]. As a result, many streams in the area are intermittent. The months of August and September are usually low flow periods while the greatest

discharge occurs in April and May. This maximum runoff period is caused by the spring melting of the winter snowpack. Many perennial streams also exist in the study area; for example, the Pit, Crooked, Chewaucan, and Sprague Rivers. Their headwaters usually originate in higher elevations where snowpack and throughflow give a constant supply of water. Several perennial streams are fed by a series of reservoir storage areas created by these higher elevations. These reservoirs help supplement summer dry periods when demand is high.

Groundwater can be found in the unconsolidated fill of the arid alluvial basins. Drinkable groundwater is found in the sand and gravel deposits of alluvial fans found near the mouths of canyons and along the many terraces on the periphery of the basins. As a result of the infiltration of the water from the many intermittent streams, groundwater quality decreases from the margins of the basins inward to their center. The highly mineralized water of the lakes infiltrate the groundwater and thus decrease its quality. Groundwater depth increases from the center of the basin outward toward their margins. Groundwater recharge results from the infiltration of the intermittent streams. Therefore, recharge of the groundwater decreases as the summer dry season approaches. Thus, the groundwater table fluctuates with the variability of recharge and is at its lowest level in the summer season.

Air Movement. Wind movement is generally from the west and

south, with occasionally cooler air masses moving from the north-northwest during the late summer. The south wind is dominant during the fall and winter while the west wind prevails during spring and summer. Greater wind velocities generally result from the west wind movement while the north winds usually have lower velocities.

Summer thunderstorms usually cause the strongest wind velocities. They move through the study area from the southwest. They are most frequent during the spring and early summer months.

The area also records diurnal winds. Increased thermal activity during the daytime causes the winds to pick up about mid-morning and then dissipate with late afternoon cooling. On hotter days, dust devils are common in the area. These dust devils are created by increased local thermal inertia, i.e., small areas that experience intense heating.

Particulate Matter. One of the major contributors to the suspended particulate matter in the dry basins and plateaus is wind-blown dust. Annually, tons of soil are picked up by the wind from the center of the dry basins, creating large dust clouds. Dry basins that contribute large volumes of dust are: Summer Lake Valley; Coleman Valley; Surprise Valley; Long Valley; and Massacre Valley. High winds distribute soil and dust particles from the Summer Lake Valley to the southeast into the Chewaucan Valley and Abert Lake area, nearly fifteen kilometers away.

Soil and Vegetation. Table 4 gives a brief inventory of the landtype associations, soil characteristics, and vegetation distribution within the study area. This table was derived using inventory descriptions developed by the Fremont National Forest. The Lands Systems Inventory for the Boise National Forest (Wendt, Thompson, and Larson, 1975) was used by the Fremont National Forest as a guide in the development of their descriptive inventory. Their results have been expanded so that the information depicted in Table 4 applies to the entire study area. The table also summarizes information pertaining to the general soil characteristics of the study area. All soils have good to excellent drainage.

The alluvial bottomland landtype association consists of level or gently sloping land, formed from recent alluvial deposits in the basins and along the drainage systems. Within this unit there are areas either devoid of vegetation or containing sparse distribution of salt-tolerant plants, such as greasewood. This usually occurs in the interior of the basin near an alkali-laden lake. Farther from the lake area, more non-salt-tolerant plants exist, such as big sagebrush, rabbitgrass, and other grasses. This area includes meadows and adjacent shrublands.

Scabland plateaus are gently sloping undulating plateaus of basaltic lava and tuff. This area is dominated by low sagebrush and juniper. Some big sagebrush is found in areas of increased drainage

Table 4. Landtype associations: Soil and vegetation.

Landtype Association	Elevation (meters)	Soil			Other	Vegetation
		Origin	Depth	Texture		
Alluvial Bottomland	1300-1900	Al	Mo-D	F-C	Rimmed with shallow residuals hardpan present in subsoil	Sagebrush, Greasewood, Rabbitgrass
Scabland Plateau	1300-2000	R	S	M-F	Stony	Sagebrush
Toeslope & Benchlands	1300-1825	R	S	F-C	Gravelly	Sagebrush, Bunchgrass, Juniper
Lava & Tuff Tablelands (Surf)	1600-2150	A-P	D	C	Weakly developed	Ponderosa, White fir,
(Sub)		R		F-M		Needlegrass
High Elevation Tablelands (Surf)	2000-2450	A-P	D	C	Weakly developed	Lodgepole, White fir
(Sub)		R		M		
Moderately Steep Smooth (Surf)	1675-2150	A-P	Mo	F-C	Poorly dev., stony	White fir, Ponderosa,
Sideslopes (Sub)		R		M	Stony	Aspen
High Elevation Moderately (Surf)	2000-2450	A	D	C		Lodgepole, Mixed
Steep Smooth Sideslope (Sub)		B		M	Stony	Conifer
Rhyolite Dome	1675-2150		D	C	Weakly developed	White fir, Ponderosa
Subalpine Eruptive Center	2150+	R	Mo-D	M-C	Rhyolite & ash development	Mixed conifer, shrubs
Steeply Dissected Ridges & Sideslopes	1675-2200	R	S-Mo	V	Rock outcrop & talus	White fir, Juniper, Ponderosa, Sage, Mtn. Mahogany
Miscellaneous Landtype	1300-2450	R	S	L	Stony, rock outcrop & talus dominate	Dryland shrub, White fir, Mtn. Mahogany

KEY:
Al = Alluvium
R = Residual
A = Ash
P = Pumice
S = Shallow
Mo = Moderate
D = Deep
F = Fine
C = Coarse
L = Loamy
V = Varies
M = Medium
(Surf) = Surface
(Sub) = Subsurface

Source: Adapted from Wendt, Thompson, and Larson, 1975.

where soils are deeper and less alkaline.

Open low sagebrush with small clumps of juniper are found in the shallow soils underlaid with hardpan of the toeslope and benchland landtype association. Big sagebrush and juniper occupy the deeper soils as well as lesser amounts of bunchgrass, needlegrass, and mountain mahogany.

The lava and tuff tablelands, high elevation tablelands, moderately steep smooth sideslopes, and rhyolite domes are all landtype associations dominated by forest vegetation. The understory vegetation is generally sparse. These landtype associations lie between the elevations of 1600 and 2450 meters [5200 and 8000 feet]. The steeply dissected ridges and sideslopes association has a forest canopy with a fairly dense understory of grasses and forbs. The juniper and mountain mahogany commonly occur in areas of more shallow stony soils.

The miscellaneous landtype is generally associated with fault scarps. Slopes up to 80 percent, rock outcrops, talus, and shallow soils are characteristic of this landtype. Sagebrush and mountain mahogany dominate, with pockets of white fir in the drainage networks on the north slopes.

Land Use Management

The land base supports a variety of uses within the study area.

Several of the major land uses include: livestock grazing; timber, recreation; and, urban development. The land is either managed by the Fremont National Forest (Oregon), Modoc National Forest (California), Bureau of Land Management (BLM), Oregon State Land Board, or privately owned. Approximately 19 percent of the land in the study area is administered by the two National Forests, 48 percent is controlled by BLM, five percent is supervised by the Fish and Wildlife Service, and 25 percent is owned by the private sector. Thus, 72 percent of the land is owned or administered by the Federal Government.

The land use distribution in the study area depicts the economic adjustments made in order to adapt to the semi-arid environment. Grazing comprises over two-thirds of the area's land use (Table 5). It also produces 82 percent of the area's income. Much of the grazing land is leased from the BLM on a per annum basis. Some parts of the BLM rangeland are opened each year to cattle.

Table 5. Land Use Percentage.

Land Use	Percent
Grazing	66.26
Forest	23.47
Intensive Agriculture	2.52
Urban	0.01
Other	7.74
Total	100.00

Source: Adapted from Valde (1973).

The area's agriculture is closely aligned with the cattle industry. Approximately 17 percent of the land is used for farmland, the majority of which requires supplemental irrigation. Only 20 percent of the farmland is planted in crops, the rest is either associated with grazing or forests. The major farm products are hay and small grains, both used primarily as forage for the livestock.

The second major land use in the study area is the forest and wood products industry. The U. S. Forest Service owns or administers 71 percent of the forested land. The private forest products industry owns 22 percent and the farmers own seven percent of the study area's woodland. The private land ownership produces nearly two-thirds of the timber harvest in the region. The other third is removed from the National Forests (Table 6). The major tree species harvested commercially are Ponderosa pine, White fir, and Lodgepole pine. These three tree types comprise 97 percent of the timber harvested in 1970. Besides timber products, the forests also supply land for grazing, wildlife habitats, watershed basins, and outdoor recreation.

The leisure use of the forested land for recreational purposes is increasing at a relatively rapid rate. Many campgrounds, state parks, and picnic sites are located in the area. Hunting is a major outdoor sport which harvests many deer, geese, ducks, and antelope annually.

Table 6. Forest Land and Timber Harvest, 1970.

	Percent Forest Land Ownership	Percent of Timber Harvest
Private (Forest industry)	22	63.8
Farm and Miscellaneous	7	36.2
U. S. Forest Service		
Totals	100	100.0

Source: Adapted from Valde (1973).

Very little of the land area is devoted to an urban (small town) environment. Table 7 lists the population of the significant towns in the study area and Figure 6 is a map indicating their locations and connecting road network.

Site Suitability

The area selected for this study is suitable as an investigative site because of its complex structural fault systems and the existence of many hydro-geothermal surface expressions. Russell (1884) discussed the fault displacement which occurs in this portion of south central Oregon. He cited the existence of numerous hot springs in the region and noted that their location indicated recent displacement. He also noted that hot springs occur in a linear fashion, which he attributed to their location along fault scarps.

Two geysers and numerous hot springs are located in the study

Table 7. Population of County Subdivisions and Towns, 1970.*

Location	Population
Oregon:	
Lakeview division	4,831
Lakeview	2,705
Bly**	600
Beatty**	100
Valley Falls**	15
Silver Lake-Fort Rock division	617
Silver Lake**	150
Summer Lake division	572
Paisley	260
Summer Lake**	30
Warner Valley division	323
Adel**	55
Plush**	70
California:	
Alturas division	3,900
Alturas	2,799
Canby**	75
Surprise Valley division	1,173
Cedarville**	450
Fort Bidwell**	130
Lake City**	75

Source: 1970, U. S. Census of Population

* County subdivision is used as defined by the Census of Population and the towns in each subdivision are indicated.

** Populations given represent on-site estimates by the author.

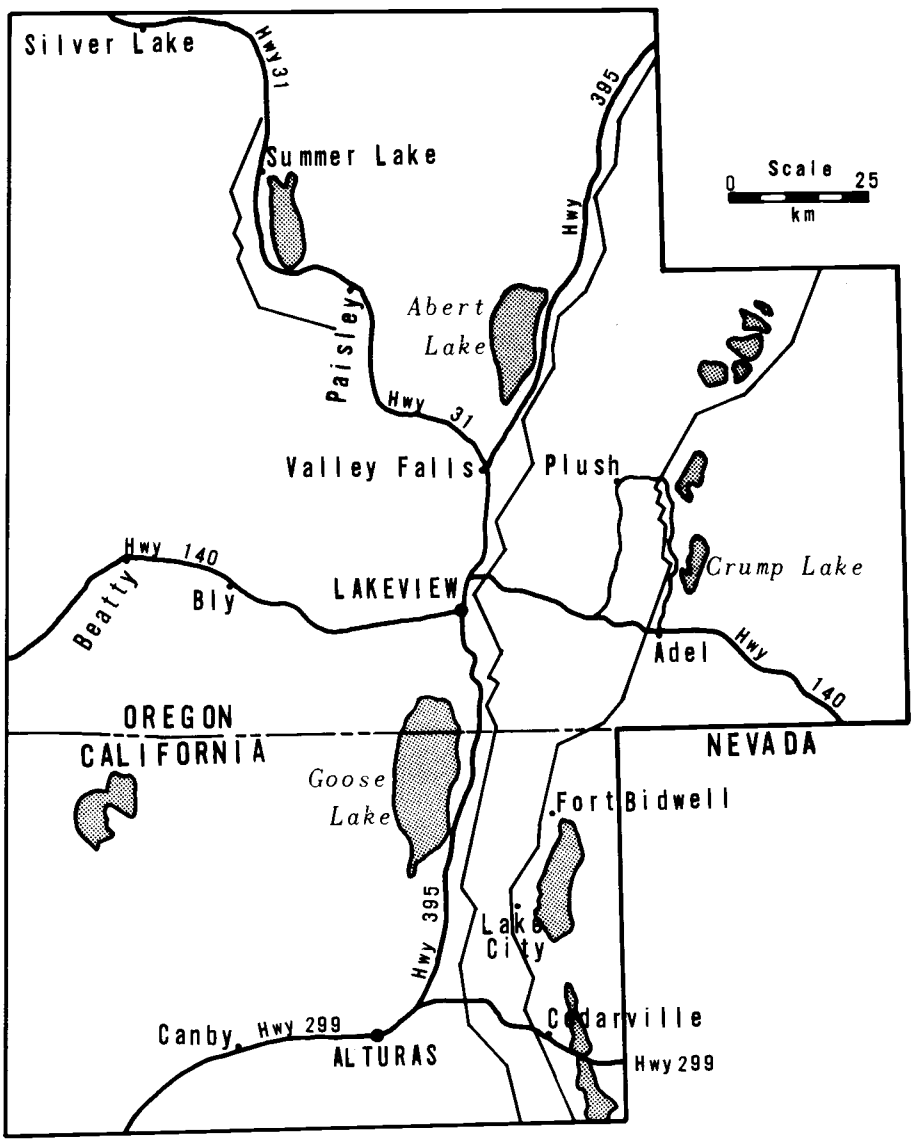

Figure 6. Study area towns and road network.

area. One geyser is located in the Summer Lake-Chewaucan Marsh-Goose Lake depression and the other in the Warner-Surprise graben. Peterson and McIntyre (1970) discussed the existence of an elongated zone of hot springs and wells from the northern part of Summer Lake to the north end of Goose Lake. These wells and springs exist on the east side of the valley along the interfaces between the graben and horst structure.

In the early 1900's, Hunter's Hot Springs at the north end of Lakeview were used as a spa. Presently, Hunter's Lodge stands adjacent to the springs and the spa no longer exists. "Old Perpetual," a shallow well drilled near the springs, erupts as a geyser approximately every thirty seconds. There are several springs at this location, all of which have temperatures near the boiling point (89^{o} C) at this altitude (1600 meters MSL). The geyser and springs are an attraction to many tourists and also to ducks.

Two other hot springs are located about three kilometers south of Lakeview. One set of hot springs is located on the Berry ranch (referred to as Berry's Hot Springs) in section 27, T. 39 S., R. 20 E. At least five different sources are located here with temperatures ranging from 64 to 88 degrees Celsius. The runoff from these springs is quite thin and is distributed into a bog-like field. Very little standing water is observed in the field and a temperature of 50^{o} C is recorded in the veneer of discharge.

Across from Berry's Hot Springs, on the east side of Highway 395, a hot spring flows from the side of a hillside owned by J. R. Brown. This is the site of the onetime Lakeview Bathhouse. Although long since gone, the bathhouse was frequently used in the history of early Lakeview. The date the bathhouse was dismantled is not known, although it was still used in the early 1900's. Present temperatures recorded are 69° C at the source (enclosed in a concrete foundation) and 66° C within three meters of the source. The spring's runoff flows into a one acre lake used by livestock. Above the inflow point, the lake's temperature is 14° C at the surface. Below the inflow point, the mixing temperature rises to 39 degrees Celsius.

The other hot springs in the Summer Lake-Chewaucan Marsh-Goose Lake depression are situated on the southeast side of Summer Lake. Summer Lake Hot Springs emits water with a temperature of 46° C at a rate of 0.05 cfs [21 gallons/minute](Phillips and VanDenburgh, 1971). This spring is presently covered over and piped into a metal-covered swimming pool. The commercial establishment has a 36° C pool temperature.

A second geyser is located in the Warner-Surprise graben six kilometers north of Adel. Peterson (1959b) first wrote about the geyser in September, 1959. The Nevada Thermal Power Company abandoned a 510 meter [1,684 foot] well on June 29, 1959 that it had drilled on land owned by Charles Crump. Two days later, the well

erupted and the Crump Geyser was formed. The geyser is situated near Crump Lake, at the base of a fault scarp forming the western boundary of the graben.

Extinct hot springs are found near Pelican Lake and Crump Lake. They can be identified by low mounds of calcareous and silicious tufa, usually devoid of vegetation (Peterson, 1959b). The mounds on the southwest side of Crump Lake range from two to six meters in diameter. Recent ground observations indicate that in the early winter and spring, the mounds are not extinct. Extremely small amounts of water seep from the mounds. The discharge is so small that only a veneer of water is observed. These seeps had a surface temperature of 25° C, however, this must not be assumed as a true water temperature but a temperature depicting the combination of hot water, calcareous and silicious tufa, and air-ground interface interactions.[1]

Other hot springs are located in this graben. Along the Middle and Upper Alkali Lakes, in the Surprise Valley, twelve kilometers east of Cedarville, California, and just off Highway 299, a hot spring and the Surprise Valley Mineral Well Motel with a swimming pool are located. Two artesian wells have been drilled adjacent to the motel.

---

[1]The temperature and other observations described herein were recorded by the author during the course of his field investigations during May, 1976.

The pools surrounding the drill holes have 84 and 92° C surface temperatures. The motel is still in operation and is slowly having its plumbing refitted. The indoor pool, built in 1959, was closed by local health authorities in 1974, because a high arsenic content was found in the spring water.[2]

A separate unnamed hot spring location is situated near the motel. This pool of water has a temperature of 90° C and is surrounded by a narrow patch of Evening Primrose flowers.

In the Pit River Valley, Kelley's Hot Springs is located approximately three kilometers east of Canby, California, on Highway 299. A four meter diameter pool, with a surface temperature of 92° C, bubbles continuously and gives off a steam cloud even on warm summer days.

The hot springs, wells, and geysers within the study area have been mapped at several different scales and times. The authors of maps that depict the largest number of surface expressions are: Stearns, Stearns, and Waring (1937); Bowen and Peterson (1970); and Phillips and VanDenburgh (1971). These maps were found to be not necessarily inclusive of all springs in the study area and do not depict the same number or location of hot springs and wells in this part of the Great Basin (Figure 7).

---

[2]Information obtained by personal interview with the motel owner, May, 1976.

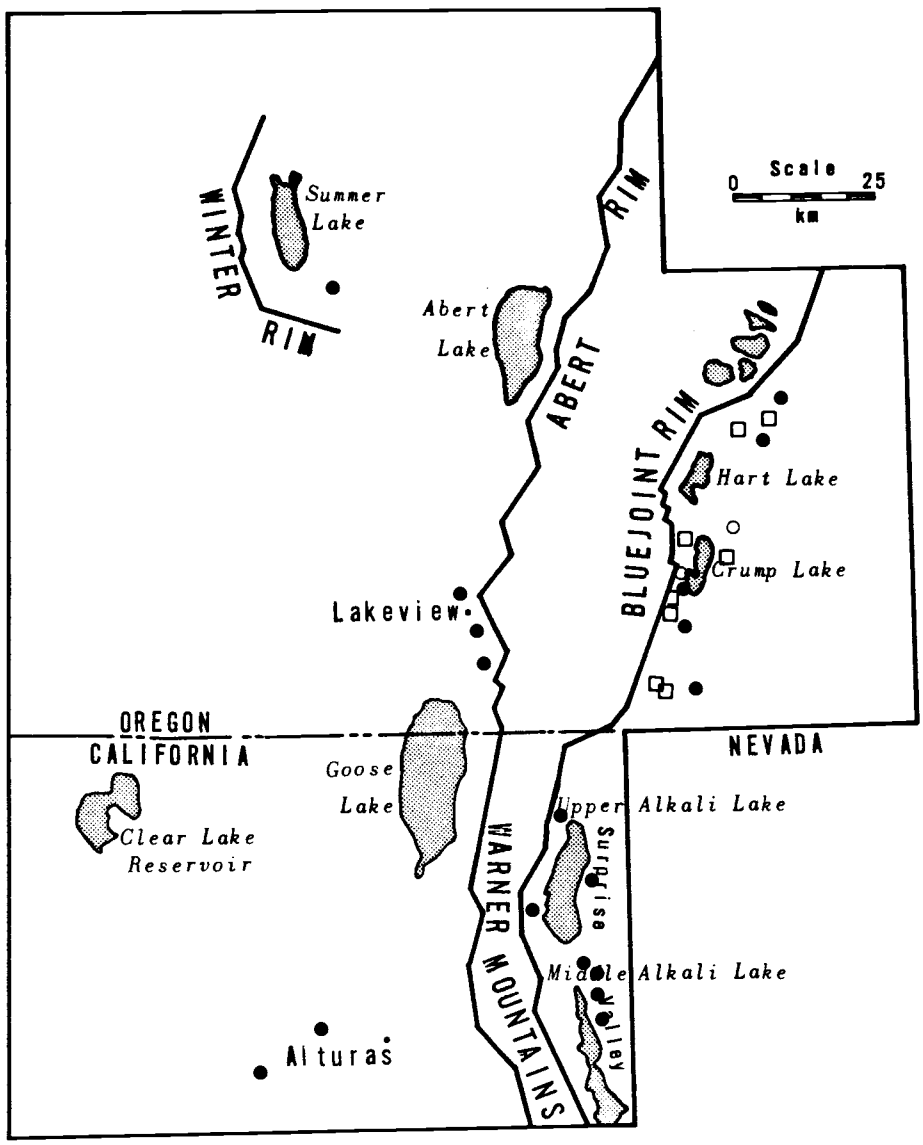

Figure 7. Previous Hydro-Geothermal sites as reported by either: Stearns, Stearns, and Waring, 1937; Waring, 1965; or Bowen and Peterson, 1970.

Hydro-Geothermal Expressions in the Study Area

The geothermal surface expressions in the study area are part of the hot-water dominated systems. The hot springs in the study area are found along the scarps of the many steeply dipping faults. Renner, White, and Williams (1975) indicate that the hot springs in this area of the Great Basin are created by surface water, infiltrating down along the fault traces, being heated by the processes of conduction and convection. A decrease in density causes the water to rise along the faults and to emerge at the surface as hot springs.

Three areas, within the study area, are identified by Renner, White, and Williams (1975) as hot-water convective systems above 150° C: Surprise Valley; Lakeview; and Crump Spring (Crump Geyser) (Table 8). The Surprise Valley location is cited as having the highest known subsurface temperature (175° C) in the study area. It also has the most massive reservoir volume, at 250 cubic kilometers. Nathenson and Muffler (1975) calculated the potential electrical energy of the location to be 637 Mw of electricity, or 2,121 Mw for thirty years. Although the Lakeview location has smaller surface temperatures, its large volume and high heat content of the reservoir also creates a large electrical potential.

Kelley Hot Springs (California) and Summer Lake Hot Springs fall into the second division of hot-water systems, i.e., 90-150° C

Table 8. Hot spring's electrical potential.

Spring	Latitude (N)	Long. (W)	Temp. Surf.	°C Subs.	Reservoir Vol km^3	Reservoir Heat Content**	Electrical Potential*** Mw e·cent
Surprise Valley	41°40'	120°12'	97	175	250	24.0	637
Lakeview*	42°12'	120°21.6'	96	160	16	1.4	37
Crump Spring	42°15'	119°53'	78	180	8	0.8	21
Kelley Hot Springs	41°27.5'	120°50'	96	130	3	0.2	-
Summer Lake Hot Springs	42°43.5'	120°38.7'	43	140	6	0.4	-

* Includes Berry and Hunter Hot Springs.

** Product of volume, volumetric specific heat of 0.6 cal/cm^3 °C, and temperature in degrees Celsius above 15° C. Heat content values times 10^{18}.

*** One Mw e·cent = 7.53×10^{14} cal/e_c where e_c = conversion efficiency of 0.02

Source: Adapted from Renner, White, and Williams (1975) and Nathenson and Muffler (1975)

category. Thus, no electrical potential is listed. Summer Lake Hot Springs has a surface temperature 53 degrees cooler than that of Kelley Hot Springs but the subsurface reservoir temperature is ten degrees warmer. The larger reservoir volume of Summer Lake Hot Springs produces higher internal pressures which creates the higher temperature differential.

Many surface expressions exist in the study area that fall into the third division of the hot-water system, i.e., less than 90 degrees Celsius. These locations with lesser heat content will be discussed in the analysis section of this research.

Role of Government

The Geothermal Steam Act of 1970 (Public Law 91-581:84 Stat. 1566) was passed by the 91st Congress to establish control over the exploration and development of geothermal resources on land owned or administered by the Federal Government. According to the act, the Secretary of the Interior can accept competitive applications for leases on Federal land. When enough competitive interest is generated (i.e., when two or more lease applications overlap by greater than 50 percent) the area of concern is designated as a Known Geothermal Resources Area (KGRA) by the Secretary or his representative, the USGS. Prior to that designation, the area may have a suspected geothermal potential and thus is referred to as a potential

KGRA. The word known in such designations may be a bit premature because no actual exploration has occurred, only the leases have been applied for. Leases applied for within a potential KGRA may be granted without competitive bidding. As of 1971, 7,300 square kilometers of Federal land (owned or administered) were classified within a KGRA by the USGS. Approximately 390,000 square kilometers are within potential KGRA's. The U. S. Geological Survey is responsible for the supervision of the operations and unitization (pooling of leases) of the act. The Bureau of Land Management supervises the exploration and leasing aspects of implementing the Geothermal Steam Act (California Department of Water Resources, 1974).

Figure 8 depicts the distribution of potential and known geothermal resources areas within the study area. Sixteen thousand eight hundred and sixty-one square kilometers are classified as areas of potential KGRA's by the USGS Conservation Division. This figure (Figure 8) is a composite of two Geothermal Land Classification Maps produced by the offices of the Western Region of the USGS. According to this distribution two percent of the total study area lies within a KGRA and 61 percent lies within a potential KGRA. There are four KGRA sites in the study area as depicted on this figure. They are: Surprise Valley, California; Crump Geyser in Warner Valley; Lakeview; and, Summer Lake.

When an organization submits a lease application to the BLM,

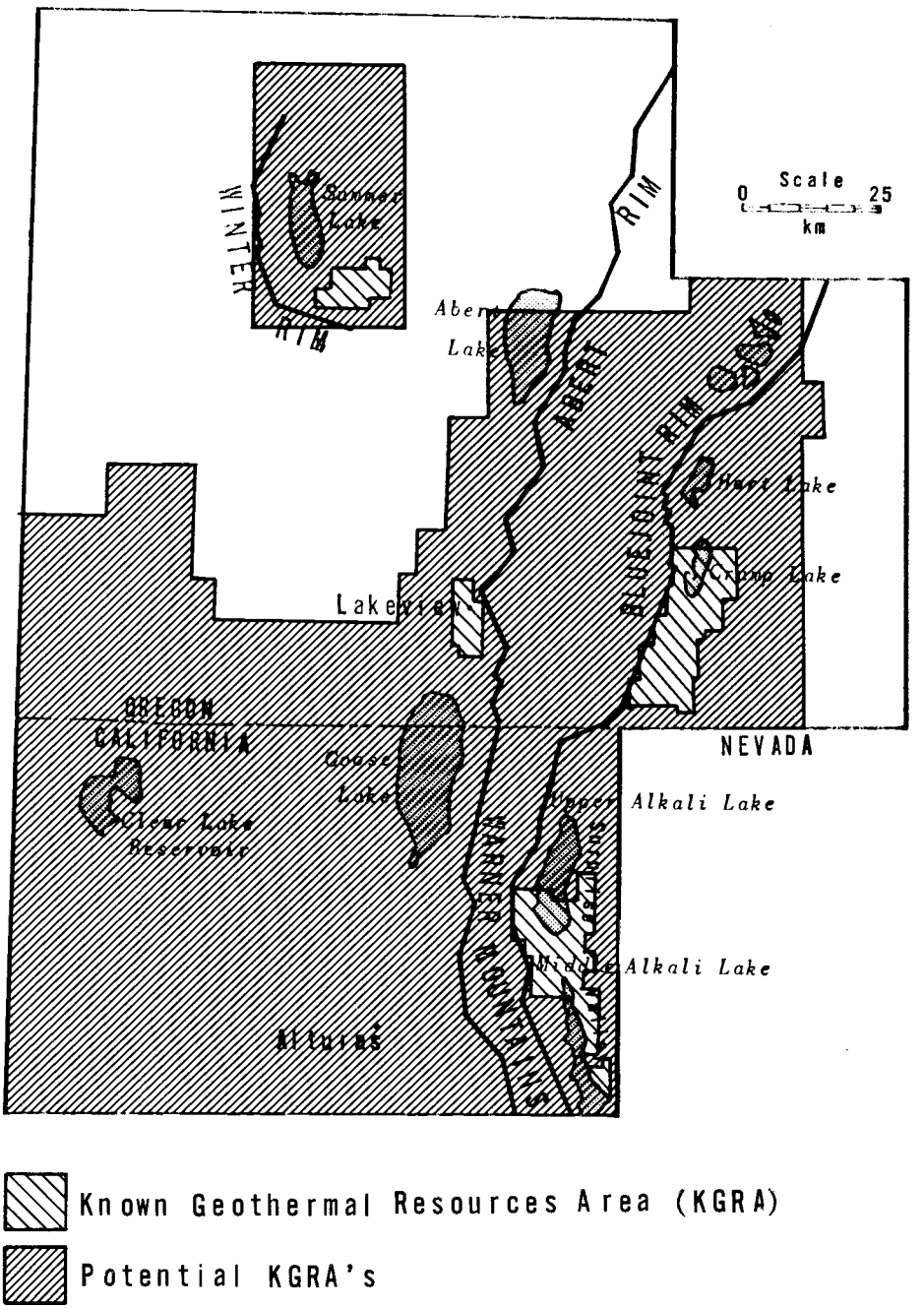

Figure 8. Known and potential geothermal resources (from USGS, 1976).

it must include an operating plan outlining their procedure for exploration, development, and reclamation. If the land to be leased is administered by the U. S. Forest Service, the lead agency (BLM) requests that an environmental analysis of the area be prepared, and that recommendations be drawn concerning the proposed actions and possible alternatives to those actions. Table 9 lists many of the environmental factors that must be considered concerning proposed actions and alternatives. These reports are termed Environmental Analysis Reports (EAR's). Three EAR's have been written for KGRA's in the study area. In 1975 the BLM released its report on the Warner and Surprise Valleys and in 1976 the Summer Lake and Upper Pit River Area EAR's were published. EAR's produced by the Forest Service are reviewed by BLM prior to release. Any recommendations concerning the lease application and its proposed actions can be overridden by the BLM prior to the EAR's release.

If the lease is granted, an environmental impact statement (EIS) must be prepared before development of the leased area is allowed. The EIS is prepared by the U. S. Forest Service. Although the Final Environmental Statement for the Geothermal Leasing Program (U. S. Department of Interior, 1973) was published as a guide for the creation of future EIS publications, no guidelines as to the actual preparation of such impact statements exist at the present time. The creation of such guidelines will be needed in the future, as nearly

Table 9. Environmental Factors.

Geology
Soils
Land use
Air
Water
Aquatic plants
Terrestrial plants
Wildlife--aquatic and terrestrial animals
Domestic livestock
Ecological interrelationships
Human values
Educational-scientific-historical values
Archaeology
Social welfare
Attitudes and expectations

Source: U. S. Bureau of Land Management, 1975 and 1976.

60 percent of the potential KGRA land in the United States is on Federal land. Therefore, the majority of land identified as having geothermal development possibilities must have environmental impact statements written prior to that development.

Exploration Techniques

In order to evaluate the environmental impact of geothermal exploration and development, much information is needed concerning the specific locations of both the hot-water reservoir and the surface expressions of that reservoir. Both Denton (1972) and Raschen and Cook (1976) discuss the different techniques used in the exploration of

geothermal resources. Table 10 and the ensuing discussion were generated from those publications.

Geological Techniques. Geological techniques provide a background for structural analysis and for historical events of a given study site. The distribution of rock types, characteristics, and interrelationships are analyzed by surface and cartographic examinations. As with the petroleum industry, geologic interpretations are key factors in exploration.

Geochemical Techniques. Geochemical techniques involve the sampling and analysis of waters and gases from geysers, fumaroles, drill holes, and surface springs. Such data are utilized to estimate

Table 10. Exploration Techniques for Geothermal Resources.

Geological Techniques
Geochemical Techniques
Electrical Techniques
Resistivity surveys
Magnetotelluric surveys
Radiometric surveys
Seismic Techniques
Passive seismic surveys
Active seismic surveys
Gravity and Magnetic Techniques
Gravity surveys
Magnetic surveys
Thermal Techniques
Drilling Techniques
Shallow temperature holes
Observation holes
Remote Sensing Techniques

Source: Adapted from Denton (1972) and Raschen and Cook (1976).

the internal water characteristics, including reservoir temperature, chemical constituency, source of recharge water, and homogeneity of water supply.

Electrical Techniques. Electrical techniques have, for many years, been the primary geophysical techniques for locating geothermal fields. The major subdivision of this group is the resistivity survey. Electrical currents are induced into the ground via electrodes spaced widely apart. The voltage potentials induced by the transmitted currents give the apparent electrical resistivity of the subsurface materials. This resistance variation can be interpreted and an analysis of the existing subsurface material can be made.

Like the resistivity survey, a magnetotelluric survey measures the apparent resistivity of subsurface materials. The difference is that the magnetotelluric survey utilizes the natural currents in the earth's crust and not those currents artificially induced.

Seismic Techniques. As the electrical methods analyze the resistivity of subsurface materials, the seismic methods analyze subsurface structure. The passive form of seismic surveys utilize small geophones, embedded into the ground, which measure the microearthquakes which are associated with geothermal areas. These earthquakes are normally found at depths of approximately six kilometers and are very small in magnitude. The careful study of earthquake patterns can help to delineate the actual fault surface which

often serves as a transport route for the geothermal fluids.

Active seismic surveys also involve the use of geophones as ground motion sensors. However, this method utilizes artifically induced vibrations produced by a heavy "dead fall" thumper striking the ground surface (for small scale shallow depth exploration) or the use of explosives in shallow drill holes on a deeper much larger scale exploration. The greater the distance between the active source and the geophone, the greater the shock waves must be in order for them to reach the sensor. Variations in the travel time of the sensed shock wave from different source points are used to locate the faults and other subsurface structural characteristics.

Gravity Techniques. Gravity surveys determine the subtle changes in gravity values as they vary over a given area. These values are measured using a gravimeter which senses the variations caused by density changes of subsurface materials. Such density changes may be related to temperature variations of the rock and fluid materials beneath the surface. Hot geothermal rocks or waters can cause these temperature variations and thus can affect the measured gravity.

Magnetic Techniques. Magnetic surveys check for variations in magnetism which may result because of temperature variations. Using a magnetometer, slight changes in magnetism can be detected and a map of magnetic variations can be constructed. Analyzing the

data of the magnetic survey in conjunction with the data of the gravity surveys, the location of potentially warmer subsurface temperatures may be determined.

Thermal Techniques. Thermal techniques can be conducted which measure the surface temperature, geothermal gradient, and heat flow. Variations in these measurements can be mapped and utilized in estimating the amount of geothermal resources.

Drilling Techniques. Drilling represents one of the more expensive techniques for determining geothermal source locations. The shallow drill hole (less than 150 meters) is similar to the holes drilled for the explosive seismic shock techniques. The temperature variations with depth determine the geothermal gradient. This gradient is projected to greater depths to determine the temperature at the suspected source point. These shallow holes are allowed by the Geothermal Steam Act without geothermal lease applications. However, if the operator wishes to continue drilling to greater depths, he must file for a lease and he must present his plan of operation and restoration. Otherwise, the drill hole must be abandoned and the surface returned to its original site characteristics.

Observation holes can be drilled under the granted lease, under the guidelines established by the lead agency (BLM). These wells are quite costly and generally the operator has already decided to continue the drilling operation to develop the deep exploratory well. However,

observation holes are used to gain as much geologic and hydrologic information as possible. These wells are drilled to depths of nearly one kilometer but the drilling ceases prior to the penetration of the potential reservoir. The information acquired from the drilling technique is accumulated over time.

Remote Sensing Techniques. The previous exploration techniques discussed demand many man-hours of on-site labor. Extended field time for travel, equipment set-up, and data collection increase both the cost and the length of the survey period. Costs and on-site survey time can be reduced by decreasing the number of man-hours required to conduct the survey. A reduction in the amount of labor required can be accomplished by the use of remote sensing.

Remotely sensed data, acquired via aircraft or satellite, alleviates the necessity of the labor intensive field survey. Specific locations for field checking can be acquired by means of the data analysis after the imagery has been acquired. Little, if any, on-site activity is required at the time of data acquisition and specifically, large scale movement of men and equipment are not required for a remotely sensed field survey. Various remote sensing techniques were utilized to determine structural variations and surface geothermal locations which are expressed along surface faults in the study area.

III. REMOTE SENSING

Remote sensing is a complex field of data collection, utilizing cameras and sensors. By definition, the acquisition of data is achieved through imaged representation of that data, while maintaining a position at some distance from the source. Not only does the term refer to acquisition of data, but also to the interpretation of that collected data.

The period of development for new forms of remote sensing was from 1960 to the present. The TIROS, NIMBUS, and LANDSAT-1 (ERTS-1) satellites were the impetus for the modern remote sensing techniques. How these techniques work is examined in the ensuing discussion.

Electromagnetic Spectrum

Both photographic and non-photographic techniques record energy impulses of electromagnetic radiation (EMR). This radiation maintains various energy levels which are exhibited by their position in the electromagnetic (EM) spectrum (Figure 9). The EM spectrum is a term which applies to all energy that moves at the constant velocity of light and that possesses a harmonic wave pattern (Estes and Senger, 1974). The three wave properties of velocity, wavelength, and frequency apply to this EMR. The velocity of the energy, as

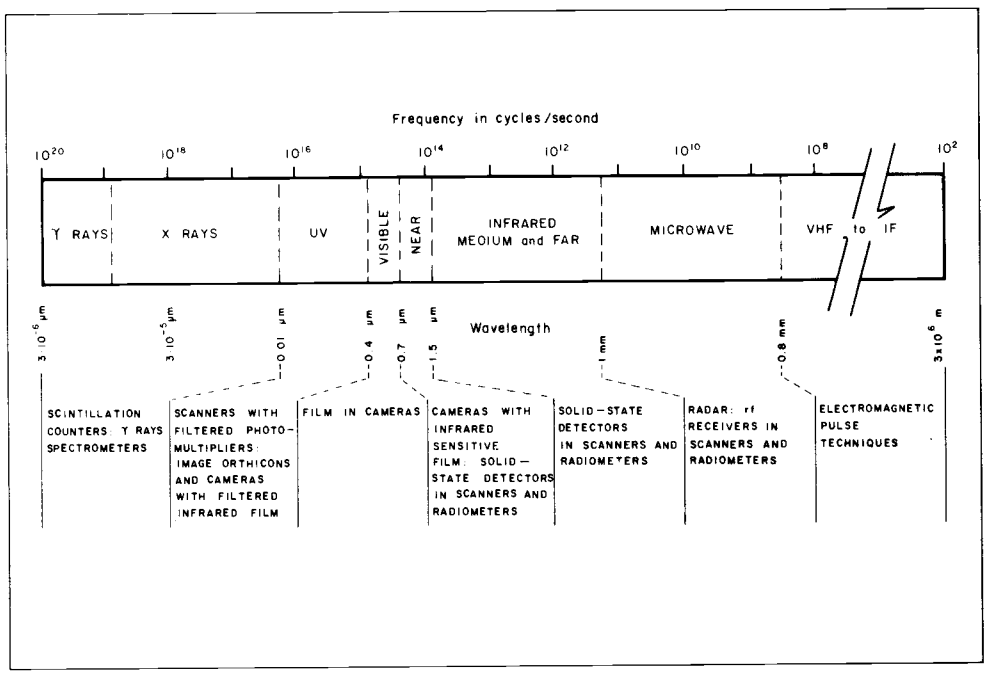

Figure 9. EM spectrum and sensors (from Estes and Senger, 1974).

stated above, is constant. Therefore, the wavelength (distance between successive wave crests) and frequency (number of wave crests per period of time) must maintain an inverse relationship, that is, the longer the wavelength, the lower the frequency.

As the solar energy reaches the earth's atmosphere, the components of the atmosphere (chiefly H_2O, CO_2, and O_3) may diminish the intensity of that radiation. This is accomplished through reflection, scattering, or absorption of the energy. Reflection of the solar radiation occurs when the atmosphere (clouds, dust particles, or other constituents) returns portions of that radiation back to space. As the remaining radiation continues to pass through the atmosphere, its path is altered or scattered by the components. The energy that is scattered may continue on and may reach the earth's surface. However, the wavelength-frequency relationship will be altered and the wave energy will be altered, as if slightly bent or refracted. Absorption is the assimilation of the solar energy. Such energy that is absorbed by the atmospheric constituents is eventually re-radiated and discharged as energy with a longer wavelength.

The EMR that is not reflected or re-radiated reaches the earth without alteration of its energy level, thus it is said to be transmitted. The amount of energy that is transmitted through the atmosphere varies with wavelength. At different wavelengths in the EM spectrum, more energy is transmitted, resulting in atmospheric windows. These

windows occur when the absorptive and reflective characteristics of the atmosphere are decreased, as a result of the physical properties of water vapor, carbon dioxide, and ozone. The distribution of these windows in the EM spectrum is depicted in Figure 10. The greater the percentage of transmission, the greater the EMR that is received by the earth's surface or from the earth's surface.

The radiation that reaches the earth's surface is either absorbed, reflected, or transmitted by all objects that comprise that surface,[3] that is, the objects are all absorbers, reflectors, or transmitters of energy. Therefore, the various energy levels emitted by these earth units can be sensed either photographically or non-photographically, depending on the wavelength-frequency characteristics. The selection of the proper imaging technique is therefore based on the understanding of the wavelength-frequency characteristics being encountered.

Four basic laws have been established which govern the radiation flux in the EM spectrum. The nature of these laws are thoroughly covered by the literature (Reeves, 1975; Estes and Senger, 1974; Wolfe, 1965; and others). The information presented below is a review of that literature.

---

[3]The objects referred to here are the surface flora, fauna, lithologic, and hydrologic units.

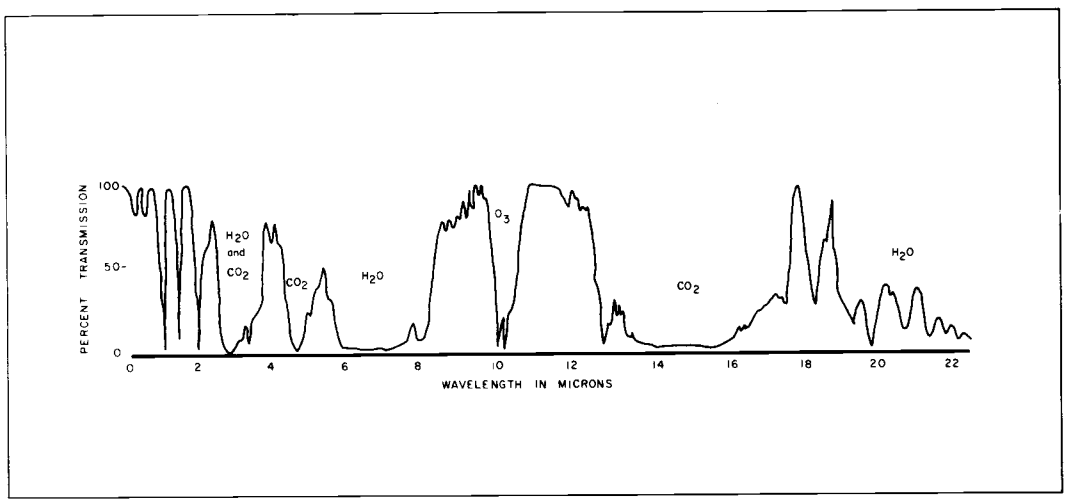

Figure 10. Percentage of atmospheric transmission (from Estes and Senger, 1974).

Planck's Law

A black body is an object that radiates the maximum possible intensity of radiation at a given temperature for every wavelength. All energy received by the black body is also emitted by it. There is, however, no true black body in nature. The sun is as close to a true black body as can be observed and is therefore defined as a black body.

Planck found that the energy of a black body is related to frequency rather than to wavelength. Planck's formula for the emittance of the black body radiator is:

$$E = C_1 \lambda^{-5} \left[\exp \left(\frac{C_2}{\lambda T} \right) - 1 \right]^{-1}$$

where:

E	=	radiant power (emissive power)
C_1 and C_2	=	constants
λ	=	wavelength in meters
T	=	absolute temperature in degrees Kelvin.

Stefan-Boltzmann Law

The following equation is obtained when Planck's equation is applied to all wavelengths:

$$E = \sigma T^4$$

That is, the emissive power of a black body radiator (in w cm^{-2}) is equal to the fourth power of the absolute temperature times the Stefan-Boltzmann constant (5.67×10^{-12} w cm^{-2} $(^{o}K)^{-4}$).

Kirchhoff's Law

Kirchhoff determined that the total amount of energy striking a surface per unit of time is equal to unity. Therefore:

$$\text{absorptivity} + \text{reflectivity} + \text{transmissivity} = 1.0$$

Reflectivity and transmissivity are not affecting the energy level of the surface, thus any energy exhibited by that surface is absorbed energy being re-radiated. Thus, for a black body, what is absorbed must also be emitted. Therefore, absorptivity equals emissivity or:

$$a = e$$

for a black body. However, all known substances do not emit all the energy that they absorb. These are referred to as gray bodies, i.e., they are not true black bodies. In such cases the emissive power (E) is reduced by the emissivity (e) of the surface. That is:

$$E = \frac{\text{emissive power of object at given T}}{\text{emissive power of black body at given T}} .$$

Applying this to the Stefan-Boltzmann Law, Kirchhoff's Law alters the equation to allow for the gray body emissive power or:

$$E = e\sigma T^4.$$

Wien's Law

This law allows for the calculation of the peak radiation (wavelength) at which a substance will emit for a given temperature. Wien's formula is:

$$\lambda \text{ max } T = \frac{2897}{\text{Temp. } {}^{o}K} .$$

Therefore, according to Wien's Law, the lower the temperature of the emitting body the longer the maximum wavelength. The reverse is also true, the higher the temperature the shorter the wavelength. The sun emits energy in the temperature range of $6,000^{o}$ K and therefore, using Wien's Law, the maximum emittance occurs with a wavelength of 0.5 μm. The average temperature of emittance by the earth's materials is approximately 285^{o} K. Thus, the wavelength of peak emittance of the earth is approximately 10 micrometers (Figure 11).

Sensors

The radiant energy of the EM spectrum can be sensed by either photographic or non-photographic techniques and can be reassembled

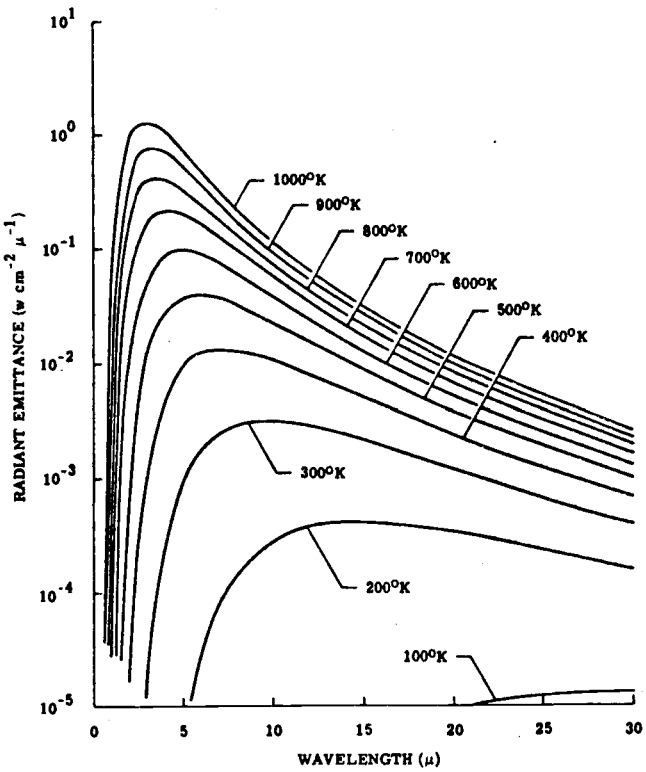

Figure 11. Wavelength peaks for blackbodies, 100-1000° K (from Wolfe, 1965).

into a photograph or image. Photographic techniques imply that the camera or sensor is passively sensing energy in the visible light (0.4-0.7 μm) portion of the spectrum or in the near-infrared (0.7-0.9 μm) portion. Therefore, the photographic technique implies the final product is a photograph, which by definition means produced by light.

Non-photographic techniques of remote sensing refer to those methods that produce images or imagery (i.e., representations of a photograph). Impressions of the energy emitted by an object are acquired by the sensor and are then converted into a facsimile (image) of that object. This acquisition of energy can be achieved by either passive or active sensors. Multispectral scanners and thermal infrared scanners are examples of passive sensors. Multispectral scanners receive the EMR reflected by the surface or object in the 0.5-1.1 μm range, while the thermal infrared scanners sense heat radiation in the range of 1-1,000 micrometers. Materials used in the construction of these passive sensors vary in their sensitivity to different narrow wavelength bands. For example, selective wavelength ranges can be detected by a different material. Therefore, the various sensor materials are associated with their particular wavelength characteristics, e.g., mercury-cadmium-telluride combination is sensitive in the 8-14 μm range.

Radar is an example of an active sensor system, utilizing the

microwave portion of the EM spectrum. Energy, at a constant level is transmitted by the radar system to the earth's surface. Just as with incoming solar radiation (insolation), this energy may be reflected, absorbed, or transmitted. The energy that is reflected back to the sensor is what determines the visual appearance of the radar imagery. The variation in signal intensity, sensed by the detector, is converted into variations in the gray scale. Thus, utilizing these gray scale variations, images are produced that represent a likeness of the surface configuration.

Both passive and active sensors are necessary in order to achieve the research objective of analyzing remote sensing techniques to locate geothermal surface expressions in the Great Basin. The sensors that are used in this research to detect surface lineaments and surface heat anomalies are: multispectral scanners (MSS) aboard Landsat-1 (ERTS-1); side-looking-airborne-radar (SLAR); and, thermal infrared (TIR) scanners.

Landsat-1

The Earth Resources Technology Satellite (ERTS-1) was launched into a sun-synchronous near polar orbit at an altitude of 920 km in July, 1972. (Recently, the term Landsat has been applied to this ERTS vehicle and will be utilized in the remainder of this discussion.) The satellite circles the earth fourteen times a day from

north to south (Figure 12). After eighteen days, the satellite returns to its original position. Thus, the entire earth is covered by the satellite and its sensors every eighteen days.

Landsat is a butterfly-shaped observation platform (Figure 13). The two sensor systems mounted on this platform are the Return Beam Vidicon (RBV) cameras and the Multispectral Scanners (MSS). The RBV consists of three cameras viewing the same 185 km square area in three different spectral bands (wavelength groups). These cameras do not contain photographic film. They electronically image (scan) the earth like a television camera. The image is transmitted to earth where the signal is converted to a photograph. The use of the RBV system was discontinued in August, 1972 as a result of functional problems.

The second sensor system aboard Landsat has been operating continually since the satellite was launched. The MSS covers the same 185 km square area as the RBV cameras. This line-scanning sensor covers the area beneath the spacecraft in a continuous fashion. Unlike the RBV's three spectral bands, the MSS collects data in four spectral bands. The four bands and their wavelengths are listed in Table 11.

Band 4 (0.6-0.7 μm) represents that range of the visible light spectrum sensitive to the color green. This spectral band is useful in examining the depth or turbidity of standing water. It tends to

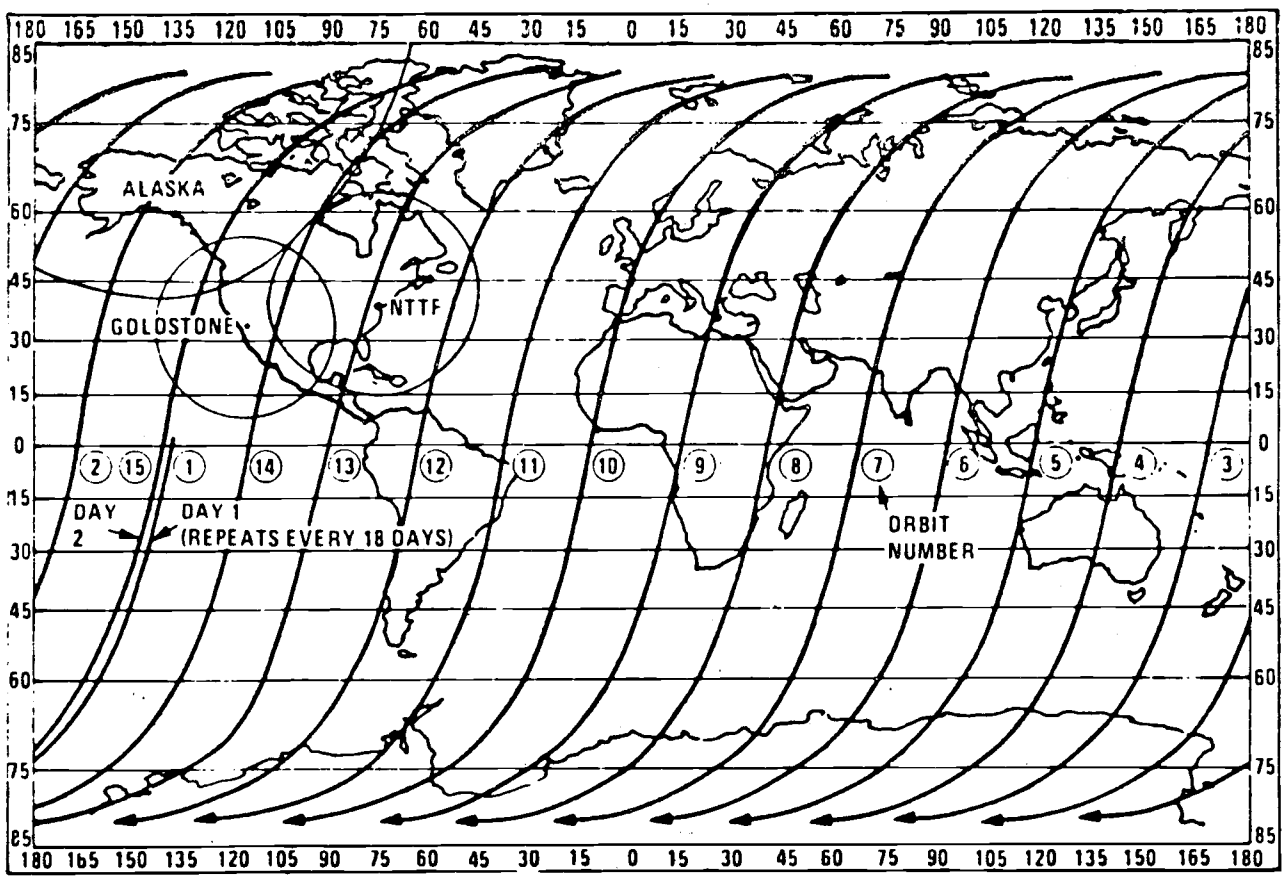

Figure 12. Landsat-1 Orbits (from NASA, 1971).

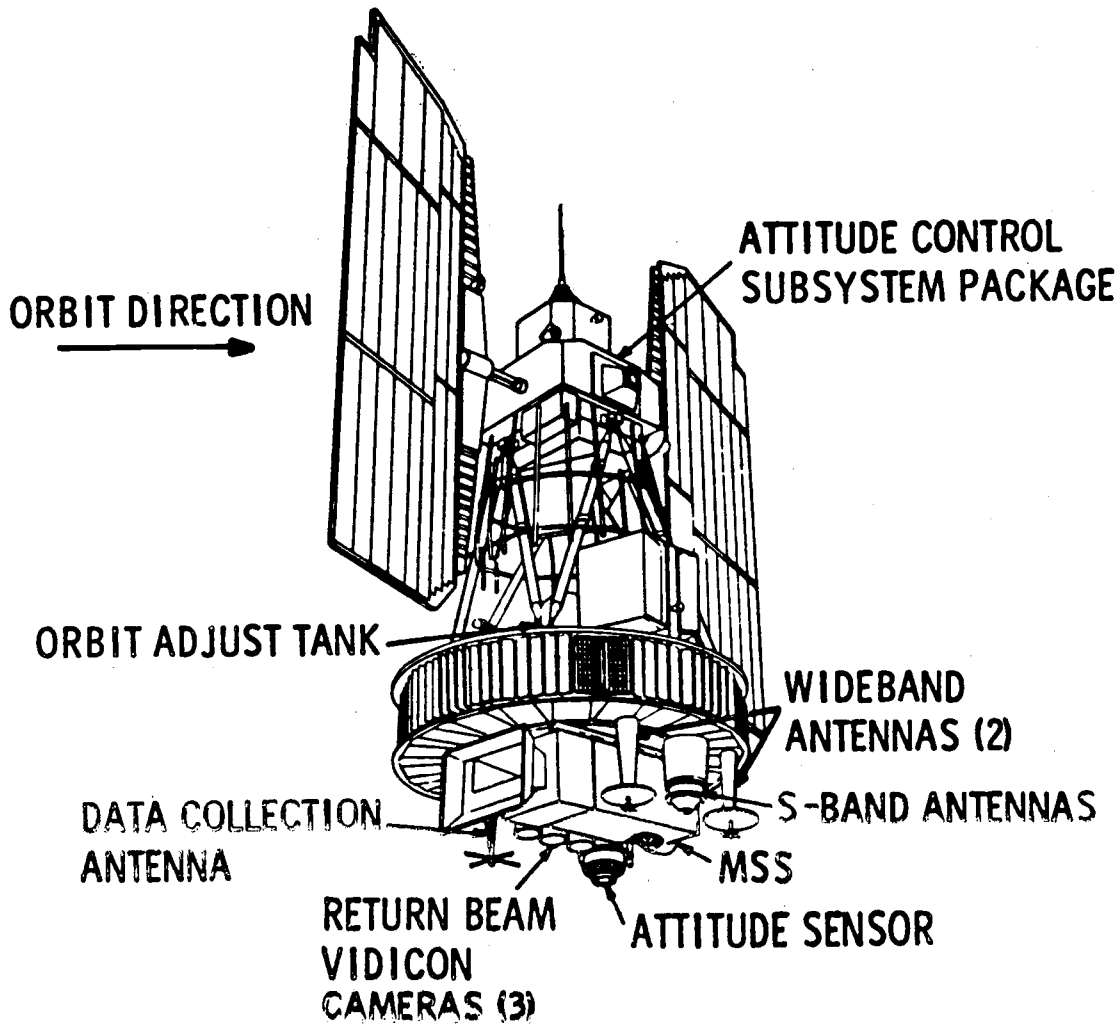

Figure 13. Landsat-1 observation platform (from NASA, 1971).

Table 11. Multispectral Scanner

MSS Band	Range (μm)
4	0.5-0.6
5	0.6-0.7
6	0.7-0.8
7	0.8-1.1

Source: NASA, 1971

enhance materials in the water, such as sediment. Band 5 (0.6-0.7 μm) is sensitive to the red division of the visible light. This band easily penetrates the atmosphere and is good in representing the variations in cultural versus physical features. Physical features, such as a drainage pattern, tend to be absorbers at this wavelength, appearing as a darker tone on the image. The cultural features are more reflective and thus their tone is much lighter.

The last two bands are both in the near-infrared portion of the EM spectrum. Band 6 (0.7-0.8 μm) produces large tonal variations that make for better discrimination in land use practices. It also allows for the best land-water relationship. Band 7 (0.8-1.1 μm) is also good for discerning the land-water variations. Water appears as black in the spectral band because it is a good absorber at these wavelengths. Vegetation is also easily identifiable with Band 7. In this spectral band, vegetation absorbs most of the green and red light

(shorter wavelengths) and reflects approximately 80 percent of the near-infrared radiation.

Many of the Landsat scenes are available in color composites of three of the spectral bands. The spectral bands are registered and are exposed through appropriate filters onto color film. The images produced are at a scale of 1:1,000,000 with the actual image size being 2.95 x 2.95 cm (7.5 x 7.5 inches). Figures 14 and 15 are synthetic color composites of the Wagontire and Modoc scenes in Oregon and northeastern California. The spectral bands of 4, 5, and 7 were used to make these composites. The negative of each band was processed utilizing color sensitive film and a diazo developer. These color images were registered and photographed, creating the two figures. Because the objective of this research is to examine the geothermal surface expressions and their relationship to structural lineations, Band 6 is most helpful in discriminating the different land use practices. Therefore, in order to bring out the natural features of water and structure, the bands most sensitive to the characteristics of those features were utilized.

Landsat imagery is noted as a useful tool in analyzing geologic joints and faults as expressed as photo lineaments. The interpretation of the imagery for delineating these linear features is well documented in the literature. Several of these studies indicate that present structural maps are missing many lineaments that actually

Figure 14. Wagontire scene of Bands 4, 5, and 7 (Landsat-1) with Lawrence's (1976) lineament interpretations.

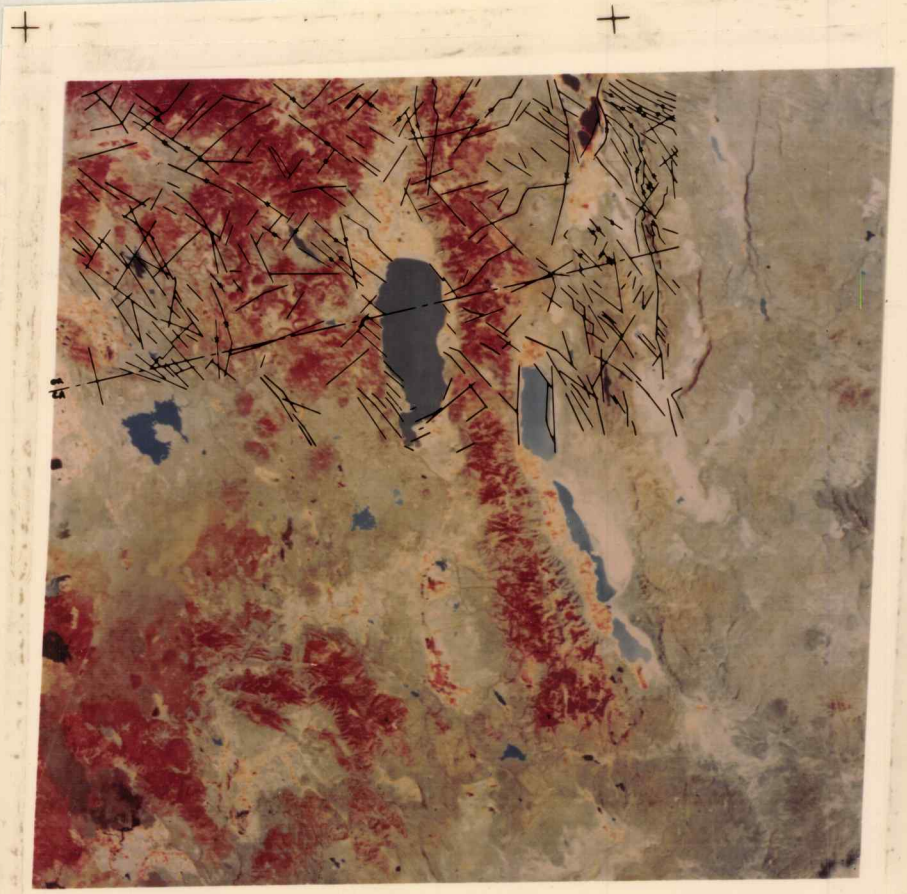

Figure 15. Modoc scene of Bands 4, 5, and 7 (Landsat-1) with Lawrence's (1976) lineament interpretations.

exist in the areas covered by the maps. Wiedman et al. (1973) identified the structural lineaments using Landsat imagery in the state of Montana, and concluded that the imagery is a potential major tool for improving geologic knowledge. They stated that the use of imagery in tectonic mapping could result in significant savings of time and money. The identification of previously unknown faults, the extension of known fault traces, and the recognition of shorter lineaments on a regional basis are bonuses of the use of Landsat imagery. New, previously unmapped lineaments have been identified by: Steffenson (1973) in the Gaspe' Peninsula, Quebec; Hoppin (1973) in the Bighorn Region of Wyoming and Montana; Pease and Johnson (1973) in the tectonic zone in Southern California; Rowan and Wetlaufer (1973) in the state of Nevada; and, Friedman, Frank, Preble, and Painter (1973) in their study of Mt. Lassen and the Warner Valley.

Lawrence (1974) produced a lineament map from Landsat imagery for the state of Oregon. He analyzed the structural lineaments on a twice size enlargement (1:500,000) of each Oregon Landsat scene. His analysis is depicted as transparent overlays for Figures 14 and 15.

The use of Landsat imagery for delineating structural lineaments is impeded by initial operation unfamiliarity, image quality, and scale. As with all skills, the degree of interpretative accuracy increases with use. The techniques necessary to delineate between

lineaments and other physical or cultural features develop through time with experience.

Image quality can also decrease the accuracy of identifying structural lineaments. Excessive cloud cover can totally obscure the ground surface, or atmospheric attenuation (i.e., a decrease in signal intensity as a result of interaction with atmosphere constituents) may reduce the clarity of the image. However, the passage of the satellite over the same location every eighteen days enables the user to select the scene with the best image quality in order to identify lineaments.

Scale is a function of satellite altitude and sensor focus. The MSS composite (Bands 4, 5, and 7) may have its 1:1,000,000 scale increased through photographic reproduction techniques. However, the largest area of image resolution is 0.4 Hectares (1.1 Acres) regardless of scale. The image size can be increased but the resolution will be only as good as the original product. Increasing image size provides for easier interpretation, but offers no more information than the original.

SLAR

Radar (radio detection and ranging) systems are sensors which operate in the microwave portion of the EM spectrum. Radar is an active sensor producing its own EMR which is transmitted to the

surface or to the object. The microwave energy which is reflected (backscattered) from the surface or from the object is received, amplified, and converted to equivalent gray scale tonal variations. These variations create an image of the surface or of the object. The variability of the EMR backscattering provides significant information about size, shape, configuration, and other attributes of the surface or of the object.

There are many different configurations of radar, each designed for its specific purposes of measurement. The type of system best suited for airborne image-depicting radar is side-looking-airborne-radar (SLAR). This system is designed to generate an image of the terrain parallel to the flightline of the aircraft. As the plane advances, the detector system scans outward perpendicular to the flightline (Figure 16).

Factors Influencing Interpretability

SLAR produces a continuous strip image of the area to either side of the aircraft. The EMR which is backscattered from the surface is dependent upon the strength of the transmitted EMR and upon the reflecting capabilities of the surface. The factors that influence the interpretability of this radar imagery are the inherent geometric characteristics of shadows, foreshortening, layover, and parallax (Reeves, 1975).

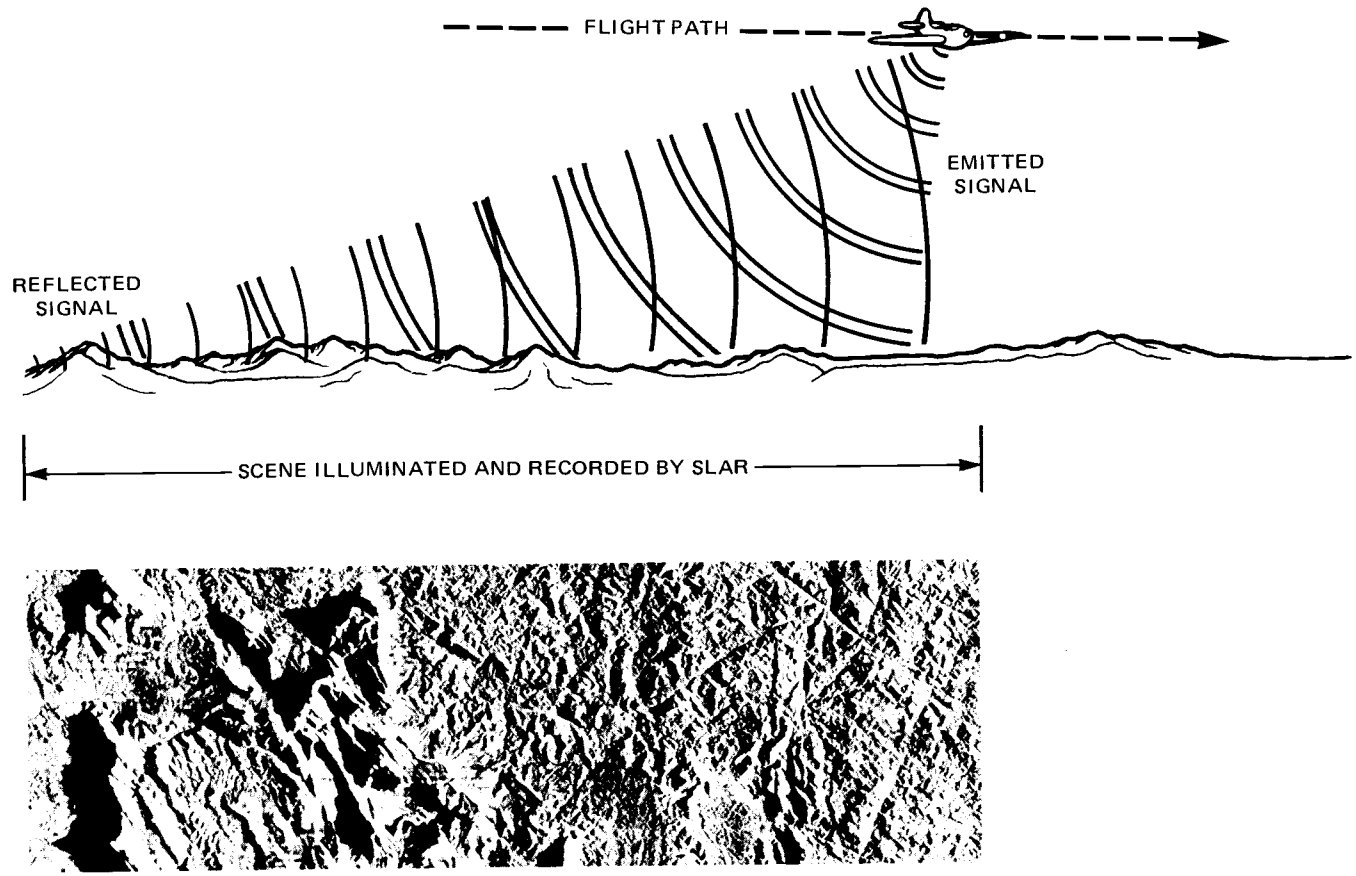

Figure 16. Side-Looking-Airborne-Radar (from Dames and Moore, 1974).

Shadows. There are two parameters that determine whether or not a shadow will be produced by a hillslope. These parameters are the depression angle (β) and the back slope angle (α_b). As depicted in Figure 17, the depression angle is generated by the propagational vector of the radar wavefront tangent to the crest of the hillslope and the horizontal plane created by the aircraft flightline. The closer the hillslope is to the point directly under the flightline the greater the depression angle. The back slope angle is the hillslope angle of the terrain facing away from the radar beam.

The relationship of these two parameters determines whether shadows occur on the imagery. Three relationships are possible:

1. $\alpha_b < \beta$, no shadow as the back slope is fully illuminated (Position A in Figure 17);
2. $\alpha_b = \beta$, radar wavefront tangent to the back slope (Position B); and,
3. $\alpha_b > \beta$, shadows form as back slope is obscured (shadow length increases in Position C through F).

The length of the shadow is directly related to the distance the hillslope is from the flightline and is inversely related to the aircraft altitude.

The condition producing a shadow, described above, is correct only when the trend of the crestline is parallel to the flightline, i.e., perpendicular to the radar wavefront. If the trend of the crestline

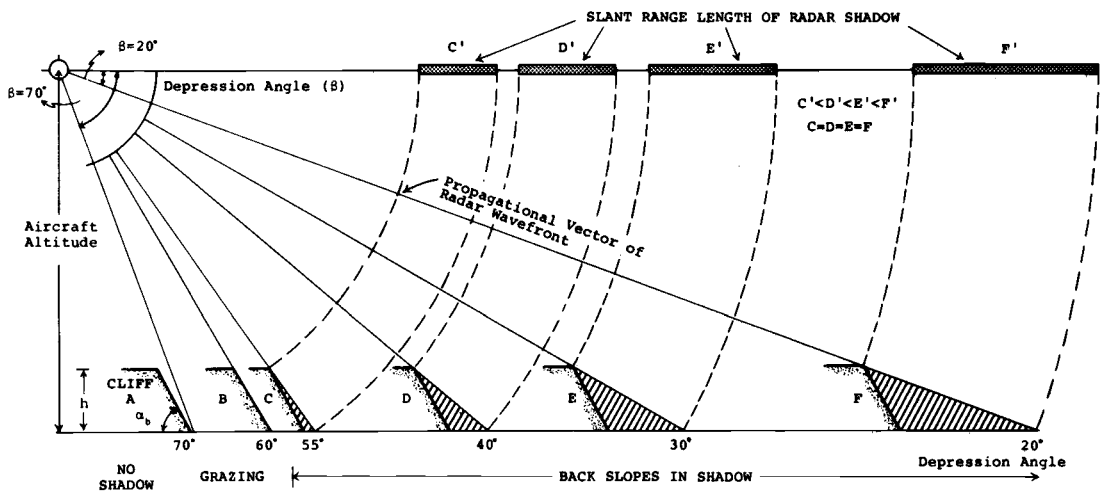

Figure 17. Radar shadowing and depression angles (from Reeves, 1975).

and the flightline form an angle (θ), the angle at which a given hillslope produces a shadow increases as θ increases. As is seen in Figure 18, with a hillslope angle of 40° and θ equalling 40°, a hillslope will not produce a shadow until the depression angle is 47.5 degrees.

The height of the hill producing the shadow (Figure 19) can be calculated according to the formula:

$$h = S_R H R^{-1}.$$

The height of the object above the datum plane is directly related to both the slant range shadow length (S_R) and the altitude of the aircraft (H). It is also inversely related to the total slant range (R) (LaPrade and Leonardo, 1969).

Foreshortening. Radar foreshortening, the apparent decrease in slope length of the slope facing the sensor, occurs in all cases except when the angle of inclination (ϕ) equals 90°. When ϕ is equal to 90° the slope on the imagery is equal to the actual hillslope length (scaled). When ϕ is zero the slope is foreshortened 100 percent. The angle of incidence and percentage of foreshortening relationship is curvilinear as ϕ decreases and foreshortening increases.

Layover. Radar layover occurs when the top of the hillslope is closer to the sensor than the bottom. This layover occurs on the foreslope. Figure 20 indicates the relationship between the hillslope angle

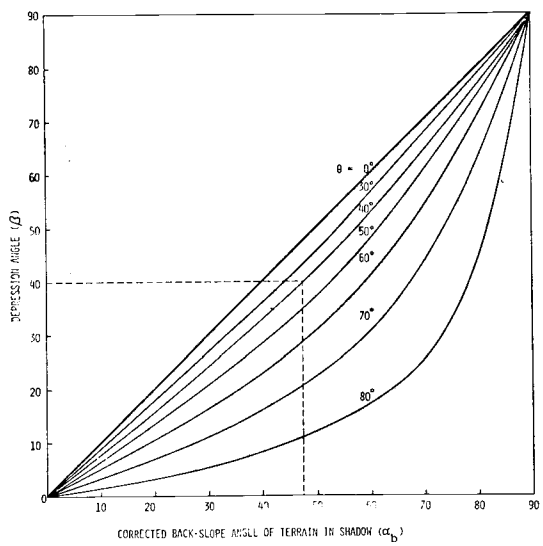

Figure 18. Depression angle relationship to angle θ, created by the intersection of the aircraft ground track and the trend of the crestline (from Reeves, 1975).

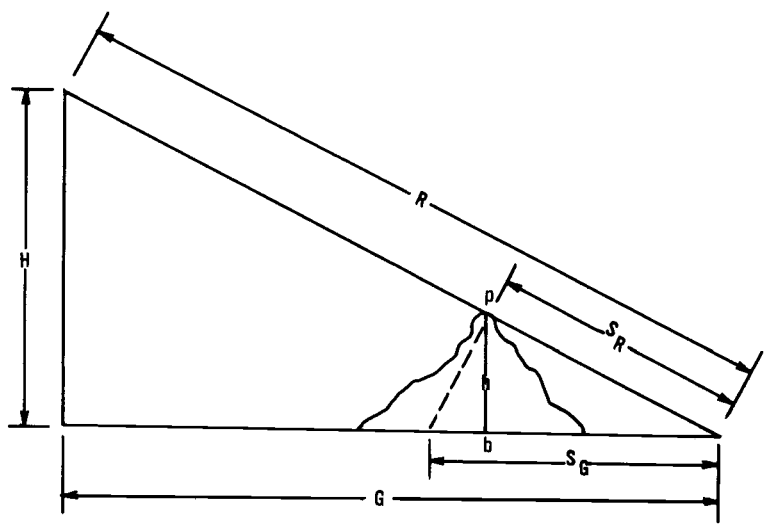

Figure 19. Hill height/shadow length geometry (from LaPrade and Leonardo, 1969).

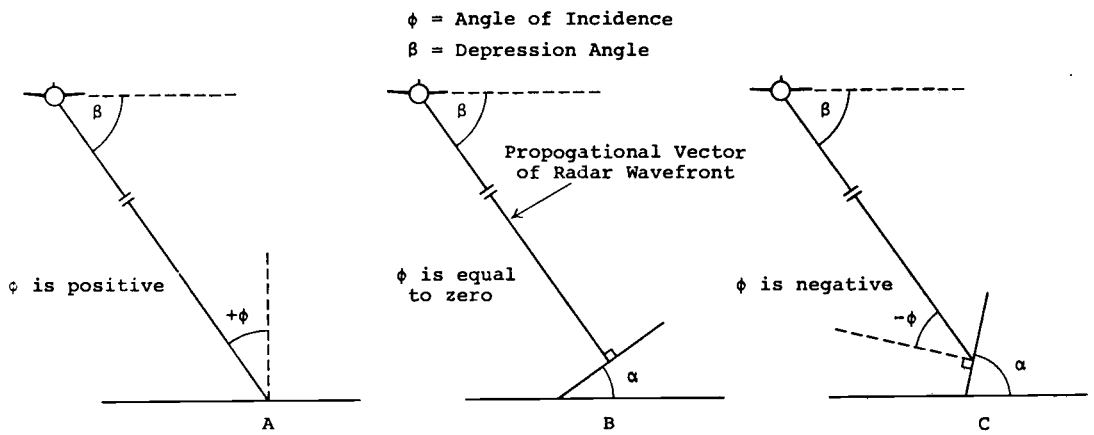

Figure 20. Depression angle and angle of incidence (from Reeves, 1975).

(α) and the angle of incidence. Radar layover occurs when the depression angle is large and the angle of incidence is negative (Figure 21). When layover is observed it produces images that are practically uninterpretable. Layover is most severe in the mountain ranges in that portion of the imagery closest to the flightline (large depression angle).

Parallax. Similar to photographic parallax, image displacement is a result of the relative position of the object and the nadir point. The relative displacement of the image is in the opposite direction of that which occurs in photographic systems (Figure 22). SLAR produces displacement toward the nadir if the object is above the datum plane, and away from the nadir if the object is below the datum plane. Parallax adjustments can be made utilizing stereopairs from overlapping flightlines or from different flight elevations.

Combined Effects. The combined effects of shadowing, foreshortening, and layover produce complex problems in interpreting SLAR imagery of mountainous terrain. Low aircraft altitude produces layover and foreshortening nearest the flightline and excessive shadowing away from the flightline. Closely spaced parallel flightlines and/or an increase in aircraft altitude reduce these effects.

Advantages and Disadvantages

The major advantage of SLAR is that it can be operated in all

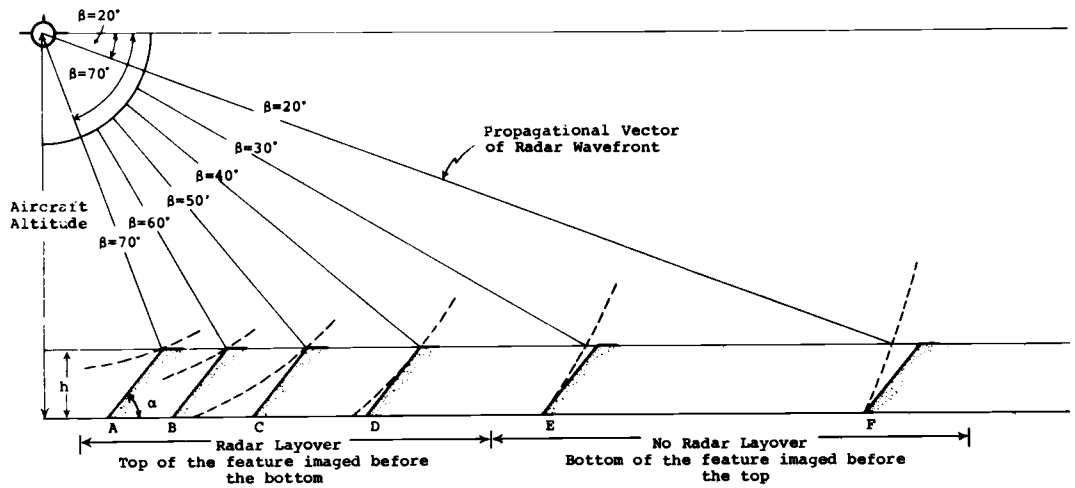

Figure 21. Radar layover and depression angle (from Reeves, 1975).

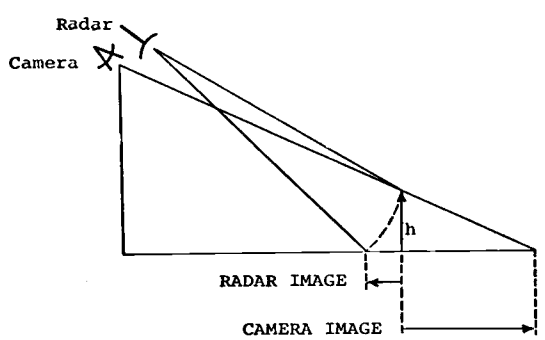

Figure 22. Relief displacement (from Reeves, 1975).

weather conditions except heavy rain, and it can produce relatively good image quality. The microwave portion of the EM spectrum is little effected by atmospheric moisture except in the most dense rain clouds.

The imagery may be acquired in either daylight or darkness. Because the non-photographic techniques do not employ the visible light or thermal emittance, the amount of insolation does not have an effect on this system.

Large scale imagery is also an advantage of SLAR. Scale is strictly a function of electronic ranging. The distance or range of scan to either side of the aircraft is determined by the operator. The choice of ranges is 25, 50, and 90 km for most SLAR systems. The shorter the range, the larger the scale. The scales produced by the 25, 50, and 90 km ranges are: 1:478,000; 1:730,000; and 1:926,000 respectively. All ranges produce imagery at a larger scale than that imagery produced by Landsat.

Therefore, because of its large scale, SLAR is more advantageous than Landsat MSS imagery for small area studies. This form of airborne radar is also useful for nighttime or poor weather data acquisition, unlike Landsat or conventional aerial photography. Basically, the advantages of SLAR result from its non-photographic microwave characteristics.

The disadvantages of SLAR result from its method of acquisition.

Aircraft motion is the catalyst in distortion problems with the imagery. The inability of the aircraft to maintain a straight linear flightline creates distortion of the imagery. This is depicted in Figure 23 and is referred to as aircraft across track deviations. Imagery distortion also results from aircraft yaw (crab).

Distortions in the form of stretch and compression of the image may result when aircraft ground speed is varied. Variable head- or tail-wind speeds may cause this distortion in the direction of aircraft flight (Figure 23). This distortion variation gives false image distance-ground distance relationships.

The second image distortion occurs at right angles to the flightline in the direction of the scan. This characteristic is inherent in the system, producing increased scale distortion outward from the flightline. Scan segments, of equal angular arc, do not cover equal horizontal ground distances as a result of increased slant range distance (Figure 24).

These image distortions must be photographically or mechanically corrected prior to their application to geologic mapping. Few SLAR systems have mechanical adjustment capabilities, i.e., where the rate of scan is established relative to the aircraft ground speed. Those systems that are not equipped with this adjustment device must have the imagery rectified (Reeves, 1975).

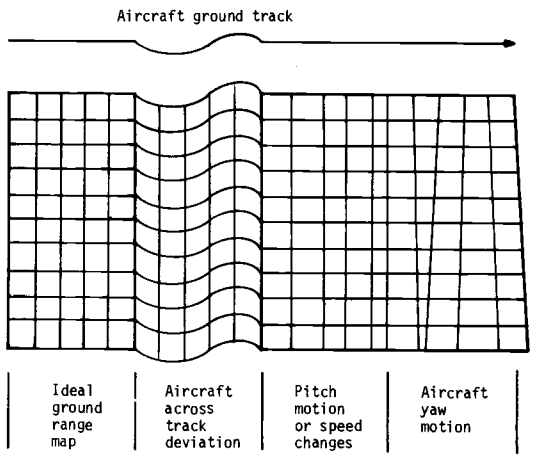

Figure 23. SLAR ground track and distortion caused by aircraft motion (from Reeves, 1975).

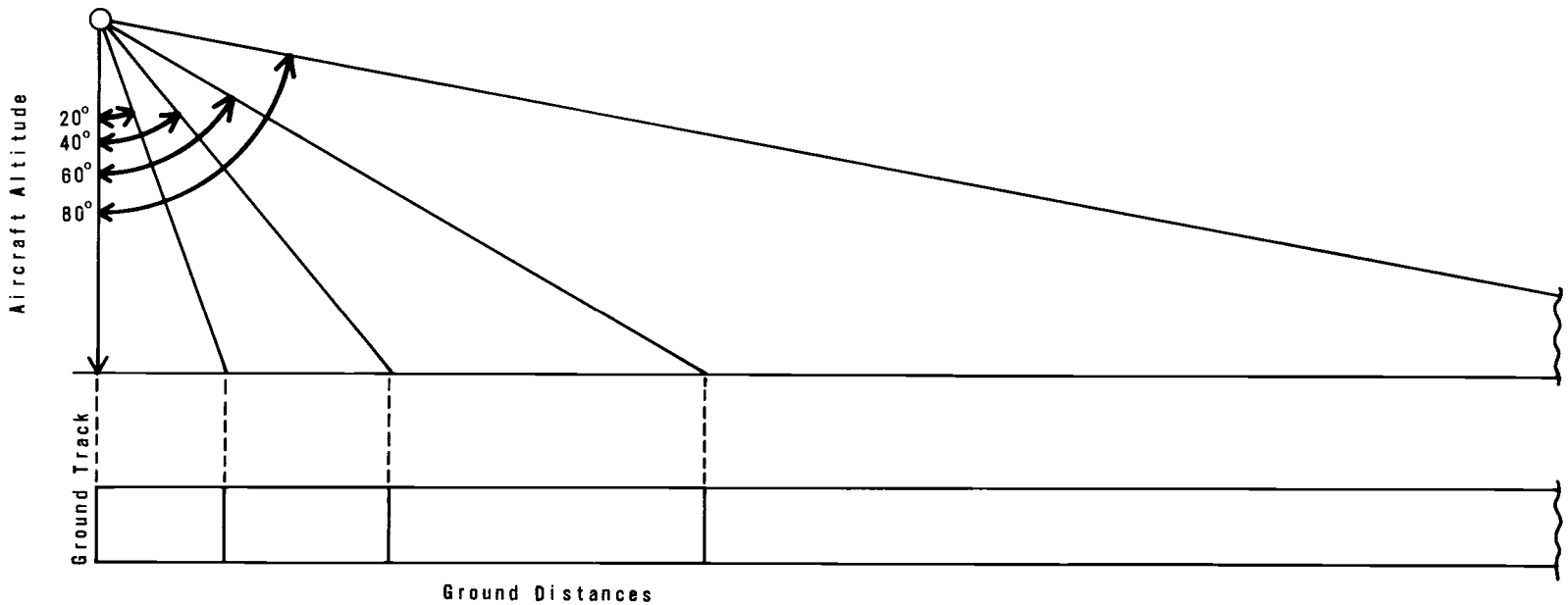

Figure 24. Variations in land distance covered by equal changes in the scan angle outward from ground track (adapted from Reeves, 1975).

Geologic Interpretation

The use of SLAR for structural analysis is well documented in the literature. According to Reeves (1975), SLAR is most useful in delineating near-surface geologic features. Various structural features are depicted on the imagery by the tonal variations of the gray scale. Surface expressions of relief, rock type, faults, and joints characteristically affect the radar return intensity.

One of the major studies producing structural analysis from SLAR was done by Wing (1971) on the eastern Panamanian Isthmus. Through the use of SLAR, he was able to determine the major strain patterns produced by crustal tectonics. Wing reiterated the discussion of MacDonald (1969), that proper interpretation of radar imagery involves consideration of the displayed tone, texture, shape, and pattern. Tone is the intensity of backscatter converted to gray scale differences. Texture is the frequency of change in the tonal arrangement. Shape relates to the telltale outlines of surface expressions. Pattern has to do with the arrangement of surface features (geologic or topographic) which allows lineaments to be observed.

Study Area SLAR Acquisition

The SLAR imagery obtained for this research was flown June 16-18, 1976 by the 1042 Military Intelligence Company (Aerial

Surveillance) of the Oregon Army National Guard (ORNG). The ground surface was scanned by an AN/APS-94C SLAR detector aboard a Model OV-1B Mohawk aircraft. The X-band real aperture system, scanning at a 0.5 microsecond pulse width, produced dual imagery (side-looking to either side of the aircraft) on a nine inch strip film.

X-band radar operates with a wavelength of 3.245 cm (9245 megacycles frequency) in the microwave radiation band. Real aperture refers to the radar systems that utilize the physical size of the antenna to determine that part of the ground that is discriminated by the beam width. Real aperture systems produce imagery that is considered to be the best source of information for geologic mapping because of its high quality resolution (Cannon, 1974). The resolution limits of the SLAR obtained for this research are 80 meters azimuthal resolution (parallel to the aircraft flightline) and an 80 meter range resolution (perpendicular to the aircraft flightline) for each 10 km range. That is, the range resolution 10 km from the flightline is 80 meters while at 20 km from the flightline the range resolution is 160 meters. The imagery acquired in this project has a range of 25 km (i.e., 25 km distance is scanned to each side of the aircraft) and yields a range resolution of 200 meters and the azimuthal resolution of 80 meters (Bunge, 1976).

ORNG flew a series of fourteen pre-selected nearly parallel flightlines in an east-west direction. This direction was selected to

take advantage of the dominant westerly air flow at the time of acquisition and thus reduce crab and cross wind effects. The flight altitude was 2,100 meters (7,000 feet) above the mean ground level (AGL). The imagery scale is approximately 1:478,000. However, the actual imagery distortion varied from flightline to flightline, a result of problems relating to aircraft motion, such as were presented earlier. The procedural steps taken to correct such problems will be presented in Chapter Five.

Thermal Infrared

The infrared portion of the EM spectrum consists of three contiguous parts: near infrared (0.7-1.5 μm) where the EMR is reflected; middle infrared (1.5-5.5 μm) where EMR is both reflected and emitted; and, far infrared (5.5-1,000 μm) where emitted EMR is dominant. According to the radiation laws presented earlier, the emitted energy of a substance is directly related to the amount of energy absorbed by that substance. Kirchhoff developed an adjustment factor (emissivity) that was a function of the radiating efficiency of the surface of that substance. In other words, only a black body emits all EMR that is absorbed, while the gray bodies (all materials of the earth) retain a portion of the EMR, therefore, decreasing the amount of EMR emitted.

Factors Influencing Interpretation

The heat energy emitted is a result of the EMR absorbed which is a function of insolation. Thus, during the diurnal cycle, the surface materials both absorb and emit EMR. However, during the nighttime when there is no incoming solar radiation, the surface materials only emit energy. Without a heat source the surface of the earth continues emitting radiation, therefore, in the diurnal cycle the smallest emitted energy levels occur prior to first light.

Atmospheric attenuation by water vapor, carbon dioxide, and ozone decreases the intensity of the thermal signal by absorbing variable amounts of emitted energy. This attenuation restricts the sensor's ability to detect thermal infrared radiation. There are two wavelength bands in the middle and far infrared portion of the EM spectrum where the atmosphere allows greater transmission of the EMR (Figure 25). These bands (atmospheric windows) have wavelength ranges of 3.4-5.5 μm and 8-14 μm. Therefore, to produce TIR imagery of high resolution and quality it is necessary to select detectors that have peak spectral response within the wavelengths of the atmospheric windows.

The windows actually fluctuate in size as a result of humidity levels (Figure 26). The humidity and mixing ratio are indicators of the amounts of water vapor actually in the air. This water vapor

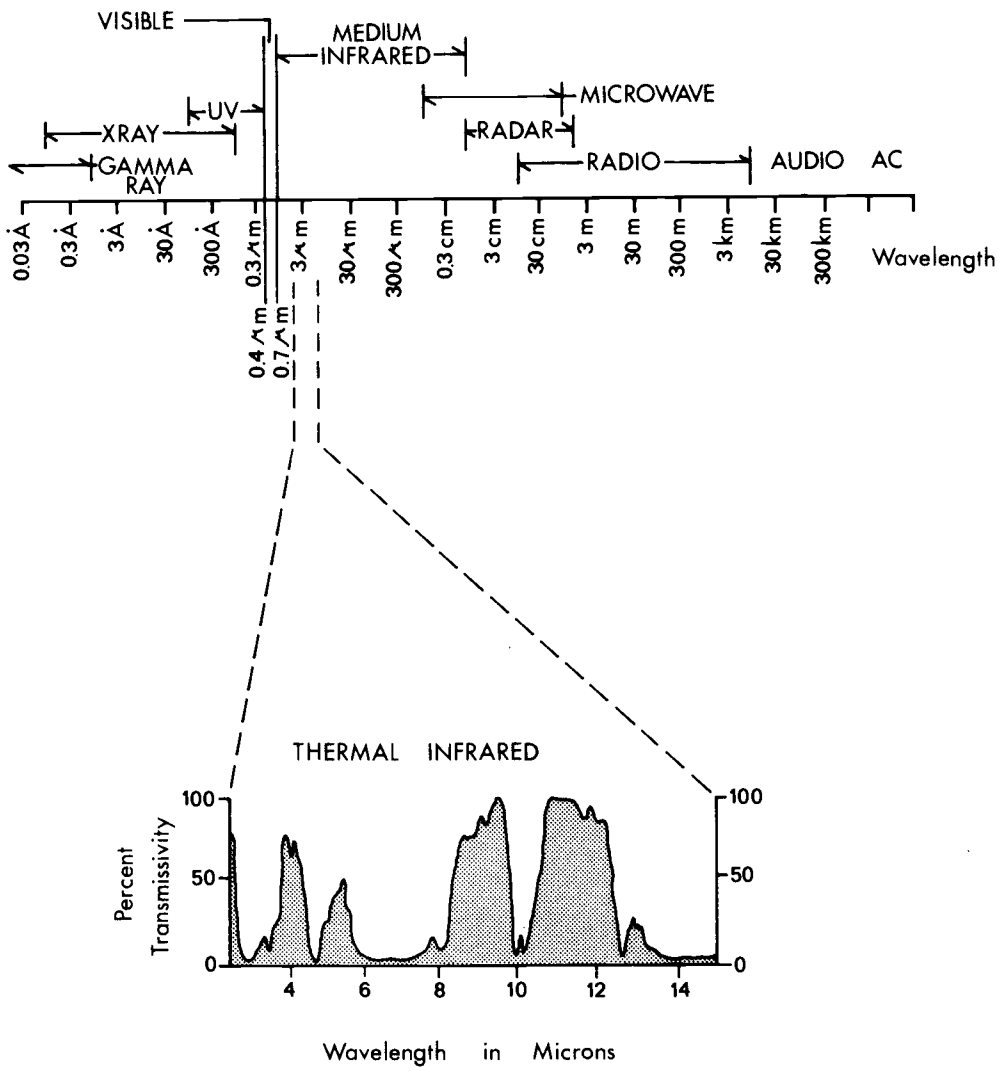

Figure 25. Electromagnetic spectrum and atmospheric transmissivity (from Estes and Senger, 1974, and Reeves, 1975).

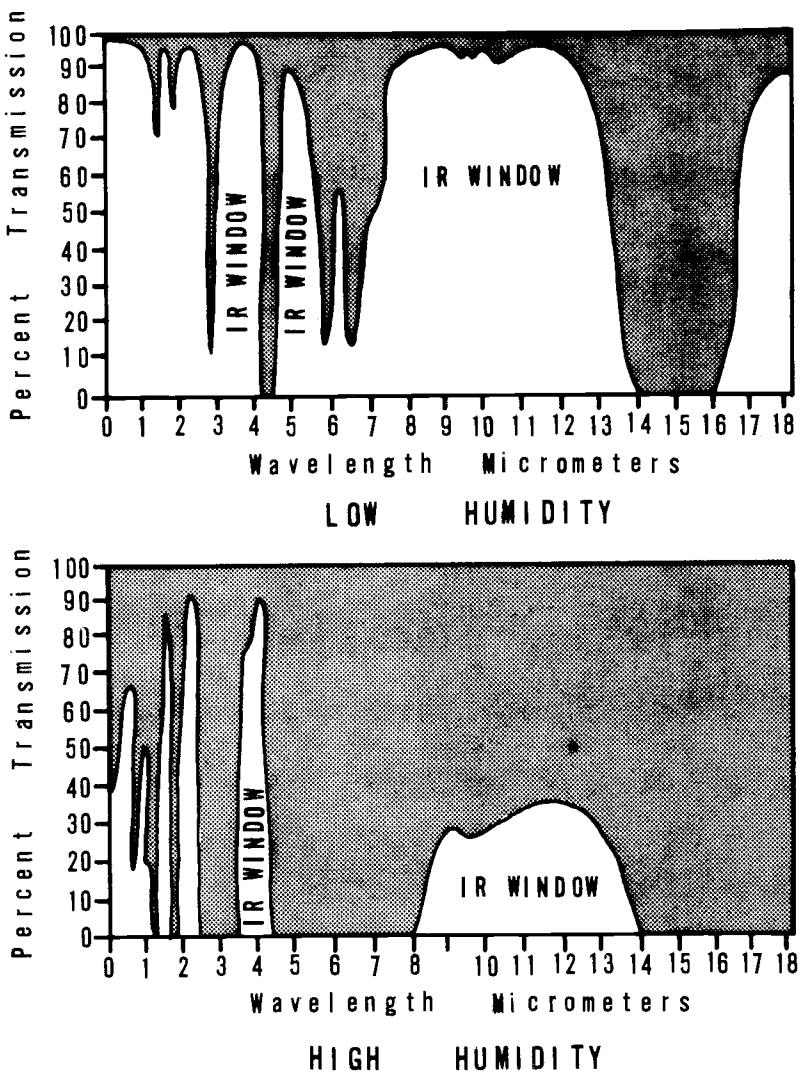

Figure 26. Humidity variations and the IR windows (from McDonnell Douglas).

absorbs greater amounts of EMR and therefore decreases the amount of transmission of emitted energy. As depicted in Figure 26, the 8-14 μm window has approximately a 95 percent transmission rate with relatively low humidity, but has only 40 percent transmission rate when the humidity is high.

There are several factors that influence the signal received by the TIR sensor and the interpretation of that imagery. These factors are: level of emitted IR radiation; textural variations in tonal quality of the imagery; atmospheric attenuation; and, detector wavelength sensitivity. In the northern hemisphere, the summer season introduces greater levels of solar radiation, providing greater heating effects. The increased surface temperatures also increase the level of heat energy emitted by that surface. Nighttime cooling creates less intense levels of emitted EMR. The winter season also produces diurnal fluctuation in the level of emitted EMR. However, the emitted energy over the entire diurnal cycle is reduced resulting from less insolation. The levels of emitted IR radiation recorded will be dependent upon both the season of the year and the time of day that the radiation is measured.

As with SLAR imagery, TIR images are composites of the gray scale produced by variations in the surface heat energy. The hotter the surface temperature the greater the emitted energy. Using Wien's Law, we are able to convert surface temperature (in ^{o}K) into

the maximum wavelength at which the surface is emitting. Variations of surface temperature (emissive power) are a function of the surface components and their characteristics. The various rock, soil, and vegetation types all exhibit different emissivities which influence the level of emissive power. For a more complete discussion of these effects, refer to Reeves, 1975.

Atmospheric attenuation is a function of the air characteristics immediately above the surface at the time of data acquisition. Temperature-moisture characteristics continually vary over time. The actual water vapor content of the air can be expressed by either the air's specific humidity[4] or its mixing ratio.[5] These measures of moisture content are altered only through the addition or extraction of water vapor (Byers, 1959). Variations in the level of specific humidity or mixing ratio will create corresponding variations in the amount of atmospheric attenuation (Figure 26). The greatest amount of attenuation will occur at or near the ground-atmosphere interface, when specific humidity, mixing ratio, and relative humidity values are high.

---

[4] Weight of water vapor contained in a unit weight of air, expressed in grams per gram or grams per kilogram.

[5] Weight of water vapor contained in a unit weight of dry air, expressed in grams per gram or grams per kilogram.

Proper detector sensitivity increases the chance of imaging surface characteristics. The detectors must have wavelength sensitivities that fall within the available atmospheric windows. Stingelin (1969), Wolfe (1965), and Reeves (1975) suggest that the indium antimonide (InSb) and the mercury-cadmium-telluride (HgCdTe) detectors are especially sensitive to the 3.5-5.5 μm and 8-14 μm windows respectively.

Thermal Infrared Characteristics

Thermal infrared scanners utilize a cylindrical revolving sensor that continually senses surface conditions (Figure 27). The geometry of the scan is quite similar to that of a SLAR system, particularly relating to the scan angles and distance are concerned. However, image distortion shows up as ground area compression at the edge of the imagery (Figure 28). The area of least distortion occurs in the center of the imagery, representing that portion of the surface directly beneath the aircraft.

Reeves (1975) discussed this and other imagery distortion which resulted from aircraft motions of roll and yaw, bank, and noise. Roll distortions result when the aircraft is unable to maintain a constant horizontal position. The resulting imagery will depict straight roads as quite sinuous and variable in width. Yaw distortions result from the aircraft varying its heading or flight path. Some systems, although

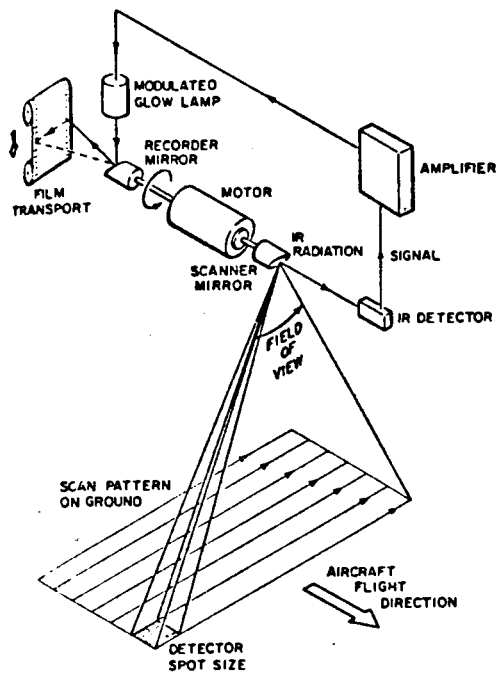

Figure 27. Thermal infrared scanner diagram (from Sabins, 1969).

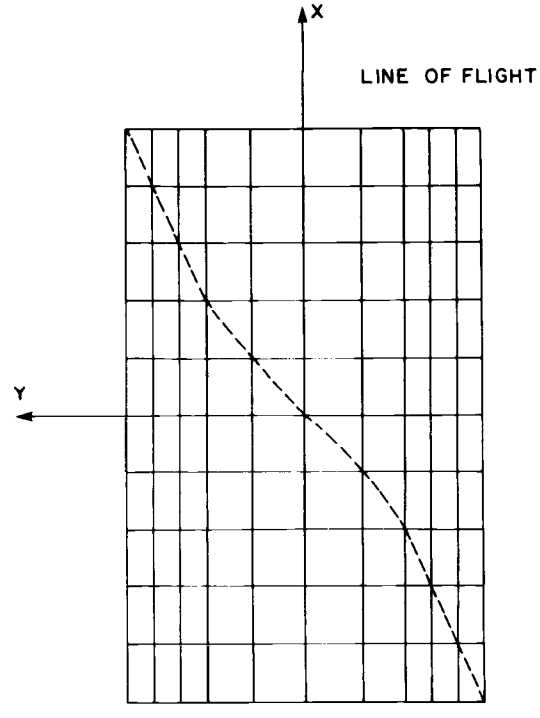

Figure 28. Potential TIR distortion (Y) perpendicular to aircraft ground track (X)(from Reeves, 1975).

not all, have compensating equipment for such distortions.

Imagery is distorted when the aircraft banks or turns. If the sensor is activated during the course change or while the aircraft is in a turn, the imagery produced has little value.

Electrical interference (noise) often results from aircraft radio transmission. Static streaks may occur on the imagery, totally obscuring the sensed image.

Variations in the scale of the imagery result when the aircraft flight speed is not constant or when aircraft altitude is not maintained. The image interpreter must utilize recognizable surface features for determining scale at any given location on the strip of imagery. Reeves (1975) said that "because these (scale) distortions reach a maximum near edges of images, an effort should be made to restrict mapping to the center two-thirds of each image."

As the sensor "drum" is activated by emitted surface energy, it heats up and thus records the energy level on the imagery. The sensor continues to scan and two image distortions may result. The first is that heat streaks or tails will be extended from the "hot-spot" across the image in the direction of scan. This is a result of amplifier saturation. These streaks obscure the images over which they are extended. Secondly, small heat sources may be amplified so that they appear larger than their true size relationship.

Thermal Infrared Investigations

Thermal infrared techniques have been used as acceptable forms of locating surface geothermal manifestations over the last twenty years (Friedman and Williams, 1968). Other studies have supported the belief the TIR scanning techniques are viable means of locating hot springs and geysers (Lattman, 1963; McLerran and Morgan, 1964; Estes, 1966; Hodder, 1970; and, Moore and Myers, 1973). One of the first TIR studies in a hydro-geothermal nature was conducted by McLerran and Morgan (1964) in the geyser and hot spring area of Yellowstone National Park. They reported that the locations of the hot-spots were easily seen. However, these locations could not be distinguished as to hydro-geothermal type.

Moxham (1969) conducted an infrared study at The Geysers steam field. He concluded that "first order manifestations of geothermal activity--hot springs and fumaroles--could be rather easily and quickly depicted by IR surveys."

The generally accepted period for conducting infrared surveys is the early pre-dawn hours. Hodder (1970) suggested that in the middle latitudes, the ideal time for imagery acquisition was two to four hours before dawn. Infrared overflights during this time occur after the soil surface had lost much of the insolation acquired during the daytime by re-radiating that energy at night. Geothermal sites should

be more easily identifiable from the surrounding terrain during this pre-dawn period. Moxham (1969) conducted geothermal overflights at The Geysers between 2:30 A.M. and 5:00 A.M. Thermal infrared images, 8-14 μm, were of better quality when the overflights were conducted in the pre-dawn hours (Valle, Friedman, Gawarecki, and Banwell, 1970).

Contrary to the generally accepted data acquisition time (above), Watson (1974) suggested that the interpretation of geothermal surface anomalies was most easily conducted at a time which most closely approximates the mean surface diurnal temperatures. His time lag analysis suggests that if the data is acquired only once during the diurnal cycle, the ideal time is either sunset or shortly after sunrise. Overflights of the Raft River in Idaho were used to conclude that 9:48 A.M. (MST) most closely approximated the mean diurnal temperature. Therefore, Watson suggests this time as the ideal period for IR data acquisition.

Thermal infrared surveys have also been utilized in structural mapping. Sabins (1969) found TIR imagery to have "greater contrast and resolution than aerial photography." He found the use of the imagery valuable in examining the surface moisture characteristics. Friedman et al. (1973) found that several of the thermal anomalies in the Warner Valley were aligned with the previously unmapped curvilinear structures of Mt. Lassen. Walker (1967) reported, however,

that infrared surveys in southeast Oregon did not yield the image sharpness or clarity that could be produced by SLAR. Relief displacement was almost lost on the TIR imagery as compared to the SLAR imagery.

Brennan, Chapman, and Chipp (1971) conducted a remote sensing evaluation of the Klondike Mining District in Nevada. To aid in the geologic evaluation of the area, they created a set of rules that applied to the acquisition of TIR imagery. The following three rules are a part of that set:

1. "No IR imagery should be obtained except under clear weather conditions;
2. At least minimal 'ground truthing' information should be collected. It should include soil and surface moisture, radiometer temperatures, and samples of sufficient size to conduct later albedo, thermal diffusivity, and IR emissivity measurements if deemed necessary;
3. (All remote sensing imagery) should be reduced to a common scale before evaluation is attempted."

These rules were applied to the acquisition of the TIR imagery for this research project.

Study Area TIR Acquisition

TIR imagery was obtained for selected flightlines within the

study area. This imagery was flown on June 21-22, 1976 and October 16, 1976 by ORNG. Grumman OV-1 (Mohawk) aircraft were equipped with AN/AAS-14A thermal infrared scanners. These TIR flights were programmed at various times throughout the evening and night.

Flight altitude was adjusted to reduce signal attenuation and to increase image resolution. The flight altitudes ranged between 600 and 900 meters above the ground level. TIR flightlines are depicted on Figure 29 along with the SLAR flightlines. The curves in the TIR flightlines represent cartographic generalizations. The flightlines were comprised of a series of linear segments connected by abrupt aircraft course corrections in order to reduce imagery distortions resulting from aircraft motion. The sensor had an instantaneous field of view of four milliradians producing a ground resolution of approximately one meter for every 300 meters of altitude above the terrain. The scan angle was 80 degrees, 40 degrees to either side of the aircraft. The scanning speed was 5,250 rpm with the film speed adjusted according to the aircraft ground speed and altitude.

The aircraft are capable of being equipped with a combination of any two of the three sensors listed in Table 12. The imagery may be obtained by simultaneous dual channel acquisition at a scale proportional to altitude or by a one channel expanded format, selected at twice the scale. The advantages and/or disadvantages of such a selection will be discussed under data analysis.

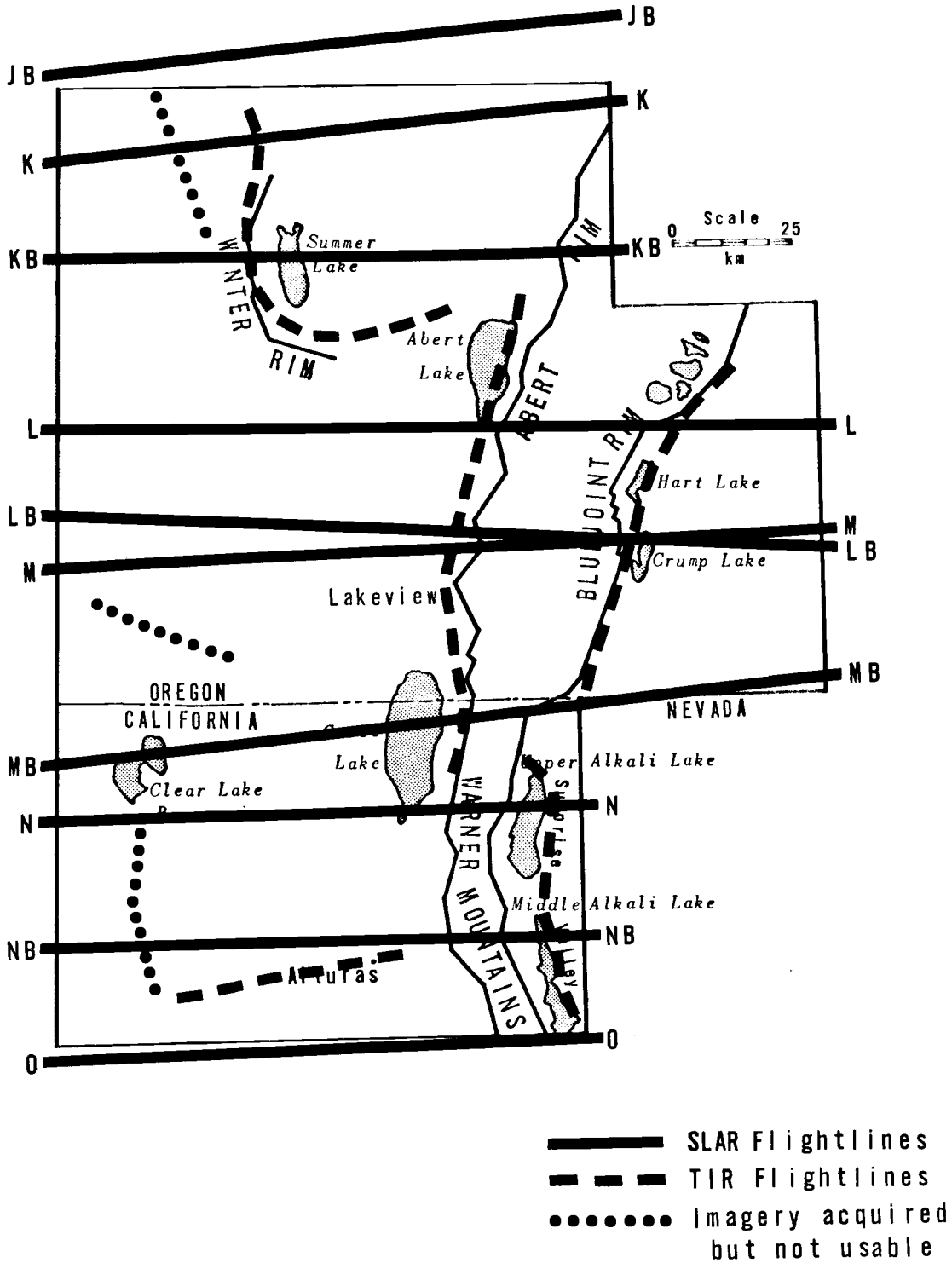

Figure 29. SLAR and TIR flightline flown in study area, 1976.

Table 12. Thermal Infrared Sensors.

Sensor	Range (μm)	Peak Response (μm)
Indium Arsenide (InAs)	1-3.4	3.0-3.2
Indium Antimonide (InSb)	1-6	4.5-5.5
Mercury-Cadmium-Telluride (HgCdTe)	8-14	10.0-13.0

Source: ORNG, 1976

The average temperature of the earth's surface materials is 285° K (Sellers, 1965), which means that the peak spectral response for the earth is approximately ten micrometers (Wien's Law). This falls within the second atmospheric window (8-14 μm). Thus, of the three detectors listed in Table 12, the HgCdTe detector senses in that peak response wavelength. This detector is capable of depicting selected surface terrain features as well as all water bodies. Valle et al. (1970) found that geothermal expressions are visible using a sensor in this wavelength. However, other water surfaces known to be at cooler temperatures appeared as bright as the hot springs.

The InSb detector has been found to provide good imagery for detecting warm spots in an ambient background (Bastuscheck, 1970). This sensor's peak response falls within the first atmospheric window (3.5-5.5 μm). As Wien's Law suggests, the maximum wavelength at which a surface will emit energy decreases in length as the

temperature of that surface increases. Therefore, for hotter targets, the detector which has a peak response in the shorter wavelengths should be utilized. The InAs detector peaks just below the atmospheric window and is subject to greater atmospheric attenuation than the other two sensors. However, because of its shorter wavelength peak response, it is capable of detecting much hotter surface targets.

The imagery acquired from these sensors should give relative temperature differences depicted by their tonal and textural variations. The level of atmospheric attenuation that occurs between the surface and the sensor can not be evaluated from the imagery. Therefore as Brennan, Chapman, and Chipp (1971) suggested, some ground truth data will be required. The information acquired through ground truthing can be utilized in evaluating the resultant TIR imagery.

IV. DATA COLLECTION

As mentioned previously, both SLAR and TIR imagery were acquired by the Oregon Army National Guard. This imagery was flown while ORNG was at summer training camp. Their operation base camp was established at Kingsley Field just outside of Klamath Falls, Oregon. The proximity of the base camp to the study area allowed for flights of relatively short duration (approximately two hours).

The field data deemed necessary for proper ground truthing of the imagery was collected by three two-man teams. Funding for the field work, equipment, and instrumentation was provided by the Fremont National Forest and the Oregon Department of Energy. The field teams were composed of members of the above agencies and graduate students[6] at Oregon State University. Each team was given specific instructions on what data was to be acquired and on the proper procedure for collecting that data. Prior to actual data collection, a series of dry runs were taken to insure uniformity in collecting procedures.

---

[6]Hugh Bunton, Marvin Crocker, Jack Hruska, Scott Kolar, S. Reid Schuller, Rick Starr, Larry Warnick, and Leonard Wilkinson.

Selection of SLAR Flightlines

Two sets of flightlines were pre-selected by the author; one set had a north-south trend and the second ran east-west. The purpose for laying out two separate flightline designs was to allow ORNG to select that set which corresponded to the dominant wind direction at the time of flight. The winds on June 16-18, 1976 were predominately from the west. Therefore, to reduce the problem of imagery distortion created by cross wind effects, the east-west flightlines were utilized.

The flightlines were designed to be nearly parallel and to be 25 km apart. The range distance on either side of the aircraft was also 25 kilometers. This arrangement was designed to create a series of flightlines where the south-facing scan of one flightline overlapped completely with the north-facing scan of the adjacent flightline. From these overlapping images, a north-facing and south-facing mosaic was to be created. This mosaic would facilitate use by having only one direction shadow displacement.

The flightline design proved to be a problem for the pilots and on-board equipment. Because the field camp was for educational training missions, the spacing of the flightlines required greater precision in flying than the pilot-aircraft were capable of performing. The subsequent flightlines varied as much as 20 km off the designated

course, providing imagery without the desired overlap.

The lack of proper overlap made the creation of the intended mosaic useless. A mosaic, created by such imagery, would have had void areas not covered by that particular north- or south-facing shadow displacement. Therefore, no mosaic was created. The analysis of the surface lineaments had to be made on each flightline utilizing both scan directions. Procedural steps and results are discussed in the next chapter.

Selection of TIR Flightlines

From the SLAR imagery and topographic maps, TIR flightlines were selected, with the approval of Fremont National Forest personnel, to coincide with both the existing major linear structures and with existing hydro-geothermal locations. The selection of these flightlines should allow for the evaluation of the hydro-geothermal manifestations along the linear fault structures in this part of the Great Basin.

Four separate flightlines were flown at various times during the evening and night.[7] The imagery was acquired using the different

[7]Three other flightlines were also flown in order to explore the Fremont National Forest for additional hydro-geothermal expressions. However, these flightlines produced uninterpretable imagery due to sensor malfunction. Areas of the Fremont National Forest not covered by useable imagery were extensively ground truthed in order to verify the lack of hot spring occurrence.

combinations of sensors previously discussed. The four flightlines for the acquisition of TIR imagery were: Canby-Alturas; Surprise Valley; Goose-Abert-Summer-Silver Lakes; and, Warner Valley (Figure 29). All four flightlines were flown on June 21-22, 1976 and the latter two flightlines were flown again on October 16, 1976. The imagery produced from the various June flights ranged from excellent to very poor. Equipment malfunction, pilot inexperience, and poor flying conditions caused various problems in acquiring useable imagery. Equipment problems occurred while imaging the Goose-Abert-Summer-Silver Lakes and the Warner Valley flightlines. These problems necessitated the rescheduling of flight dates for these two areas.

The Canby-Alturas flightline trends east-west along the Pit River and roughly corresponds to the path of Highway 299. This flightline exists in an area of known fault structures which exhibit little surface expression. The flightline was selected because of the existence of the Kelley Hot Springs east of Canby. This spring was a site for ground truthing and instrumentation. Three separate flights were made along this flightline. These flights were made at approximately 2100 hours (PDT) on June 21st and 0001 and 0400 hours (PDT) on June 22, 1976. The variations observed in the imagery will be presented in a later chapter.

The Surprise Valley flightline had two hot spring locations that served as ground truthing sites. The first location was at the hot

spring and pool near the airport 13 km east of Cedarville. This hot spring, on the east side of the Middle Alkali Lake, is a kilometer away from the motel and swimming pool that recorded high arsenic content in their geothermal water. The second ground truthing site for this flightline was at a spring four kilometers northeast of the northern tip of the Middle Alkali Lake near the old Leonard homestead. This hot spring is the source of a small warm creek that flows into the Middle Alkali Lake. Three flights were made along this flightline as well: at 2200 hours (PDT) on the 21st and at 0100 and 0300 hours (PDT) on the 22nd of June.

The imagery flown the evening of October 16th was originally designed to be collected by six different overflights. However, the need to refly the imagery necessitated combining the original six into two longer flightlines. One ground truthing site was located along each flightline. Hunter's Hot Spring, just north of Lakeview, Oregon and Crump Geyser at the edge of Crump Lake were the sites for the Goose-Abert-Summer-Silver Lakes and Warner Valley flightlines respectively.

Ground Truthing Teams

Ground teams were situated at previously known hydrogeothermal sites. Each team consisted of two members whose responsibilities were to collect selected field data at half hour intervals.

These data were used for the better understanding of the surface radiation response over time. More elaborate sets of data at the moment of aircraft overflight were also collected.

Ground Truth Parameters and Instruments

Half Hour Data

Following the suggestions by Brennan, Chapman, and Chipp (1971), soil (1 cm depth) and radiometer temperatures ($1/2^{o}$ C accuracy) were acquired at half hour intervals. These temperatures indicate the general soil response and emitted energy response with time. A recording ambient air and soil thermograph was installed at Hunter's Hot Spring from May 4, 1976 through June 24, 1976. From the temperature graphs, a lag time of approximately two hours was recorded between change in air temperature, an indicator of incoming radiation, and soil temperature response. The minor air temperature fluctuations (generally recorded in the early afternoon) caused little to no change in the soil temperature. As is expected, therefore, the soil temperature reacts slowly to changes in incoming radiation. The soil temperature record indicates that the minimum diurnal soil temperature occurs just after dawn.

The radiometer temperatures were measured utilizing two economical radiometers mounted on a stand one meter above the

ground surface. Each radiometer was constructed[8] according to Suomi and Kuhn (1958) and consisted of either two black- or two white-surfaces. Therefore, on a half hour basis two black-surface temperatures (one side facing up and one down) and similarly two white-surface temperatures were recorded. This equipment design is useful in calculating surface albedo and net radiation inputs if daytime flights are made. However, since all data for this research was collected at night, no significant insolation is assumed to have occurred. Therefore, the down facing black-surface radiometer reading is most useful as an indicator of the emitted energy received one meter above the ground surface. The difference in ground surface temperature and the down facing black-surface temperature is an indicator of the level of atmospheric attenuation in the air-ground interface and/or errors in instrumentation, most probably the latter.

The readings recorded at various times throughout the night reflect an integrated signal from the entire hemisphere below the radiometer. The area, approximately three meters in diameter, produces radiation emitted from the grass, rock, and bare soil. The soil temperature recorded represents the ground temperature of the bare soil (1 cm depth) at a point within the area measured by the radiometer.

---

[8] The economical net radiometers were constructed by members of the course G-531 (Climatology), Department of Geography, Oregon State University, Spring, 1976.

Thus, the soil-radiometer relationship is biased by the point soil temperature source at the recording depth possibly indicating higher surface radiation than that which actually occurs.

The economical net radiometers were calibrated[9] against the more sophisticated Swisstico hemispherical net pyrradiometer (Funk type) which works on basically the same principle. The three sets of economical net radiometers proved to have plus four, minus one, and minus eighteen percent accuracy levels. The eighteen percent variation possibly resulted from poor thermometer contact with the surface material (sensor).

Soil temperature was acquired at each site. A shallow hole was dug and the thermometer was inserted horizontally into the soil in the top centimeter. Care was taken not to disturb the soil cohesiveness. This temperature measurement is an indicator of the heat flux just beneath the surface.

The heat flow from near the surface at each ground truthing site is indicated in Figure 30. The value of emitted energy is listed as watts per meter squared (Wm^{-2}) which is an accepted meteorological standard for the expression of radiant energy. To convert the soil temperature in ^{o}C to Wm^{-2} the following formula was employed:

$$\text{heat flow } (Wm^{-2}) = \sigma T^{4} \times 698$$

---

[9] Conducted with the aid of Dr. H. Richard Holbe (Oregon State University, Forest Research Laboratory) and Mr. Ted McDowell.

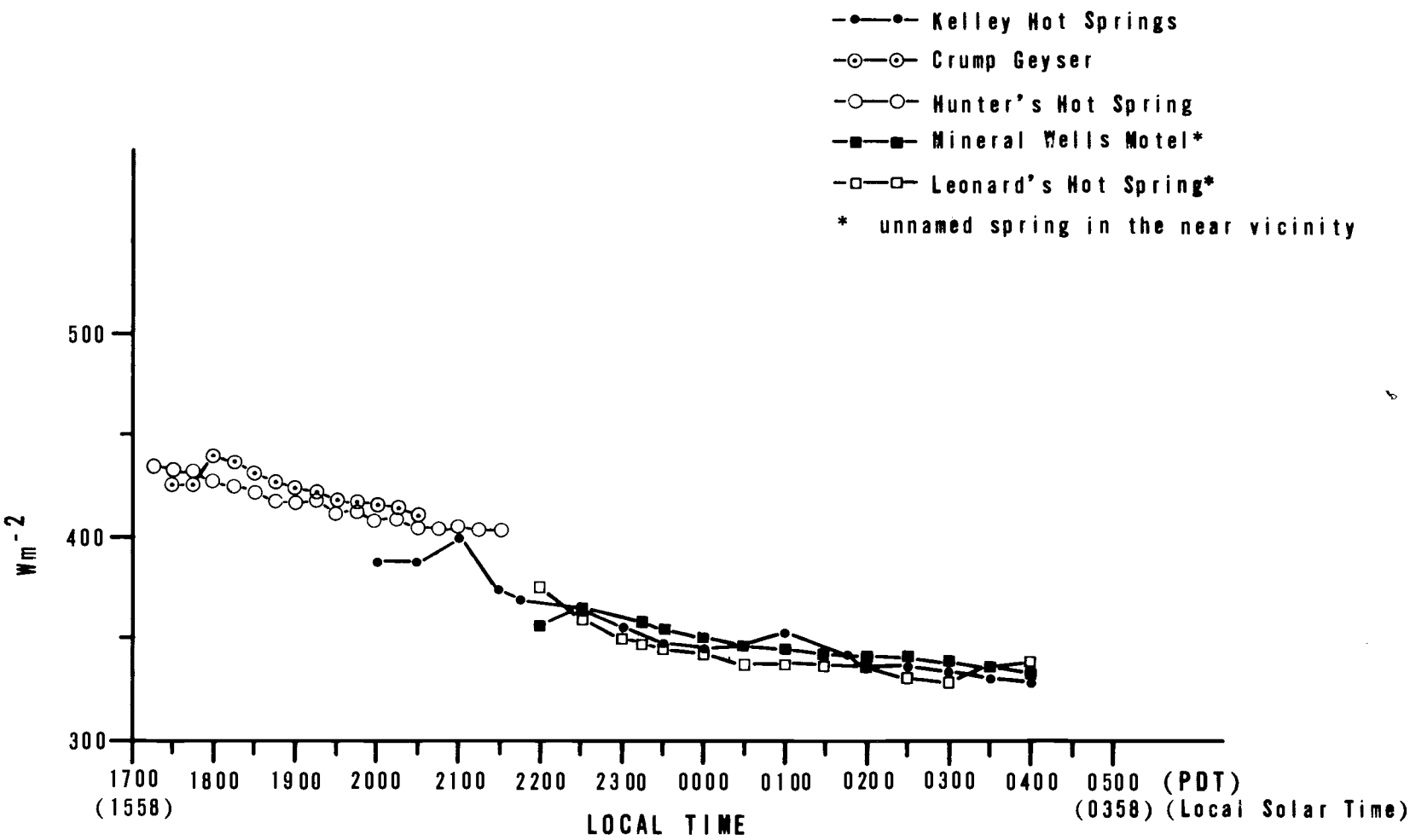

Figure 30. Heat flow from soil surface.

where:

σ = Stefan-Boltzmann constant

T = ^{o}K

698 = conversion factor from langleys to Wm^{-2}.

As indicated by the figure (30), the soil heat flux in the early evening hours is greater and tends to decrease with time. As would be expected, the least heat flux occurs just before dawn.

The percentage decrease in measured heat flow between the surface and the one meter level is plotted in Figure 31. The curves represent the percentage decrease of the soil heat flux as measured by the radiometer. The decrease rapidly becomes larger shortly after dusk and then begins to stabilize. It was anticipated that these measurements would produce an estimate of the degree of atmospheric attenuation occurring within the one meter layer. However, the resulting curves suggest instrumentation positioning errors.

The radiometer reacts to the changes in energy being emitted from the surface (top 20 micrometers) of the soil. The measured readings of the radiometer was compared to the soil temperature at depth (one centimeter). The heat flow occurring within the top centimeter of the soil is not representative of the energy being emitted by the soil at the surface. Therefore, the positioning of the thermometer measuring soil temperature introduces the instrumentation bias suggested previously. The steep rise of the percentage decrease curve

between 1700 and 1900 hours represents the rapid radiation loss from the surface (measured by the soil) as the incoming solar radiation decreases at dusk. Once the adjustment has been made (i.e., radiation loss at dusk) the curve stabilizes over the rest of the nighttime hours. Contrary to what had been anticipated, this curve (Figure 31) does not represent atmospheric attenuation, rather the incompatibility of the instrumentation selected.

The affect of wind movement on the Crump Geyser heat flow curve is seen in Figure 31. The rising heat flow curve made a sharp drop starting at 1900 hours. At that reading a five knot wind, gusting to 8-10 knots, was blowing. This wind was not present at the time of any prior readings. The turbulent heat exchange and convection of the wind altered the atmospheric heat and/or moisture conditions, and is depicted by the drop in the curve. At 2015 hours the wind subsided and the curve began to rise again.

The heat emitted from the hot spring surface at the time of overflights is depicted in Figure 32. The differences between the heat emitted by the soil and by the hot springs are greatest during the early morning hours. This is the result of the decreasing soil temperature and the relatively constant hot spring surface temperature. However, the order of magnitude is relatively small (Table 13). For example, utilizing the Stefan-Boltzmann Law, the fourth power of the absolute soil and water temperatures for the hot spring near the motel site was

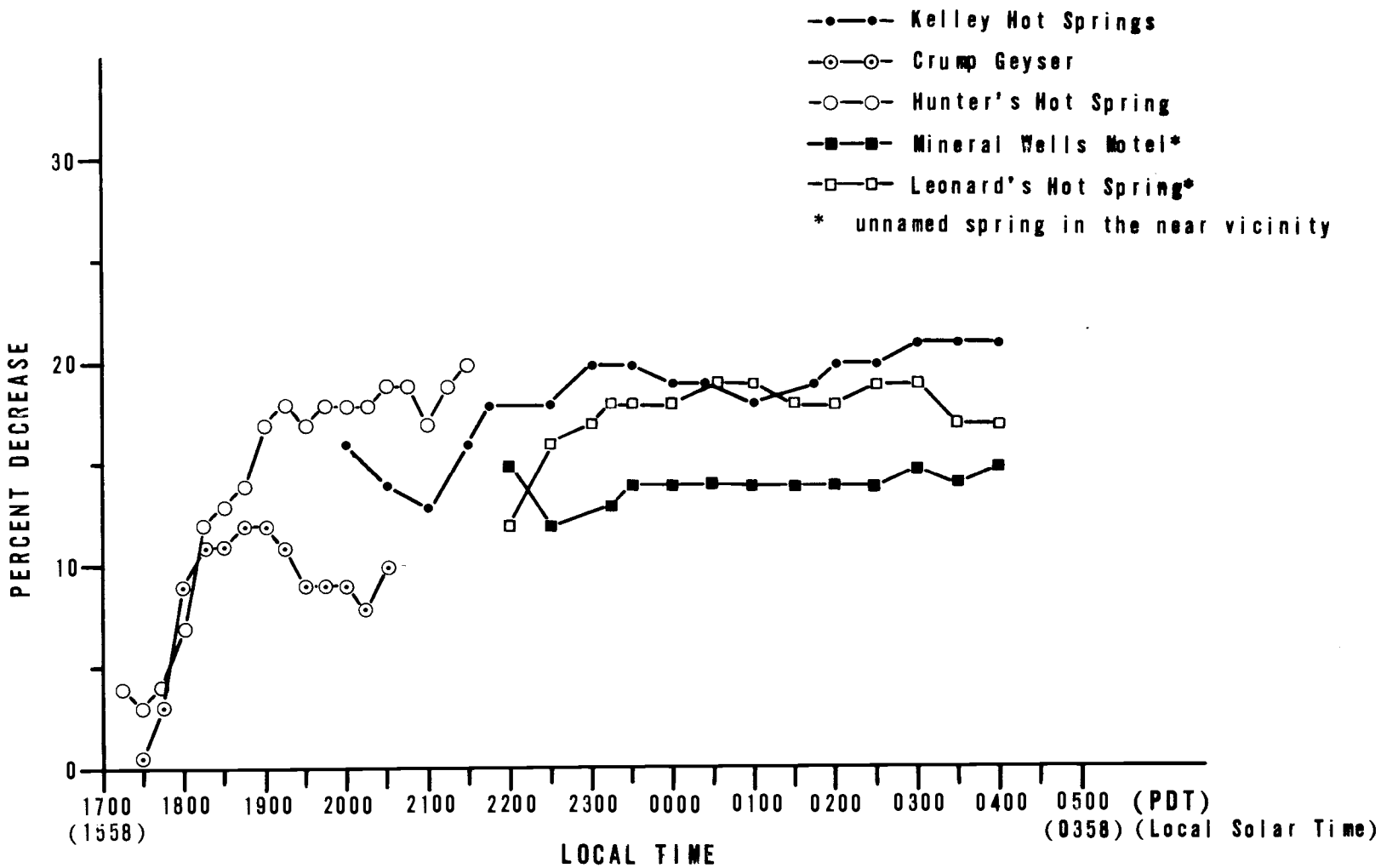

Figure 31. Percentage decrease in measured heat flow between ground surface and the one meter level.

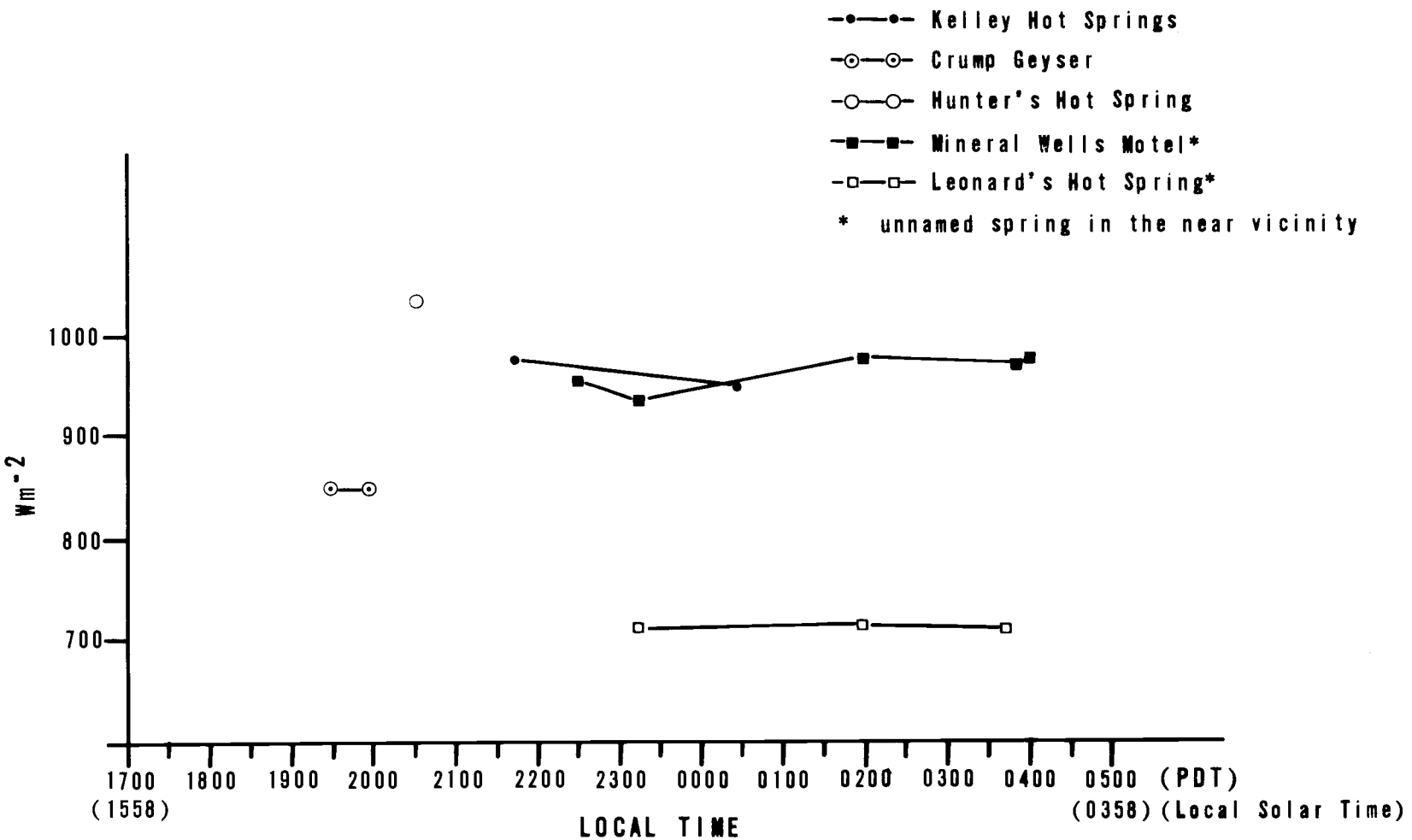

Figure 32. Heat flow from hydro-geothermal sources at time of TIR overflights.

Table 13. Absolute water surface temperature as a function of the surrounding absolute soil temperature.

Site	Order of Magnitude	Flight Time (hours)
Spring near Leonard Hot Spring	1.77	2317
	1.82	0159
	1.85	0345
Kelley Hot Springs	2.18	2144
	2.19	0035
Motel near Cedarville	2.30	2230
	2.26	2328
	2.45	0159
	2.50	0352
Hunter's Hot Springs	2.52	2034
Crump Geyser	2.02	1930
	2.03	1957

2.30 times hotter than the surrounding surface at 2230 hours. However, it was only 2.50 times greater at 0352 hours when the soil temperature was at its recorded minimum. Flights in the pre-dawn hours acquired surface temperature-hot spring temperature variations of only 0.24 magnitude increase.

Overflight Data

Just prior to the aircraft beginning its pass along a given flightline, air-to-ground communication was established. Ground teams

were notified, and readied themselves for the aircraft overflight. All ground truthing data had to be measured at the moment of aircraft passage. This method was utilized in order to evaluate the atmospheric-ground characteristics as they applied to the imagery. Therefore, data collection and TIR sensor passage occurred simultaneously.

At the time of the June flights, two fusee type phosphorous road flares were placed sixty meters apart parallel to the flight path. The flares were placed a minimum of two kilometers from the nearest known geothermal expression, so that the sensed images would not interfere with one another. Sixty meters from the flares, a foot square, one-inch thick piece of dry ice was positioned in a linear fashion with the flares. These flares and dry ice were to be used to establish maximum and minimum recording gray-scale levels in the imagery. This procedure was abandoned for the October flights as a result of June imagery evaluation and an additional literature search. The June overflights yielded only one flightline on which the flares and/or dry ice were visible. Such a variability in recording can be accounted for in one of two ways. First, the phosphorous flares are noted for producing variable amounts of IR radiation even though they possess high-temperature flames. The gaseous reactions have been proven to be poor radiators (Engineering Design Handbook, 1971). Second, the occasional recording of the flares on the imagery suggests that a sensor configuration may be the cause. The ground

distance spacing of the raster lines may frequently create a situation where the relatively small flares are not recorded. Most probably the flares were not shown on the imagery as a result of both possibilities.

The field data that were collected at the time of aircraft overflight for each sampling site are listed in Table 14. Radiometer readings, soil temperatures, and water surface temperatures were collected according to the same procedures followed in collecting similar data on the half hour. The following information was collected to gain a better understanding of the air and soil moisture characteristics.

Air Characteristics. The local barometric pressure was obtained at the time of overflight from a recording microbarograph, housed in a weather shelter at Hunter's Hot Springs and calibrated from the readings supplied by the Lakeview Airport. These readings were used in conjunction with the wet and dry bulb air temperatures to determine the specific humidity, relative humidity, and mixing ratio of the air.

The wet bulb and dry bulb air temperature were acquired using a sling psychrometer. Care was taken in installing new dry wicks on each psychrometer. Distilled water was applied to the wicks without physically touching the wicks. The psychrometer was operated in its accepted manner at the one meter height. Successive readings were

Table 14. Site data.

Time	Date	R	Wb	Wd	Wv	Wd	Ts	Tw	N	E	S	W
Kelley Hot Springs:												
2144	6/21	10	8.3	8.9	-	-	24	88	11	10	14	7
0035	6/22	6	5.6	6.7	-	-	22	85	11	9	12	8
Motel near Cedarville:												
2230	6/21	9	7.2	9.2	-	-	18.5	86	5	10	7	4
2328	6/21	7	5.8	7.2	-	-	18	84	*	*	*	*
0159	6/22	4.5	3.9	4.4	2.2	N	15.5	88	11	8	3	4
0352	6/22	3	1.9	2.8	-	-	14	88	*	*	*	*
Spring near Leonard Hot Spring:												
2317	6/21	6	5.0	6.7	2.6	NNW	20	65	7	*	14	5
0159	6/22	3	3.3	4.4	-	-	18	65	5	14	*	14
0345	6/22	4	3.9	5.0	3.5	NNW	17	65	7	5	*	13
Crump Geyser:												
1930	10/16	12	6.7	13.3	4.8	NW	19	75	3	2	2	4
1957	10/16	12	8.9	14.4	8.7	NW	18.5	75	*	*	*	*
Hunter's Hot Springs:												
2034	10/16	2.5	1.7	3.9	-	-	17.5	93	29	25	9	27

Time = Pacific Daylight Time
R = Radiometer Black-Bottom Surface Temperature (^{o}C)
Wb = Wet Bulb Temperature (^{o}C)
Wd = Dry Bulb Temperature (^{o}C)
Wv = Wind Velocity (Knots)
Wd = Wind Direction
Ts = Soil Temperature (^{o}C)
Tw = Water Surface Temperature (^{o}C)
N = Percent Soil Moisture North of Site
E = Percent Soil Moisture East of Site
S = Percent Soil Moisture South of Site
W = Percent Soil Moisture West of Site
* = No values obtained

taken until the temperature readings stabilized. They were then recorded on the field forms provided. The psychrometer readings were taken in degrees Fahrenheit and later converted to degrees Celsius. This later conversion accounts for the level of accuracy exhibited in the readings cited in Table 14.

The psychrometer temperatures and local barometric pressure were plotted on a Skew T, log p Diagram. From the diagram the mixing ratio (w) and saturation mixing ratio (w_s) were determined. Applying these ratios to the formula for determining the relative humidity, the results obtained are cited in Table 15.

The relative humidity at the time of each overflight is plotted in Figure 33. The curves suggest the increase of relative humidity as nighttime temperatures decrease. The curves of the Kelley Hot Springs, Leonard Hot Springs, and motel sites are slightly higher than expected, however, as it had been raining sporadically during the six hour period prior to the first flight.

The mixing ratio at the time of each overflight is plotted in Figure 34. Except for the Crump Lake location, the general trend is that mixing ratio decreases as the night progresses. This indicates that the mass of water in the air is greater after sunset when the air is warmer than just prior to dawn when the air temperature is lower. The increase in mixing ratio at the Crump Lake site can be attributed

Table 15. Site humidity and mixing ratios.

Time	Date	Relative Humidity (percent)	Mixing Ratio (gm/kgm)
Kelley Hot Springs:			
2144	6/21	96	7.0
0035	6/22	94	5.6
Motel near Cedarville:			
2230	6/21	87	7.2
2328	6/21	91	6.3
0159	6/22	97	5.1
0352	6/22	93	4.6
Spring near Leonard Hot Springs:			
2317	6/21	88	5.6
0159	6/22	93	5.1
0345	6/22	94	5.3
Crump Geyser:			
1930	10/16	63	9.6
1957	10/16	69	10.2
Hunter's Hot Springs:			
2034	10/16	85	4.9

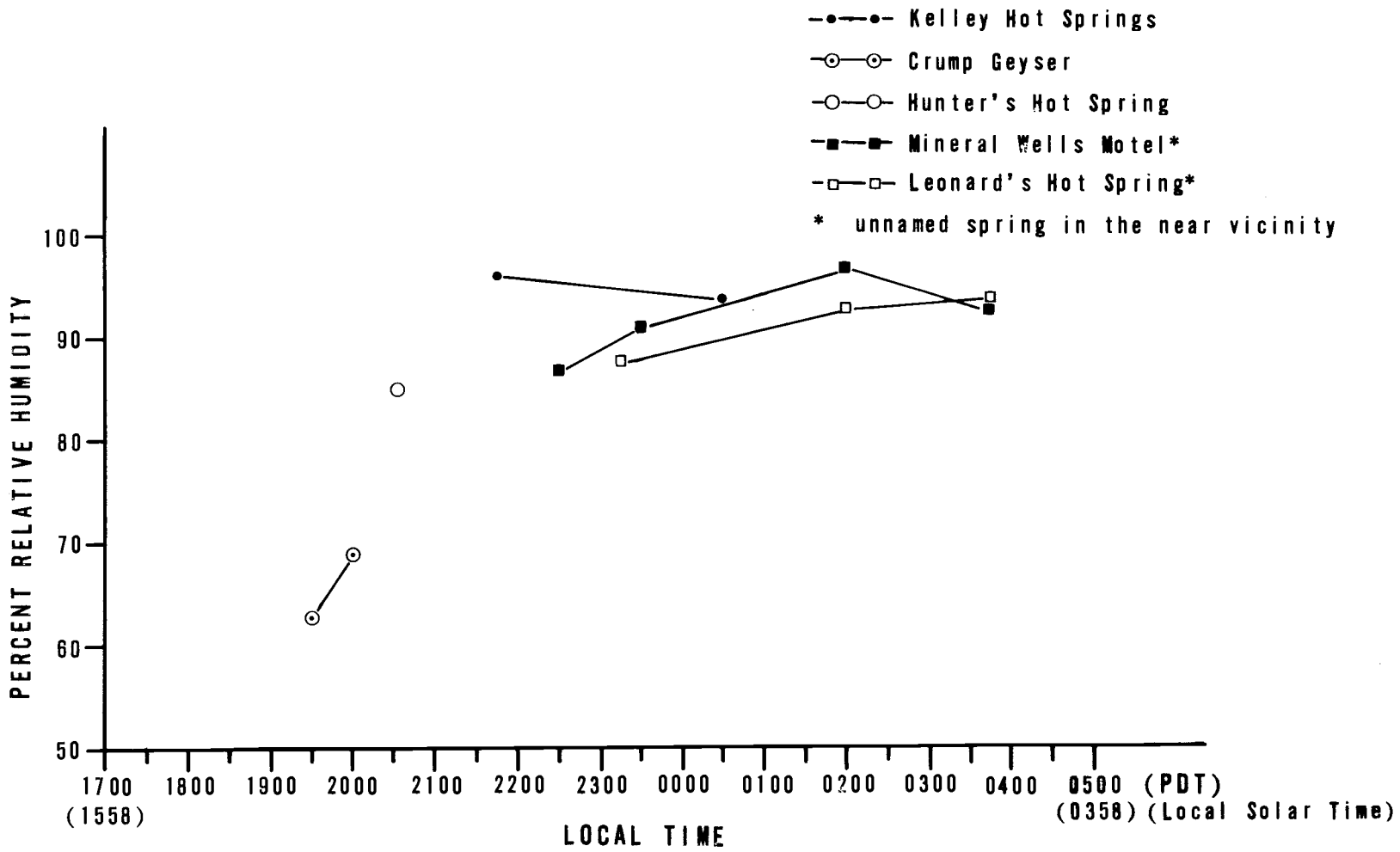

Figure 33. Relative humidity trends.

to the winds encountered during this period apparently adding water vapor to the air at that location.

The determination of the ideal time for data acquisition can be made through the comparative evaluation of Figures 30, 32, and 34. The flow of heat from the soil continues through the night until the lowest soil temperatures are observed at dawn. The hydro-geothermal sources continue to emit heat energy at relatively constant rates throughout the night. Therefore, the difference between soil and hot spring temperatures are greatest during the early morning hours. Mixing ratio values are at their lowest also in the early morning hours. Low mixing ratio, a function of water vapor in the air, is desirable for reducing atmospheric attenuation effects in acquiring TIR imagery. Therefore, the collected ground truthing data supports the contentions of Hodder (1970), Moxham (1969), Valle, Friedman, Gawarecki, and Banwell (1970), and others that TIR data acquisition should occur in the early pre-dawn hours. Since no post-sunrise flights were conducted, Watson's time lag conclusions for a 0948 hour overflight could not be evaluated.

Wind direction and velocity were obtained using a hand held anemometer. Readings were taken in miles per hour and later converted to knots. Wind direction refers to the direction that the wind is blowing from. The wind direction was determined by the observer's direction of view as the wind blew directly at him. The effects

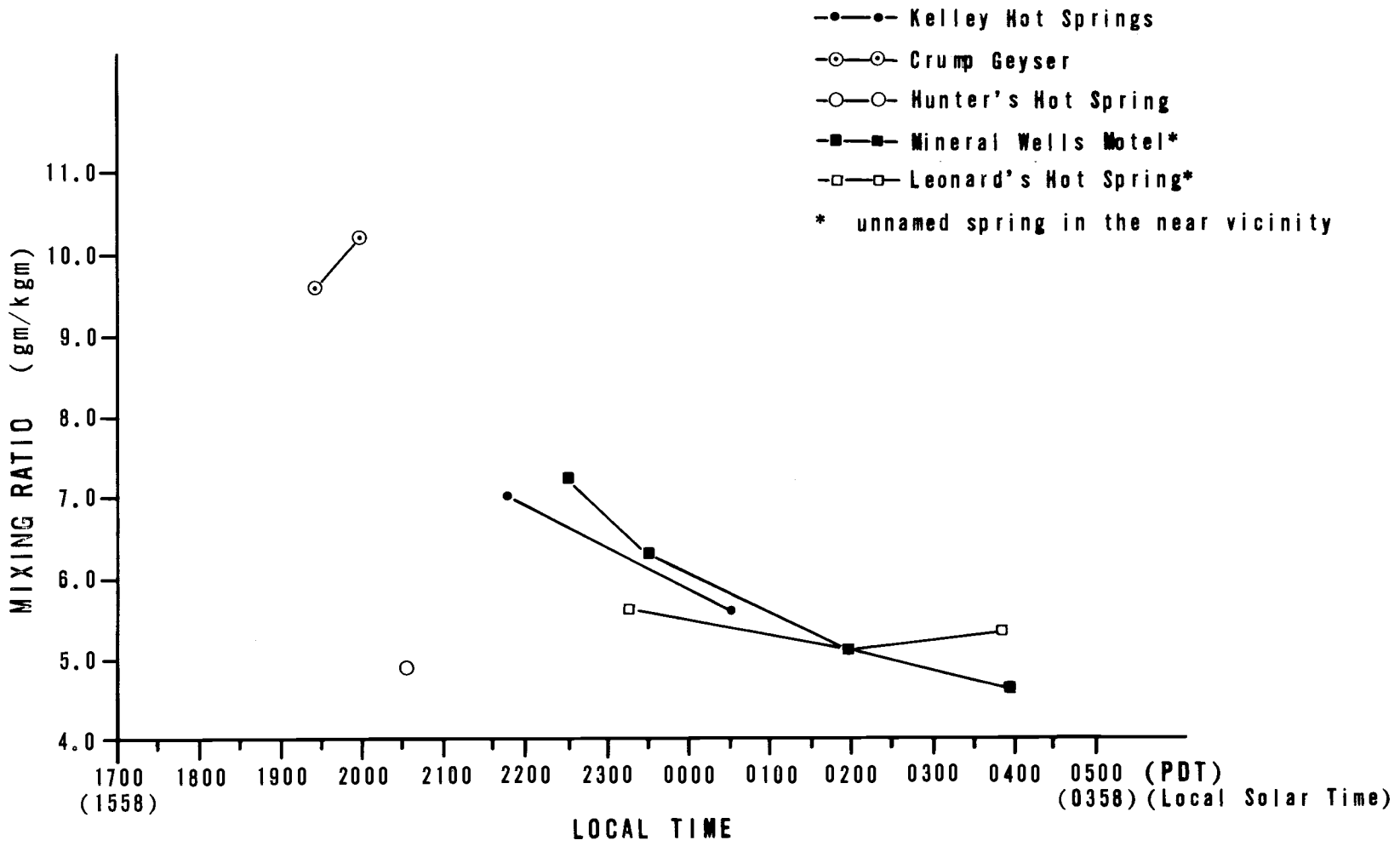

Figure 34. Mixing ratio trends.

of wind on surface air characteristics, specifically relative humidity, were referred to previously in the discussion concerning Figure 31.

Soil Characteristics. Soil moisture percentage was calculated for the soil within twenty meters (where possible) of the hot spring sampling site. Conventional soil cans were utilized to collect four disturbed soil samples at the time of each overflight. One soil sample was collected in each of the four major coordinate directions. The samples were hermetically sealed and taken to the Fremont National Forest Soils Laboratory within six hours of the overflights.

The previously gravimetrically weighed empty soil cans were re-weighed containing soil samples on the same precision scale. The samples were dried in a 105^{o} C drying oven for twelve hours. The samples were weighed again. The differences in their dry weight as opposed to their wet weight was calculated as a percentage of the wet weight. Such computations yielded the soil moisture percentage of each soil sample. The results of the calculations are listed in Table 14.

Examination of the soil moisture information yields the fact that except for Hunter's Hot Springs, no sample site had soil moisture greater than fifteen percent by weight. This fact indicates an area with soil high in alkaline and pumice materials. As discussed previously, the evaporation/precipitation characteristics of the study area are such that low soil moisture percentages should be expected.

The higher soil moisture at Hunter's Hot Springs is a result of the closeness of the samples area to the geyser. The spray from the geyser, which erupts every thirty seconds, supplies a relatively constant water supply to the surrounding area. The spray also accounts for the relatively high humidity (85 percent) experienced in the early evening hours.

More problems occurred in the collection of soil samples than in any other ground truthing information. At three different times soil samples were not taken by the ground teams at the time of overflight. Some soil samples were lost when part of the sample was spilled after drying. This, of course, gave incorrect readings when applied to the wet soil sample weight.

Vegetation Moisture. Vegetation immediately surrounding the sample sites was extremely sparse. Bare soil and lithologic material were dominant. The scarce vegetation was composed of small grasses and a limited amount of sagebrush. Samples taken during the June overflights were inadvertently destroyed in the drying oven. However, the samples examined from the October overflights yielded vegetation moisture percentages less than or equal to soil moisture percentages. Therefore, it is believed that the sparse distribution of vegetation surrounding the data site had little impact on the TIR signal, as compared to soil temperature and moisture.

Surface Water Temperatures. The water temperature was measured for each sampling site location at the time of aircraft passage (Data in Table 14). A Celsius thermometer was inserted into the water at an oblique angle until the bulb was just below the surface (1 cm). The temperature was read to the half degree and recorded. In small pools where more than one source is located, the hottest source temperature was recorded. The heat flow from the measured sources is depicted in Figure 32.

Summary. The ground truth parameters can be used as site-specific indicators of the physical attributes depicted on the thermal infrared imagery. The information can only be applied to that source for which it was collected. However, it can be used to infer the moisture attenuation occurring at other sites along the same flight-line.

The data collected indicates that the attenuation levels decrease at fluctuating rates with time (from dusk to dawn). As air temperature and mixing ratio decrease over time, the relative humidity increases. This relationship generally holds true except when altered by wind movement. The movement of the air tends to alter the air characteristics by introducing or removing water vapor from the air and therefore potentially can cause variations in the amount of atmospheric attenuation experienced at the air-ground interface.

The differences between the soil temperature, which slowly

decreases with time, and the relatively constant water temperature is greatest just before dawn. However, the order of magnitude of this difference varies slightly between sunset and sunrise.

From the ground truthing information obtained from this study, it is suggested that the most ideal time to obtain thermal infrared imagery is in the pre-dawn hours. Thus, the conclusion substantiates earlier research. The relationship between air, soil, and water characteristics at this time appear best suited for TIR imagery acquisition with the level of the mixing ratio or water vapor content in the air being the determining factor. The interpretation of the TIR imagery obtained should support the above conclusion.

V. SLAR INTERPRETATION AND ANALYSIS

The SLAR imagery in this research was obtained in the form of continuous-strip film negatives. To increase the ease of interpretation, the imagery was converted to print positives. The interpretation and analysis of each continuous-strip (flightline) yielded approximations of surface lineaments existing along that flightline. Interpreted data along the north-looking segment of the flightline were also observed on the south-looking segment of the adjacent flightline. This phenomenon results from the variable flightline side-overlap. Therefore, where side-overlap occurred, the surface lineaments were interpreted and analyzed twice, once in opposite scan directions. This side-overlap and interpretation of individual flightlines produced a very segmented approach to the analysis of the lineaments found within the study area. To overcome this segmentation, a composite of all flightlines was created, producing a map overlay of the surface lineaments in the study area. This overlay was used to produce the structural lineaments observable in Figure 49.

Three separate stages were needed in the manual interpretation and analysis of the SLAR imagery to produce the surface lineament map. These stages included printing, interpreting, and compiling the imagery and data. Each stage required systematic procedures to correct the various problems previously discussed which are

inherent in the acquisition of SLAR imagery. These procedures are briefly depicted in the flow diagram of Figure 35.

Printing Imagery

The imagery from the June overflights was in the form of continuous-strip film negatives. In order to increase interpretative accuracy, print positives were required. The black-and-white imagery was printed according to the procedures discussed below.

Initial Flightline Printing

All flightlines were reviewed and Flightline J was observed to most closely match the 1:500,000 scale of the selected basemap (U.S.G.S. shaded relief map composite). This flightline was then printed in a non-continuous fashion. Ample overlap between consecutive prints was necessary so that a continuous-strip mosaic of the flightline could be created. By matching the overlap and similar photographic images, the photos were indexed, cut, and joined together using a dry mount press.

Consequent Flightline Printing

Utilizing the mosaic of Flightline J, the adjacent flightline, JB, was processed according to the above procedure which was applied to Flightline J. However, when comparing the distortion

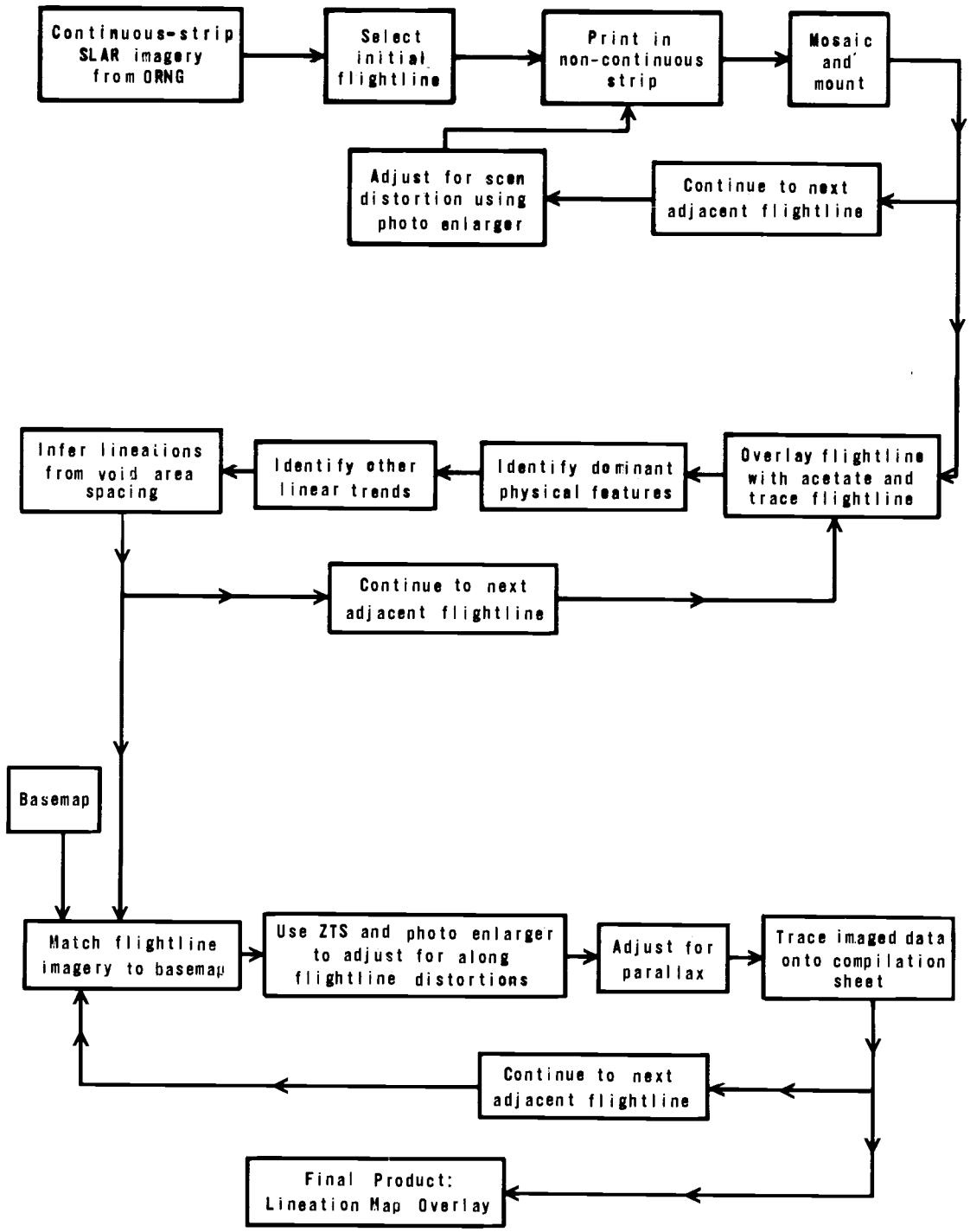

Figure 35. Flow chart of steps performed to construct lineament map.

characteristics of Flightline JB to that of J, it was apparent that distortion variations in both the direction of scan and the direction of flight occurred from flightline to flightline. Variations occur in the scan direction as a result of the scan angle adjustments required to maintain a 25 kilometer side-scan distance. The resulting image is either stretched, so that it appears longer than the same image on the adjacent flightline, or compressed into a shorter image. Variations in the direction of flight occurred as a result of changing aircraft ground speed.

The scan direction distortions were adjusted, through the use of a photo enlarger, so that the image length on one flightline matched the image length of the adjacent flightline. The photo enlarger technique was restricted to adjusting the image by enlarging its size. It could do nothing to alter the shape of the image. Therefore, on the imagery where distortion variations occurred perpendicular to each other, the photo enlarger could adjust only for variations in one direction. As a result, the variations were adjusted in the scan direction. Distortion along the flightline remained and were adjusted for in a later procedure.

Similar topographic features on adjacent flightlines were utilized as reference objects to photographically adjust the image. This procedure was duplicated from flightline to flightline throughout the study area. Once distortion was adjusted, the imagery existed in

photo positive prints of the individual flightline mosaics. These continuous-strip mosaics were utilized in the interpretative procedures for imagery analysis.

Imagery Interpretation

The flightlines printed according to the procedures discussed above were utilized individually in order to interpret the lineaments along each. The following procedures were followed for each flightline consecutively until all flightlines were analyzed.

Overlay Positioning

Matt acetate overlays were secured over the flightline mosaic. To aid in repositioning at a later time, the line of flight or ground track superimposed on the imagery by the radar scanner, was traced onto the acetate. Lake outlines and outstanding cultural features, such as powerline locations, were also traced onto the acetate at this time.

Imagery Review

During the initial review of the imagery, the dominant physical features, such as ridge or crest lines, major fault traces, and other sites of observable displacement, were traced on to the acetate (Figure 36). This usually produced approximately half of the observable

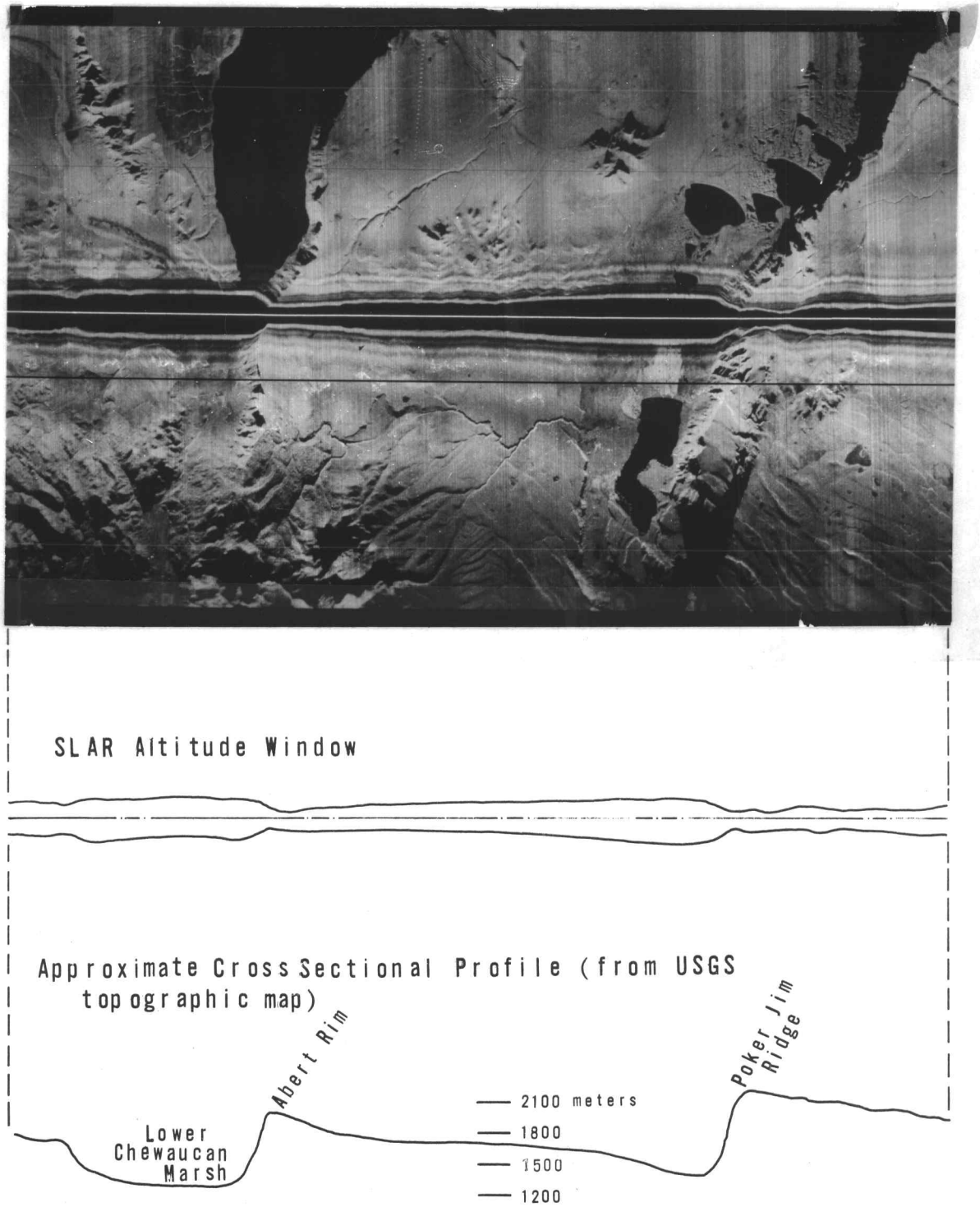

Figure 36. SLAR and interpreted lineaments near Abert Lake, Oregon.

lineaments on the flightline.

In the second review of the imagery, river trends and the linear occurrence of physical features were subject to author scrutiny. The less observable extensions of features noted in the first review were also delineated at this time. These two interpretative passes produced the majority of the linear features noted on the imagery. However, two interpretative problems were found to exist which momentarily restricted analysis.

Problems

The major problem encountered was shadowing. Mountain peaks and crestlines produced shadows that totally obscured the physical information behind the peaks or crests. These shadows extended outward in the direction of scan. Shadow length increased with increasing distance from the ground track. This problem was inherent with the system and no adjustments could be made when interpreting from one flightline. However, some correction was accomplished by using adjacent flightlines and this correction will be explained in procedure three to follow.

The second problem was created by the design characteristics of the SLAR system. Utilizing a zero delay scan angle, i.e., scan begins directly beneath the aircraft and outward to the selected 25 kilometer range, a void area or altitude window was created in the

center of the imagery. The altitude window was produced by rapid or near instantaneous recording of the transmitted signal or "raster burn" (Figure 36). A 10 kilometer radar delay option could have been selected, however, valuable information would have been lost.

The rapid or near instantaneous recording of the transmitted signal also created serious distortions on the imagery within the first seven-and-a-half kilometers on either side of the aircraft's ground track. Within this distance many smaller scarplets were not visible resulting from the distortion. Side-overlap of the imagery compensated for many of these problem areas. However, ample side-overlap did not occur throughout the entire study area. Where side-overlap was lacking, the imagery analysis created areas with a low density of lineaments. Such an area of lower lineament density can be observed on Figure 49 in the area north and west of Alturas, California.

The shape of the altitude window, produced on the imagery by the sensor, actually depicts a profile of the terrain passing beneath the aircraft (Figure 37). Therefore, changes in ground elevation are recorded as changes in the profile or width of the altitude window. Where this window is narrow, the land mass below the aircraft is quite high or relatively close to the aircraft. Abert Rim makes quite an impression on the altitude window, as seen in the figure. Where the window area is wide, the land elevation is relatively far from the aircraft. Observing the changes in this window, along the ground

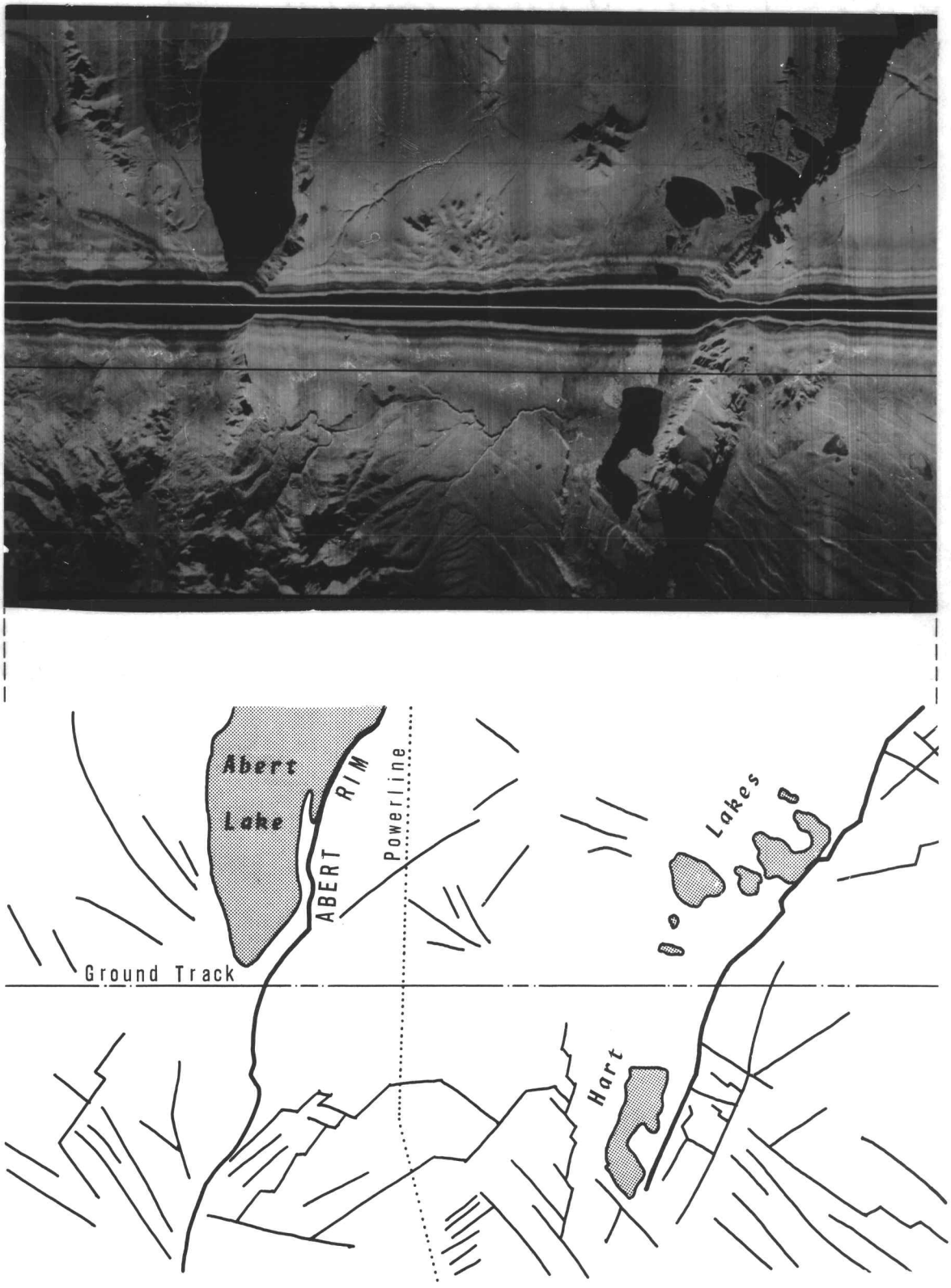

Figure 37. Comparison of SLAR altitude window and approximate cross sectional profile.

track, allowed the author to interpret the additional lineaments not interpreted in the first two passes of imagery analysis. The ground track altitude window also allowed for lineament determination in areas where little terrain variations occurred. Therefore, by utilizing the inferred terrain profile, linear features were identified and located as to their intersection with the line of flight in the area of the distortions near the altitude window. All linear features were analyzed and recorded on the acetate overlay after three consecutive reviews of the imagery.

Imagery Compilation

The third procedure involved the transfer of individual flightline lineaments into a composite of all flightlines in the study area. Scale adjustments of the imagery were necessary so that the final map product was at the scale of the basemap. Proper flightline positioning required the alignment and orientation of the imagery line of flight over the equivalent basemap line of flight.

Along Flight Distortions

Beginning with Flightline J, the interpreted information of each flightline was transferred to a composite or compilation map. During this stage of production, adjustment of image distortion along the flightline resulting from the variable aircraft ground speed was

performed. Using a Bausch and Lomb Zoom Transferscope (ZTS) Model Number ZT4H, the imagery was adjusted for distortion variations through the instrument's enlargement and 360 degree stretch properties. The versatility of this instrument allowed for such corrections along each flightline. The variability of aircraft ground speed was not constant and therefore continuous instrument adjustment was required while using the ZTS.

Parallax

Side-overlap of adjacent flightlines created a parallax distortion when overlaying the interpreted information common to opposite scan directions. That is, the north-facing scan of one flightline appeared to produce a parallax offset of the same land feature when it was overlaid with the south-facing scan of the adjacent flightline. Thus, two lineaments were observed when only one actually existed. Because a true photo stereographic relationship did not exist, the parallax problem was adjusted by creating a line of approximation between the two lineaments. The distance between the two lineaments was weighted against their relative distance from their respective line of flight. The lineaments drawn on the composite of all flightlines represent both the adjustments for along-ground track distortions and parallax variations.

Shadowing

Lineament information hidden by the shadowing effect of the SLAR along a particular flightline frequently became observable when overlapping adjacent flightlines were utilized. What was hidden by a north-facing scan of one flightline was exposed by the south-facing scan of the adjacent flightline. Except for areas where the shadowing effect of opposite facing scans overlapped, the linear features hidden by the remaining shadows were exposed and included in the lineament map product.

Lineaments observed in the study area overlay the 1:500,000 basemap mosaic of selected portions of the U.S.G.S. Oregon and California shaded relief maps (Figure 49). The three heavier lines represent the major fault line scarps (Winter Rim, Abert Rim, and the extension of Poker Jim Ridge) found in the study area. The other linear features represent the many lineaments of lesser relief displacement which are observed throughout this section of the Northern Great Basin. This figure (49) will be utilized along with the information acquired in the thermal infrared section to examine the potential of SLAR and TIR imagery for the exploration of surface hydrogeothermal expressions.

Imagery Comparison

A comparison was made between the lineaments depicted on Figure 49 and those exhibited by both Lawrence's (1976) Landsat-1 analysis (Figures 14 and 15) and Walker's (1973) geologic map. All three were analyzed at their common scale, 1:500,000. The area, within the study area common to all three, was overlaid with a ten lines to the inch grid network. Each grid cell that possessed a lineament was counted, producing a total that represented the number of grid cells in which a lineament existed per map.

The lineaments of major displacement were common to all three maps. However, the lineaments produced from the SLAR imagery were observed 12 percent more frequently than those lineaments indicated by Walker and 26 percent more frequently than the lineaments interpreted from the Landsat imagery. The increased number of potential structural lineaments observed on the SLAR imagery resulted from a greater number of the smaller scarplets (small vertical displacement) being more easily identifiable from the SLAR imagery.

VI. THERMAL INFRARED ANALYSIS

Previous studies indicate the existence of various hot springs and geysers in the study area (Walker, 1967b; Bowen and Peterson, 1970; and Friedman et al., 1973). By flying over the major surface lineaments, utilizing various thermal infrared sensors, it was possible to locate these hydro-geothermal surface expressions. The level of accuracy in locating and analyzing such expressions was dependent upon the selection of a particular sensor or a combination of sensors to secure the imagery.

ORNG had the capability to use three separate detectors either as a single sensor or in a simultaneous dual channel two sensor combination. The three detectors utilized by ORNG in securing the thermal infrared imagery were mercury-cadmium-telluride (HgCdTe), indium antimonide (InSb), and indium arsenide (InAs). The wavelength characteristics (range and peak response) of each detector were discussed above and were summarized in Table 12. Both the mercury-cadmium-telluride and the indium antimonide have peak response characteristics that fall within available atmospheric windows and thus are sensitive to various levels of the earth's infrared radiation (Stingelin, 1969; Wolfe, 1965; and Reeves, 1975).

Detector Analysis

The major advantage of utilizing a one channel detector, instead of a dual channel arrangement, is that the imagery is produced at a larger scale. The single scan imagery is nine centimeters wide with the scale directly dependent upon flight altitude. This larger scale simply aids in user interpretation and does not improve image resolution. The dual channel detector depicts the imagery on two four-and-a-half centimeter strips. The imaged land surface depicted on each channel is identical, only sensed at different wavelengths.

Depicted on Figure 38 is Kelley Hot Springs located just east of Canby, California. The image is created by a single mercury-cadmium-telluride detector flown over the target at 4:19 A.M. PDT (local time) on June 22, 1976. The hot spring's surface temperature was 88° C and the spring was producing a large volume of vapor at the time of overflight. The vapor is visible just below and around the hot spring as an intermediate gray scale value. Roads, vegetation, and other physical features are also depicted on the imagery. These too are represented by variations in the gray scale. Variations in water temperature are quite difficult to observe. As was suggested by Valle et al. (1970) water surfaces of various temperatures appear as bright as the hot springs when using a mercury-cadmium-telluride detector. This is apparent on the imagery when comparing the gray

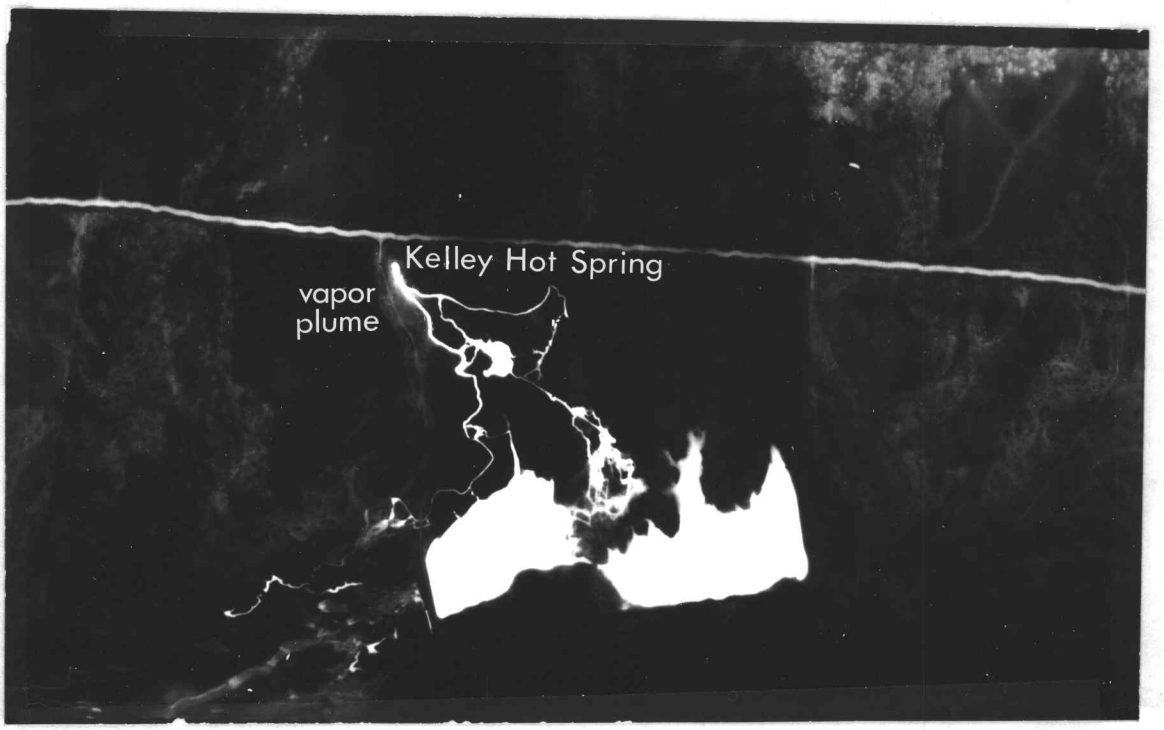

Figure 38. Kelley Hot Springs, HgCdTe [June 22, 0419 PDT].

scale level of Kelley Hot Springs to that of the slightly cooler lakes through which it flows. The relatively higher water temperatures produce much darker gray scale tones than those created by the cooler soil and vegetation.

A single channel image of Kelley Hot Springs created by the indium antimonide detector (Figure 39) possesses characteristics similar to those of the mercury-cadmium-telluride detector discussed above. The image depicted in this figure was flown at 12:20 A.M. PDT (local time) on June 22, 1976. The steam effect visible on the previous figure is not as easily observed when using this detector which senses in the shorter wavelength range (1-6 μm). The streaking effect coming off the hot springs is indicative of censor overload or overheating as was discussed in an earlier chapter. Thus, when actual hot spot locations are not easily distinguishable from other water bodies, these streaks can be utilized to infer locations of higher temperatures.

Fusee Flares

Along each flightline two phosphorous fusee road flares were placed at 60 meter intervals. The purpose of these flares was threefold: (1) to aid the pilots in locating and verifying their ground track (flightlines); (2) to aid in the scaling of the imagery along track; and (3) to aid in evaluating temperatures depicted by the various gray

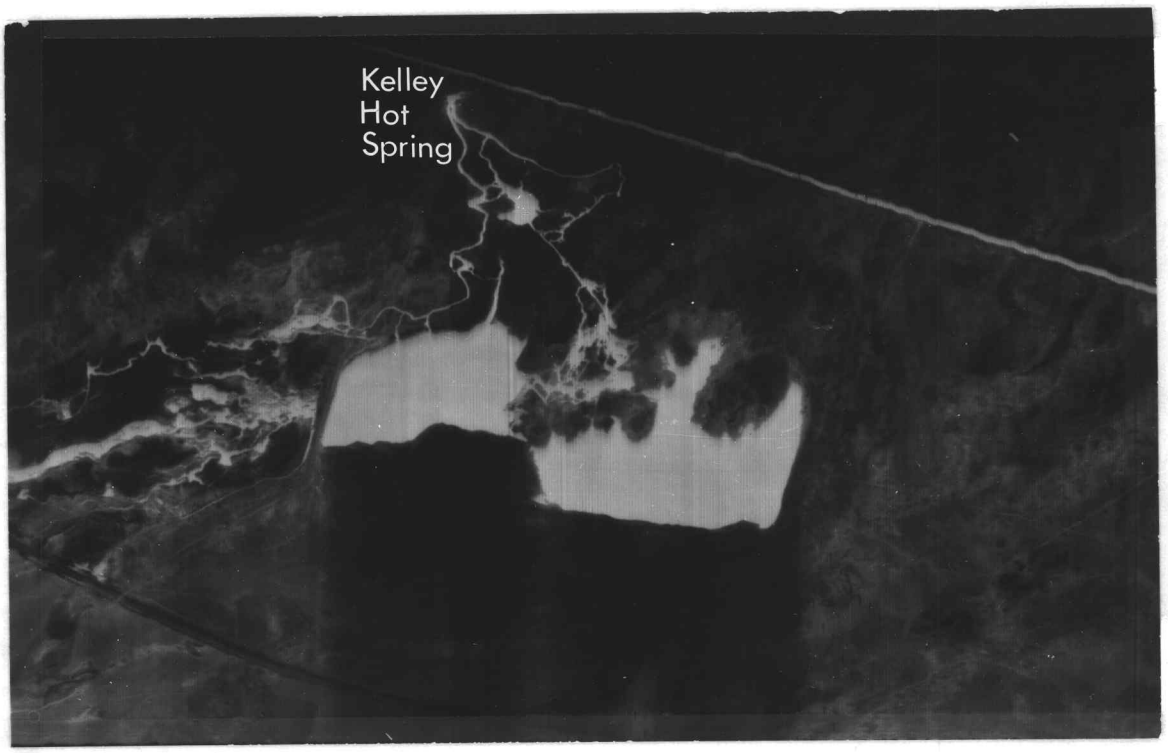

Figure 39. Kelley Hot Springs, InSb [June 22, 0022 PDT].

scale values. In nearly every instance the pilots reported visual sighting of the flares and were able to make in-flight adjustments to their ground tracks. The road flares proved very useful for this purpose.

The sites where the flares were to be placed were selected during the planning stage of flightline design. Each flare site was to be no closer than two kilometers from the nearest known or suspected geothermal site. This distance was selected so that the flares would not interfere with the imaging of the actual hot spot location. The flares were placed paralleling the aircraft's ground track 60 meters apart. This distance was paced off by the ground team stationed at the flare locations. Upon communication from the aircraft's crew that they were approaching the area, the flares were ignited.

The use of flares for scaling the imagery was only partially successful. As a result of greater sensitivity to the shorter wavelengths and thus higher temperatures and radiation levels, only the indium arsenide consistently recorded the flare's radiation. The mercury-cadmium-telluride detector never recorded the flares, while the indium antimonide (the intermediate of the three sensors) picked up the radiation levels sporadically. Both flare locations are visible on the indium arsenide portion of Figure 40. However, the complementary channel (indium antimonide) has picked up only one of the two flares.

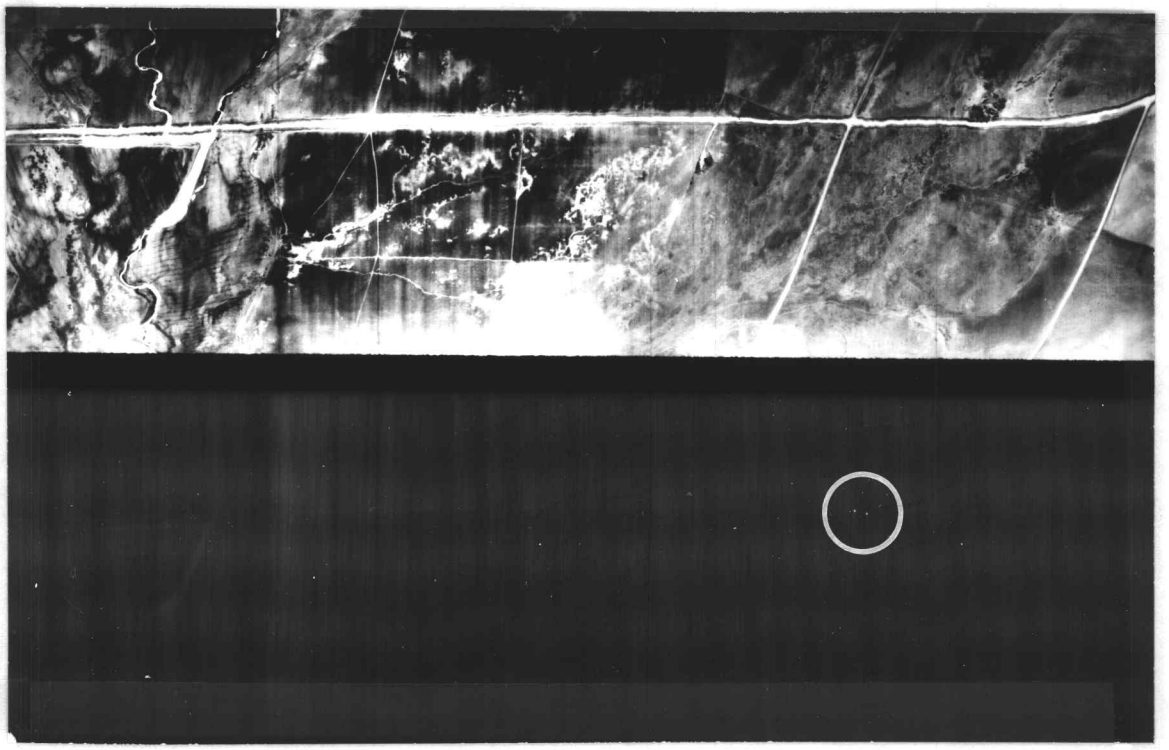

Figure 40. Fusee flare locations, InSb/InAs [June 21, 2145 PDT].

This intermittent imaging of the flares by the indium antimonide and the total lack of imaging by the mercury-cadmium-telluride results from interference by surrounding features, from detector sensitivity, and from atmospheric attenuation of the gaseous vapors given off by the burning phosphorous. Figure 40 presents a good example of where the radiation of the road surface and that of the second flare became integrated. The slight tonal variation of warmer objects and the resolution of the imagery of the indium antimonide detector caused the second flare to be unobservable. Considering the characteristics of the three detectors, the indium arsenide senses radiation in the shorter wavelengths (higher temperature) and is therefore more consistently prone to depicting the imaged object.

The unusually high burning temperature of the phosphorous flares produces only minor amounts of IR radiation (Engineering Design Handbook, 1971). Much of the radiation is absorbed by atmospheric attenuation. The combination of variable attenuation and variable IR radiation amounts produced by the flares generated a situation where the flares were not consistently detected by the sensors. As a result of this, the flares could not be used to infer temperatures on the imagery. Also, as a result of this variability, in the October 1976 overflights, the flares were used only to help the pilot verify his ground track.

Crump Lake

The Crump Geyser area, one of the best known hot springs in southern Oregon, is depicted in Figure 41. This single channel mercury-cadmium-telluride image was obtained at 12:38 A.M. PDT (local time) on June 23, 1976 at a flight altitude of approximately 825 meters. The water surface temperatures at the time of overflight were 94° C for the geyser, and 85° C for the hot spring which is located one quarter of the way between the geyser and Crump Lake (20° C). Also visible are several seeps, which possessed only a thin veneer of water with a surface temperature of 25° C. These seeps were indicated by Russell (1884), however, until the present research no indication as to their actual location has been made. The imagery clearly indicates these small seeps. The observable gray scale variations between the geyser, hot springs, seeps, and Crump Lake are negligible. Water surfaces of varying temperatures appear of equal gray scale value. However, soil areas of potentially higher moisture content also appear relatively light (on an image positive). The drainage and fan-like pattern on this image appears to be as light as various surface water locations on Crump Lake. Therefore, the single channel sensor (especially the mercury-cadmium-telluride) does not directly distinguish between hydro-geothermal locations and other water surfaces.

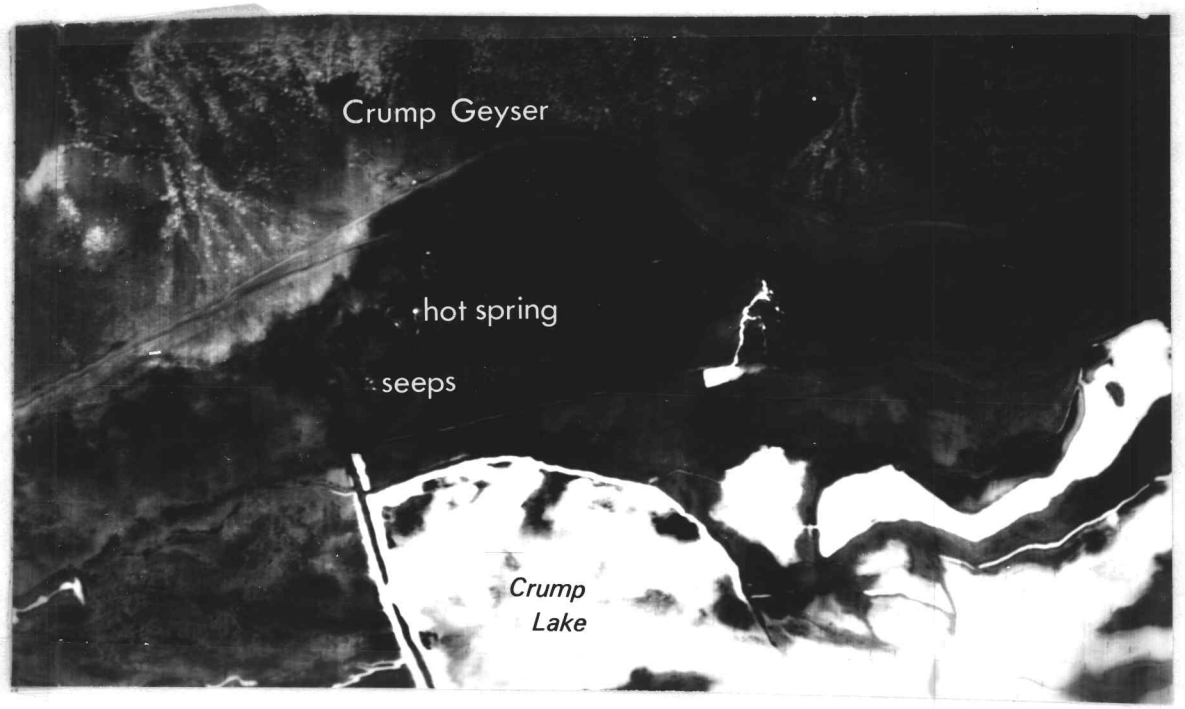

Figure 41. Crump Geyser area, HgCdTe [June 23, 0038 PDT].

Surprise Valley

The most intense area of hydro-geothermal activity was found to exist along the eastern side of the Middle Alkali Lake in the Surprise Valley. The greatest number of hot springs were found in the vicinity of the Surprise Valley Mineral Wells Motel. Four separate pools (unnamed springs southwest of the motel) yielded a minimum of twenty separate sources. The four pools are imaged on Figure 42 (single channel mercury-cadmium-telluride flown June 22, 1976 at 3:50 A.M. PDT). Sensor saturation results from the high levels of IR radiation being emitted from the pools (94° C).

A dual channel image of the same source area is depicted in Figure 43 (mercury-cadmium-telluride and indium arsenide flown June 21, 1976 at 11:25 P.M. PDT). Although at a smaller scale, the mercury-cadmium-telluride detector exhibits the same characteristics as depicted in Figure 42. However, the relative hot spring pool area is smaller on the indium arsenide imagery. This results from the indium arsenide detector's sensitivity to the hotter IR targets. The steam flume does not register on the indium arsenide imagery and because of this the pool area is depicted on the imagery.

Also visible on Figure 43 are the actual runoff traces of the warmer water. The runoff can be traced on the indium arsenide detector until the water cools sufficiently below the detector's sensitivity

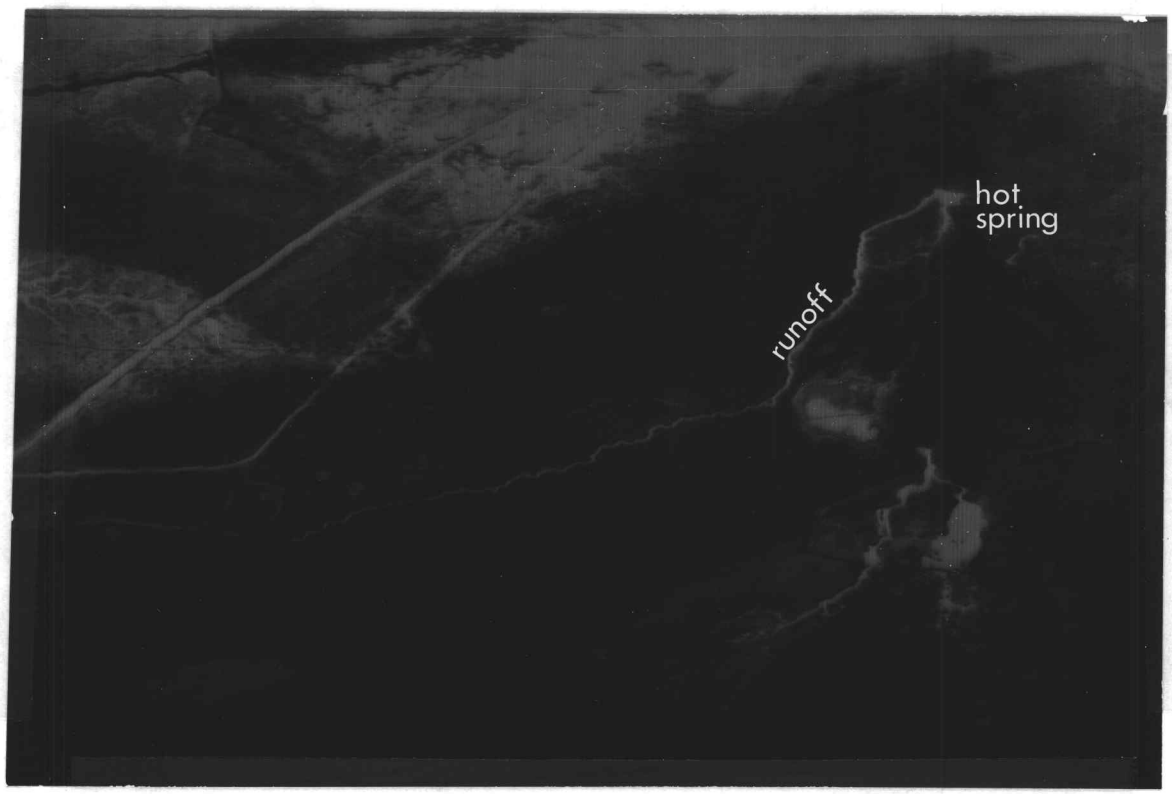

Figure 42. Surprise Valley: Mineral Wells Motel area, HgCdTe [June 22, 0350 PDT].

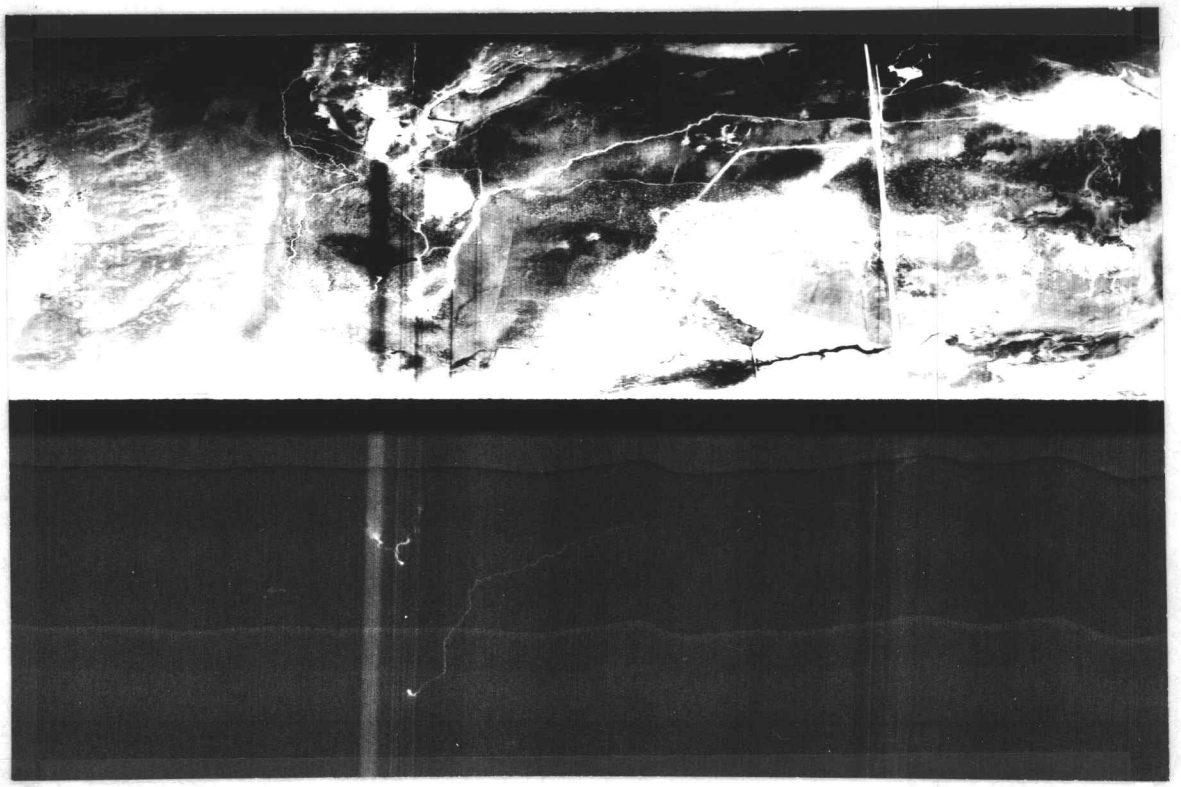

Figure 43. Surprise Valley: Mineral Wells Motel area, HgCdTe/InAs [June 22, 2325 PDT].

level either by mixing and dispersing into a cooler water body or by losing heat to the lower atmosphere at the water-air interface. Either way, the indium arsenide detector produces a more accurate view of the size and extent of the heated water surface.

One advantage of the TIR sensor is depicted in Figure 43. Exact location of the hot springs, number of hot springs, and extent of the channelized hydrothermal water are not easily found in existing literature or maps. This dual channel acquisition allows for such analysis.

Although the indium arsenide detector shows a more accurate depiction of the shape and location of the pool in Figure 43, only the pool's surface area is shown. One limitation of the TIR sensor is that it does not indicate to the observer that sixteen separate sources of geothermal water, observed in subsequent ground truth data, exist at the bottom of that one hydro-geothermal pool. This limitation is not a factor when examining non-hydro-geothermal sources, such as fumaroles. Non-fluid heat sources can be accurately located and examined (Rosenfeld and Schlicker, 1976). Figure 44 is a graphic depiction of the pool shape, along with the location and relative temperatures (i.e., surface water temperatures directly above each source) of the sub-surface sources. Some of the source temperatures were impossible to acquire because of their inaccessibility at the center of the pool. The temperatures of the surface water ranged from

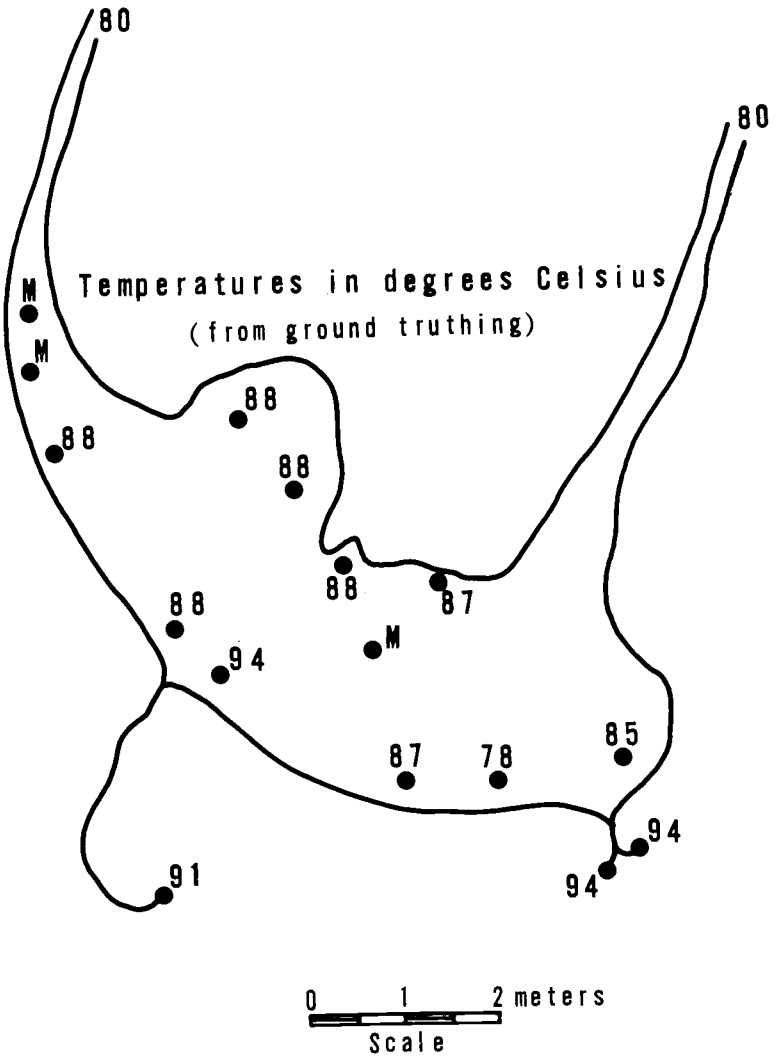

Figure 44. Diagram of unnamed hydro-geothermal pool near Surprise Valley Mineral Wells Motel.

94 to 78 degrees Celsius. The combined runoff temperature twenty meters from the pool was 80° C. To acquire detailed information concerning the pool areas depicted on the infrared imagery, some amount of ground truthing was required. Otherwise, information concerning the number of sources would be purely speculative. Figure 45 was flown over the eastern side of Surprise Valley at 0153 (PDT) utilizing the expanded format of the mercury-cadmium-telluride detector. Eleven distinct sources or hydro-geothermal sites were observed from the imagery. Only half of the sources were producing runoff or discharge. The springs occur at the edge of the Upper Alkali Lake and the discharge flows into the lake. These sources do not exist in any of the present literature.

Figure 46 depicts the geothermal sites reported in previous reports. Those sites surrounded by the large circles were confirmed from the TIR overflights while those surrounded by the large square were confirmed only through on-site ground truthing. Those sites not encompassed by either the circle or the square were not confirmed by this investigation. Through discussion with area natives, it is suggested that many of these unconfirmed sites are capped drill holes that no longer are expressed at the surface.

Need for Gound Truthing

Besides the need for ground truthing mentioned above, field

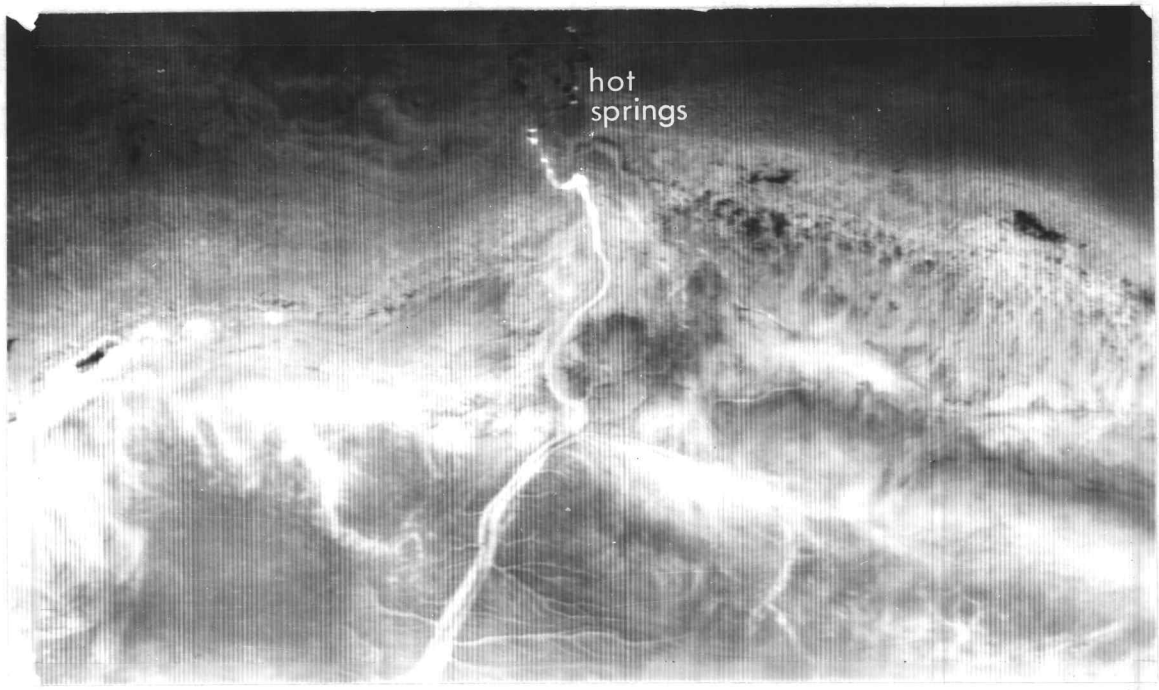

Figure 45. Surprise Valley: Mineral Wells Motel area, HgCdTe [June 22, 0153 PDT].

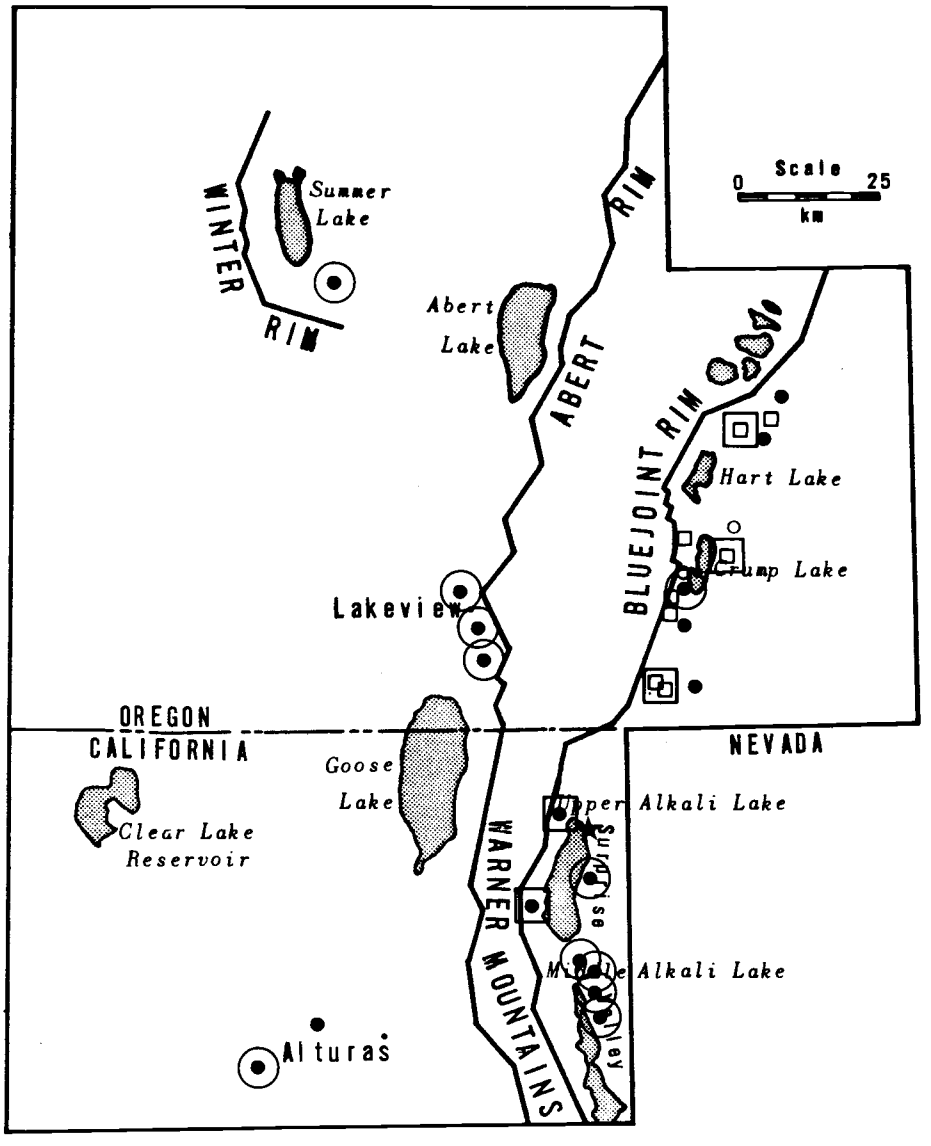

Figure 46. Confirmed hydro-geothermal sites as reported by either: Stearns, Stearns, and Waring, 1937; Waring, 1965; or Bowen and Peterson, 1970.

checks must be conducted after the imagery is acquired and analyzed. Figure 47 is a dual channel (mercury-cadmium-telluride and indium arsenide) image collected October 16, 1976 at 9:55 P.M. PST. The indium arsenide portion of the figure depicts a cluster of five heat sources plus one other source a short distance away. The sources had not been observed on any of the June imagery. Subsequent ground truthing yielded five campfires and one house location. Therefore, either subsequent verification by ground truthing or pre-existing knowledge of the area is necessary to guarantee that the hot spots interpreted from the imagery are truly hydro-geothermal locations, and not locations of other heat sources.

Single vs. Dual Channel Detectors

The use of the two channel detector system proved to be the most useful in the search for hydro-geothermal locations. The limitations of a single channel system required extensive ground truthing. The mercury-cadmium-telluride and indium antimonide detectors, when used individually, tend to blend terrestrial radiation and the hydro-geothermal radiation in such a manner that all water bodies appear of equal brightness on the imagery. Therefore, the cooler water surfaces would be indistinguishable from the geothermal sources. The mercury-cadmium-telluride detector registers terrestrial radiation from soil moisture and from some vegetation sources

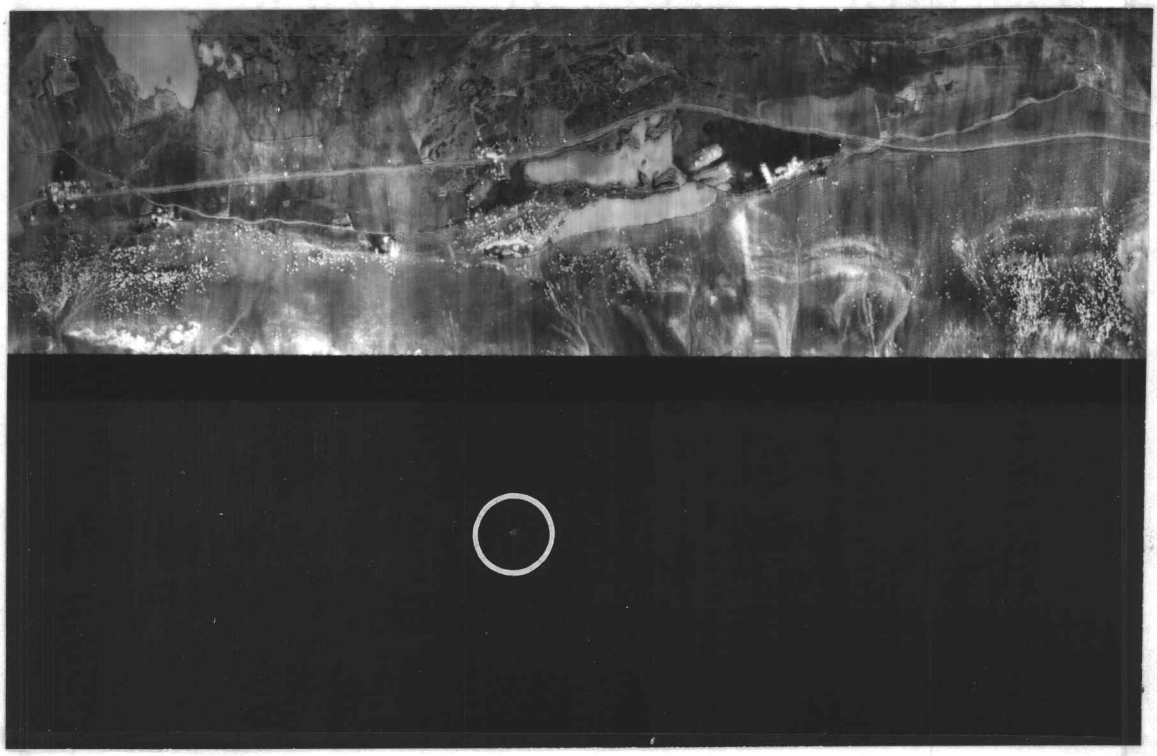

Figure 47. Campfires near Summer Lake, HgCdTe/InAs [October 16, 2155 PST].

in the same manner as that from geothermal sites. If a one channel system is the only option available, the indium antimonide detector should be utilized. The indium antimonide system is more apt to sense the higher temperature geothermal sources, as a result of its shorter wavelength sensitivity, and to register them in brighter gray scale values than would be recorded by the mercury-cadmium-telluride detector.

Although navigation and other aircraft equipment problems hindered the collection of a sufficient sample of dual channel combinations, the research indicates that the best combination of the three detectors for locating hydro-geothermal surface expressions is indium antimonide in association with the indium arsenide. The indium antimonide allows for terrain interpretation and thus relative ease in determining one's geographic location. The indium arsenide senses only the hotter sources, above 50° C, which is advantageous for locating potentially useful hydro-geothermal sources. This combination (indium antimonide and indium arsenide) would allow for the greatest accuracy in locating the sources, with the least amount of ground truthing. Further research, however, would be necessary to confirm this contention.

Densitometer Analysis

It was a major objective of this research to examine the

predictability of surface hydro-geothermal temperatures using the infrared imagery. The theory was that by knowing selected ground truth information about one particular hydro-geothermal site, it would be possible to predict other site temperatures on the same piece of imagery by relating the measured gray scale levels to temperature.

The three best pieces of imagery were taken to the Environmental Remote Sensing and Applications Laboratory (ERSAL) on the Oregon State University campus. Housed at ERSAL is a Welch Scientific Company 3830X Densichron Model 1 Photometer. The instrument is operated manually to obtain gray scale density levels for selected point sources. The greatest accuracy of this instrument is acquired through the use of the lucite plastic aperture one millimeter in diameter. The instrument was calibrated using a precision density step wedge and instrument correction factors were determined.

Figure 48 represents the density-temperature plottings of three separate imagery strips over the same hydro-geothermal source area. The relative density levels ranged from 0.465 to 2.21 and the temperature levels ranged from 65 to 94^{o} C (Table 16). It can be noted that the indium arsenide imagery registered density levels well below that of either mercury-cadmium-telluride images. By means of examining both Figure 48 and Table 16 it can be concluded that no

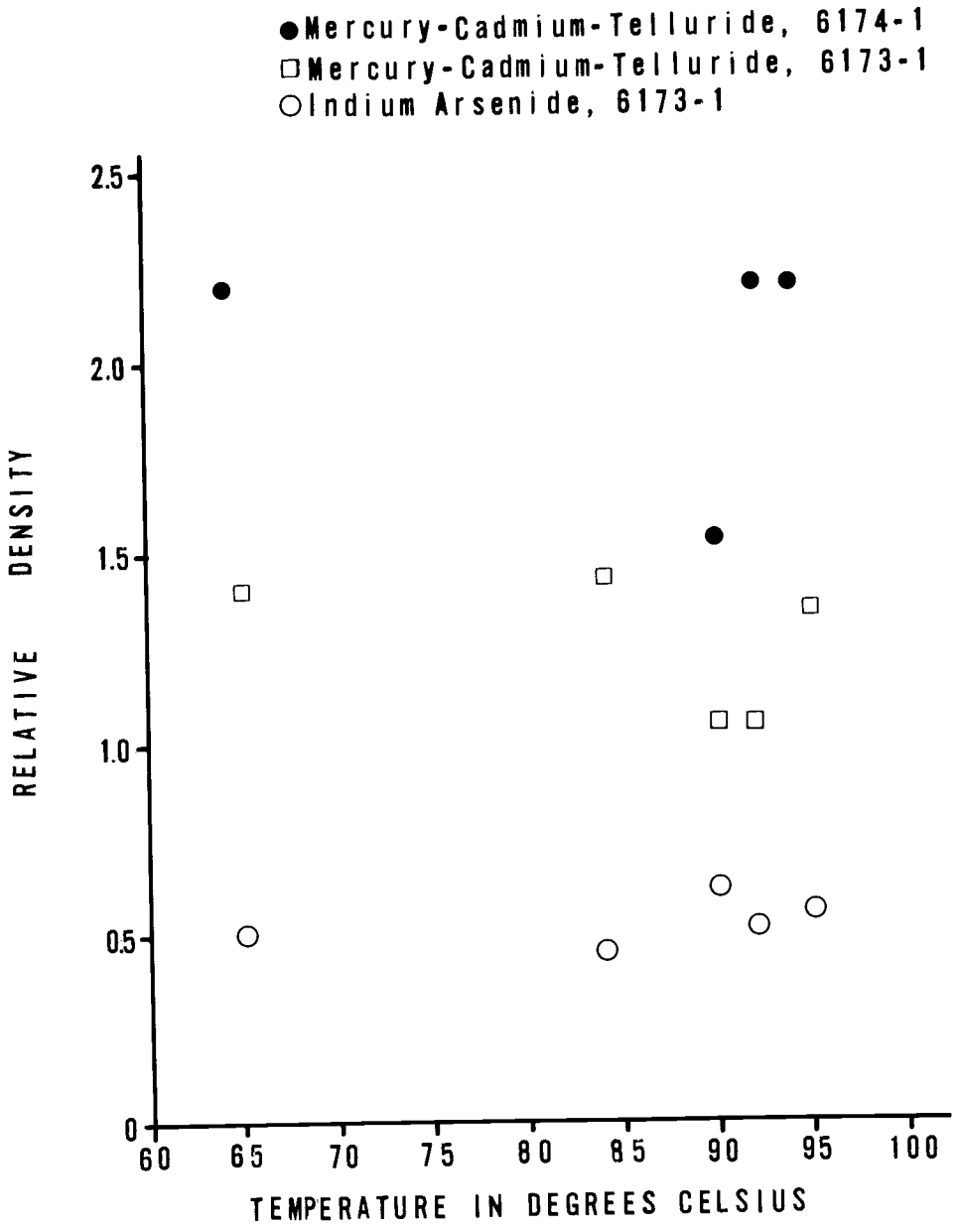

Figure 48. Relative density values versus temperature.

Table 16. Density-temperature relationships.

Temperature °C	6174-1 HgCdTe	6173-1 HgCdTe	6173-1 InAs
65	2.20	1.41	0.51
84	M	1.44	0.465
90	1.54	1.06	0.63
92	2.20	1.04	0.52
94	2.21	1.36	0.56

M = aircraft did not pass over this spring on this overflight.

apparent predictive relationship holds true between the temperature and gray scale levels. The 6174-1 mercury-cadmium-telluride imagery produced maximum gray scale values for the 94° C temperature as should be expected, however, the 65° C and 92° C temperatures each recorded the same density reading. The 6173-1 mercury-cadmium-telluride flight produced a maximum density level at the 84° C temperature level while all hotter temperatures were registering lower density levels. The indium arsenide imagery produced an even different relationship, where the 90° C produced the maximum density reading. The overall density range for the indium arsenide was smaller than either of the mercury-cadmium-telluride flights.

The TIR scanners were set at pre-selected contrast and gain levels prior to aircraft overflight. Such pre-calibration of the sensor is imperative for the establishment of temperature-density relationships. The sensor's settings were adjusted in flight by the

aircraft's crew. This in flight adjustment produced the non-relationship between temperature and density depicted in Figure 48.

The distribution of the density levels for each detector considered in Figure 48 strongly relates the detector's sensitivity response to that of emitted energy. The hot spring temperatures (65-94^{o} C) were easily equated to wavelength (7.89-8.57 μm) via the use of Wien's Law. The greater density levels of the two mercury-cadmium-telluride imageries are indicative of the 8-14 μm wavelength in which it senses. The hot springs are emitting very closely to the detectors range. Therefore, greater impact (density) is made by the hot springs on the imagery. Two levels of density were created by the various inflight sensor adjustments. The indium arsenide detector senses in the 1-3.4 μm wavelength and is therefore only imaging partial radiation levels of the hot springs. This accounts for the lower density readings of the indium arsenide imagery.

The attempt to predict temperature on one strip of imagery was based on the assumption that the surface characteristics observed and recorded at one site along a flightline apply to all the sites along that flightline. The dynamic characteristic of the air-ground interface, discussed previously, tends to negate such an assumption. The variability of atmospheric attenuation based upon changes of air temperature and moisture characteristics hinders the application of such an assumption.

Considering the above mentioned limitations of establishing a temperature-density relationship, extended field checking was necessary either at the time of actual flight or after imagery analysis. The imagery collected in this research can be utilized for establishing potential hydro-geothermal locations. However, verification of site location and temperature determination will require actual on-site observations.

VII. SLAR AND TIR COMPATIBILITY

Map Product

The compatibility of using side-looking-airborne-radar and thermal infrared detectors for locating hydro-geothermal surface expressions was examined in this study. A map has been produced which depicts the interpreted data (either from detector analysis or ground truthing)(Figure 49, in pocket). The scale adjusted imagery was registered to the 1:500,000 U.S.G.S. shaded relief basemap. The map product graphically depicts the structural relationship between the surface hydro-geothermal sites and the fracture traces.

Study Area

The heavy boundary line delineates the study area limit. This area included parts of south central Oregon and a northeastern portion of California. The area is composed of land both privately owned and publicly administered by many branches of government. The government's involvement, specifically the Fremont National Forest, in this area was the impetus for seeking the evaluation of the existing geothermal potential. Such an evaluation was conducted utilizing SLAR and TIR in a complementary fashion and is summarized pictorially in Figure 49.

Lineaments

From the SLAR imagery and U.S.G.S. topographic quadrangles, three lineaments were found to have major vertical displacement (greater than 500 meters). Winter Rim, Abert Rim, and the Poker Jim Ridge and their extensions were easily identifiable on the imagery. Available reference maps confirmed that sections of these faults possessed greater than 500 meters vertical displacement. The distinction between these major lineaments and the many lineaments of lesser vertical displacement is shown on Figure 49 by line weight variations.

The two fault trends, discussed previously, of NW-SE and NE-SW are easily seen on the figure. The lineaments of greater displacement have a tendency to run NE-SW and are relatively few in number. The lesser displacement lineaments are quite numerous and trend NW-SE.

Hydro-Geothermal Sites

The relationship between the hydro-geothermal source locations and the structural lineaments is also depicted on the figure. The two hot spring sites and the geyser at Hunter's Lodge fall within meters of the Abert Rim fault scarp which passes just east of Lakeview. The hot spring locations near Crump Lake and Hart Mountain also fall

within close proximity of a major fault lineament (Poker Jim Ridge). The TIR locations depicted from this study represent only those sites that fell within the area of TIR flightlines. The flightlines, as previously discussed, were flown along structural lineaments and thus a causal relationship is implied. However, there may be locations not considered by the TIR imagery where such an implied relationship does not exist.

The Surprise Valley hot spring locations lie in an area of deep sedimentary deposits. The valley is surrounded by fault lineaments. However, interpretation of such lineaments in the valley was not possible as they were hidden by the sediments. The location of these hot springs suggests the existence of sub-surface fault traces that possess no surface expressions. Grabens, such as Surprise Valley, may possess hot springs originating from the sub-surface faults. Therefore, it is advisable to acquire TIR imagery of the valley periphery in searching for surface hydro-geothermal expressions.

In the portion of the study area imaged by TIR overflights, the hydro-geothermal sites tend to be located near the lineaments of greater vertical displacement. Of the twenty-three different hot spring locations, all but two occur in close proximity to a major fault trace. Those two are located in the Pit River Valley west of Alturas, California.

The TIR imagery allowed for the accurate location of all the

hydro-geothermal sites confirmed in the study area (Figure 46). The geographic grid coordinates for the following sites were found to be incorrectly cited by Bowen and Peterson (1970) and Stearns, Stearns, and Waring (1937): Summer Lake Hot Springs; Crump Geyser; Berry's Ranch Hot Springs; Leonard Hot Springs; and the two unnamed sources near Leonard Hot Springs. The unnamed stream with eleven sources was identified from the imagery and is new to the literature.

The temperatures of the hot springs and geysers were established by ground truth in the field. These are cited in Table 17 along with their geographic grid coordinates. These sources were grouped into five degree Celsius classes above 60° C and ten degree classes below 60° C for their display of Figure 49. Those temperatures represent the maximum temperatures recorded at each site. Two California sites (unnamed stream with eleven sources and Boyd Hot Springs) were either dry or were totally inaccessible at the time of ground truthing. However, interpretation from the TIR imagery indicates a temperature value of at least 30° C determined by minimum threshhold levels of the sensors and a visible vapor plume, indicative of a geothermal hot spring. Therefore, these sites are included in the 30-39° C classification on the figure, but are listed only as "warm" in the table. This was done in order to maintain an accurate listing of measured temperatures.

Table 17. Hydro-geothermal sites: Temperature and location. Hydro-geothermal locations and temperatures referenced on the map "Lineations and Hydro-Geothermal Locations in the Northern Basin and Range Province: Oregon/California" by Thomas W. Hodler and Charles L. Rosenfeld.

	Max. Temp.* (°C)	Section	Township	Range
OREGON:				
Summer Lake Hot Spring	48	1	T33S	R17E
Fisher Hot Spring (Cox Ranch) 2 sources	67	10	T38S	R25E
Crump Geyser	94	34	T38S	R24E
Unnamed springs (2) near Crump Geyser	85	34	T38S	R24E
Hot Spring Campground Bathhouse	38	32	T35S	R26E
Twentymile Creek (Cahill Ranch)	67	30	T40S	R24E
Hunter's Lodge (Hot Spring and Geyser)	93	4	T39S	R20E
Brown's Ranch (Leithead Hot Springs or Joyland Plunge)	69	27	T39S	R20E
Berry Ranch Hot Spring	88	27	T39S	R20E
CALIFORNIA:				
Ft. Bidwell	45	17	T46N	R16E
Unnamed stream (11 sources)	warm	36	T46N	R16E
Boyd Hot Spring	warm	31	T45N	R17E
Leonard Hot Spring	39	15	T43N	R16E
Unnamed spring (Cow Bone Hot Spring)	65	18	T43N	R17E
Unnamed spring (Railtie Hot Spring)	84	12	T43N	R16E
Surprise Valley Mineral Wells Motel	92	6	T42N	R17E
Unnamed spring southwest of motel (16 sources)	94	6	T42N	R17E
Unnamed spring southwest of motel	90	12	T42N	R16E
Kelley Hot Spring	88	29	T42N	R10E

*Derived by on-site measurement.

Three sites are indicated on Figure 49 as being other sources and no temperature is given. These sources were consistently cited in previous publications: Phillips and VanDenburgh (1971); Bowen and Peterson (1970); Waring (1965); and, Stearns, Stearns, and Waring (1937) (Figure 46). Their inclusion in this study occurs as a result of the author's inability to prove or disprove their existence. The sites were not covered by the TIR imagery and were inaccessible as a result of either their physical location or their presence on posted private land. There is no evidence, either on the imagery or through ground truthing, that substantiates their location or temperature. Therefore, the author chose to include them on the figure as other sources and suggests further research to verify their existence.

Four of the identified hydro-geothermal sites are located outside the boundary of areas designated as KGRA's by the U. S. Geological Survey. In Oregon, the Bathhouse Hot Spring is not included in a KGRA. However, this site is located in the interior of the Hart Mountain National Wildlife Refuge. Fort Bidwell and the unnamed stream with eleven sources near the northern end of the Upper Alkali Lake do not fall within the KGRA boundary, nor does Kelley Hot Springs near Canby, California. Kelley Hot Springs is of significant interest because of its 88^{o} C temperature and continuous surface boiling action. All hydro-geothermal sites identified by this research fall within the area designated by the U.S.G.S. as potential KGRA's.

Temperature Decay Rings

The hydro-geothermal hot springs in the study area have a tendency to cluster in groups of three or more springs within a very short distance. There are three locations where this clustering effect can be observed: near Lakeview, Oregon; at the south end of Crump Lake, Oregon; and, on the eastern side of the Middle Alkali Lake, California (Figure 49). Within each of these clusters there is at least one hot spring or geyser with a 90^{o} C or hotter surface water temperature. There is also a single hot spring source west of Alturas, California, with a temperature near the 90^{o} C value (Kelley Hot Springs, 88^{o} C). No other single source approaches this water temperature.

These four centers are visible on both the larger scale principal map and the smaller scale inset map of Figure 49. On the inset map, the centers serve as centroids for a series of concentric isothermal range rings that represent highly generalized temperature decay with distance transport. Kruger and Otte (1973) reported that geothermal waters could be transported in a concrete insultated steel pipe a distance of 18 kilometers with only a five degree Celsius temperature loss. Reistad (1976) suggested that such a temperature decay value is realistic in the Northern Great Basin.

The isotherms are not closed circles. Rather, the isotherms

stop at the two major lineaments of the extensions of Abert Rim and Poker Jim Ridge. These fault scarps serve as physical barriers to the transportation of the geothermal water. In places, these escarpments rise nearly 900 meters above the level of the hot springs. Such a barrier is, in the practical sense, insurmountable. The construction of the isotherms allowed for these barriers and, therefore, they are not enclosed.

Other terrain features occur at greater distances from the source areas. These areas of relief can be avoided through the selection of different pipeline routes. These different routes would, of course, increase the transport distance and thus cause a greater temperature decay. For ease of displaying the theoretical isotherms, these terrain features were disregarded, and the isotherms represent linear distances from the hot spring source.

The isotherm distance was calculated from the centroid with an estimated temperature decay value of 0.27° C/km (5° C/18 km). Therefore, potentially all the area within the 90° C isotherm can be supplied with at least 90° C water by the hot spring(s) at its origin. The areas within the 80° C and 70° C isotherms can be supplied respectively with 80° C and 70° C geothermal water. Some locations have similar isotherms overlapping from different sources. For example, in the extreme northeast corner of California and the extreme northwest corner of Nevada, two 80° C isotherms overlap.

Therefore, the area bounded by the two isotherms can be supplied with geothermal water of at least 80° C by two separate sources, the Crump Lake and Middle Alkali Lake centroids.

A similar situation can be found in the south central portion of the study area. Here in southern Oregon and northern California, two 70° C isotherms overlap. Theoretically, this area could be supplied by 70° C water from both the Kelley Hot Springs and Lakeview centroids. The Kelley Hot Springs area does not possess a 90° C isotherm because the source area temperature is only 88 degrees Celsius.

Potential Applications

The isotherms delineate areas in which geothermal waters can be supplied at consistent temperatures. The isotherms also delineate zones of potential application for the geothermal resource. A listing of various applications is found in Table 18. These uses are temperature dependent and are recorded according to descending temperature characteristics. The uses cited assume the water is uncontaminated from harmful salts and mineral deposits.

The temperatures recorded in the study area are 94° C and below. Therefore, uses cited in Table 18 above that temperature are for reference purposes only. Except for surface steam, flashed at the water-atmosphere interface, only hydro-geothermal sites were

Table 18. Temperatures required for various geothermal applications.

	°C	Applications	
Saturated Steam	200		Temperature Range of conventional power production
	190	Evaporation of highly concentrated solutions	
	180	Refrigeration by ammonia absorption	
		Digestion in paper pulp	Present expected temperature range for binary power plants
	170	Heavy water via H_2S processing	
		Drying of diatomaceous earth	
	160	Drying of fish meal	
		Drying of timber	
	150	Alumina via Bayers process	
	140	Drying farm products at high rates	
		Canning of food	
	130	Evaporation in sugar refining	
		Extraction of salts by evaporation and crystallization	
	120	Fresh water by distillation. Most multiple effect evaporations.	
		Concentration of saline solutions. Refrigeration by	
	110	medium temperatures.	
		Drying and during of light aggregate cement slabs.	
	100	Drying of organic materials, seaweeds, grass, vegetables, etc.	
		Washing and drying of wool.	
	90	Drying of stock fish	
		De-icing operations	
	80	Space heating	
		Greenhouses by space heating	
	70	Pasteurization (Harmful bacteria killed at 74.4° C)	
		Refrigeration by low temperatures	
Water	60	Animal husbandry	
		Greenhouses by combined space and hotbed heating	
	50	Mushroom growing	
		Balneological baths	
	40	Soil warming	
	30	Swimming pools, biodegrading, fermentating	
		Warm water for year-around mining in cold climates.	
		De-icing.	
	20	Hatching of fish. Fish farming.	

Source: Adapted from Raschen and Cook, 1976.

found to exist in this portion of the Basin and Range province. Those hydro-geothermal sites failed to show heat potential for near surface direct electrical production. However, these sources may possibly be utilized for electrical production when used in a binary means with another energy mode. The potential applications of the geothermal resource must, therefore, be conducive to either direct use of the water or the indirect use of the water through the application of heat exchangers.

The most practical applications of the geothermal waters fall in the realm of space heating of homes, schools, greenhouses, and other structures and also for the heating of swimming pools, fish hatcheries, or soil beds. These uses are best suited for application by means of a heat exchanger to transfer the geothermal heat. The geothermal water located in the study area, in most cases possess higher salt and mineral deposits than can safely be utilized directly, for example, Berry Ranch Hot Spring possesses 905 ppm dissolved solids and Crump Lake hot springs possesses 662 ppm dissolved solids (Phillips and Van Denburgh, 1971). Therefore, uses of the geothermal waters should occur in the form of indirect applications.

Any area which lies within the 80° C isotherm can be supplied with geothermal water hot enough for home heating. The techniques for utilizing the water were discussed earlier in Chapter Two. These may vary, including either a direct flow of the geothermal water

through a pipe network in the dwelling floor, or a simple conductive heat exchange into a fresh water closed-system with radiators.

Other potential uses depicted in Table 18 relate to agriculture. Geothermal waters are being successfully used in a year-round greenhouse just north of Lakeview. The geothermal water is used to heat air in the greenhouse. The water is conveyed through pipes buried in the ground to warm the soil environment. This protects the plants' root structure, aiding the plants' growth and well being.

The use of the hot water for bathing has occurred in the past at both Lakeview and at the motel east of Cedarville, California. The prior use was discontinued some years ago, while the latter application has only recently been discontinued. Arsenic levels in the water were too high for safe exposure. However, if the pool were to utilize strictly the heat from the water, via a heat exchanger, this health problem could be eliminated.

The potential for utilizing the hydro-geothermal resource in the study area is quite significant. The principal study area towns of Lakeview, Alturas, Cedarville, Ft. Bidwell, and Canby all lie within access of 80^{o} C or warmer geothermal waters. Nevertheless, very few structures yet utilize the resource for space heating, and only one year-round greenhouse is in operation.

Review

The analysis of the potential application for the hydrogeothermal resource was made directly from the map product of this research. Figure 49 is the result of SLAR and TIR imagery interpretation in an area where the surface expressions of hydrogeothermal phenomena were known to be related to the fracturing and faulting of geologic materials. Utilizing a realistic estimated temperature decay factor, concentric isotherms were constructed delineating areas of equal temperature supply. These isotherms were utilized, along with a known temperature-application relationship, to evaluate the potential uses for the resource. This resource potential can and should be considered in future cultural development in the Northern Basin and Range province.

VIII. SUMMARY AND CONCLUSIONS

Summary

The need for developing alternate energy sources is a political, economic, and social concern of many nations. Geothermal energy could provide one such source. Restricted by its geographic location, this energy resource must be developed and utilized in relatively close proximity to its origin.

Study Area

The Northern Basin and Range physiographic province has been geologically active since the Miocene epoch. Vulcanism was followed by Pleistocene and post-Pleistocene sedimentation. The extension of the substratum beneath the Basin and Range province creates the surface structure exhibited in the Great Basin, i.e., tilted fault blocks, horsts and grabens, and internally drained basins (Stewart, 1971). Two fault trends have been identified in the study area; NE-SW and NW-SE. The NE-SW trending faults have been identified to be normal faults with large vertical displacement of 500 meters or more, e.g., Abert Rim. The area is dominated, however, by many scarplets of lesser vertical displacement. These smaller faults are strike-slip in nature and trend NW-SE. Lawrence (1976) identified two zones of strike-slip faults that extend across a portion of the

study area. These zones produce a right lateral offset of 10-20 kilometers. Donath (1962) noted that no one trend consistently offset the other. Thus, he concluded that movement along each set of faults was concurrent and that the fault trends were contemporaneous in origin.

The study area included the northernmost part of the Basin and Range Province, i.e., the Great Basin of southern Oregon/northern California. This area contains a great deal of hydro-geothermal activity, such as hot springs and geysers. The locations of these surface manifestations are known to be structurally dependent upon the subsurface geology. The faults serve as transport routes for water heated within the earth's crust. Therefore, the exploration for surface hot springs and geysers should be confined to the periphery of the fault lineaments observable within the study area boundary.

Conclusions

SLAR

The use of SLAR for delineating the surface expressions of faults and other similar features produced 26 percent more structural lineaments than previous Landsat analysis and 12 percent more than existent geologic mapping. Major expressions of 500 meters vertical displacement or more, such as Abert Rim, were easily observed on all three data products and topographic maps. The SLAR imagery

allowed for more frequent interpretation of the many smaller scarplets existing in the study area. The interpretation of these surface expressions of lesser vertical displacement is a major advantage of SLAR imagery.

The acquisition of the imagery in strip form with non-continuous side-overlap proved to be quite labor intensive. The utilization of the SLAR imagery in generating a final map product required the matching of adjacent flightlines manually and scale-distortion adjustments by means of the photographic enlarger and a Zoom Transfer Scope. These scale-distortion characteristics are inherent in imagery acquired by aircraft-sensor combinations that do not adjust for variable ground speed or for altitude variations of the aircraft.

The near instantaneous recording of the transmitted signal produced a seven-and-a-half kilometer wide area on either side of the ground track where image distortion occurred. This area provided the lowest density of interpreted surface expressions. At the center of the distortion, a void area or altitude window was superimposed on the imagery by the sensor. This window created an inferred terrain profile that was used to interpret the surface lineaments where they crossed the ground track. When sufficient side-overlap of the adjacent flightlines occurred, one flightline complemented the adjacent area of distortion. However, when overlap was non-existent, void areas of image interpretation were created. These areas

produced blank areas on the lineament map inferring the areas to have relatively low density lineament occurrence.

TIR

Analysis of the thermal infrared imagery located one new potential hydro-geothermal site and allowed a more accurate designation of geographic coordinates for five other sites than were provided in previous studies. Location was more easily accomplished through the use of a dual channel sensor system. Four of the hot springs were found to exist outside the areas designated as Known Geothermal Resource Areas (KGRA's), established by the U. S. Geological Survey.

The mercury-cadmium-telluride (8-14 μm) imagery, as proposed by Valle et al. (1970), did not distinguish between the various water temperatures. The hotter temperatures of the hydro-geothermal sources were equal in gray scale brightness to that of the cooler lake temperatures. This was apparent on the single channel mercury-cadmium-telluride imagery of both Crump Lake and Kelley Hot Springs.

Heat variations on the mercury-cadmium-telluride imagery were inferred by the streaking on the imagery created by sensor saturation. An example of this was observed on Figure 38. The revolving drum of the detector streaked the imagery when ample

cooldown did not result after sensing a hot target. Frequently the streaking can be utilized to locate the hydro-geothermal site.

As has been suggested by numerous studies, the mercury-cadmium-telluride detector depicts all surface radiation (terrestrial) and is helpful in relating the imaged surface to the actual geographic location. The detector produced pseudo-photographic images on which the various terrain features were identified. This imagery, in association with available topographic maps, was used for relating the imagery to the actual surface location.

The mercury-cadmium-telluride detector was utilized in locating both the seeps near Crump Geyser and an unnamed stream with eleven sources on the east side of the Upper Alkali Lake. These sources were easily identified as water bodies, but their actual identification as hydro-geothermal sites required ground truthing.

The indium arsenide detector (1-3.4 μm) produced imagery which depicted the greater levels of IR radiation created by the hotter surface targets (generally over 50° C). The examination of the hot spring area near the Mineral Wells Motel proved the advantage of using the indium arsenide detector for determining accurate hot spring location and the extent of its size. The detector's wavelength sensitivity creates this characteristic. The use of this sensor is indicated when a more accurate view of the size and extent of the hotter temperature water source is desired.

The indium arsenide detector does not sense in the wavelengths generated by the earth's surface radiation and therefore, geographic location is difficult to obtain. Logically, therefore, this sensor is not advisable for use in a single channel mode unless exact geographic location is not an objective.

As presented earlier in this research, the indium antimonide detector (1-6 μm) exhibits partial traits of both the mercury-cadmium-telluride and indium arsenide detectors. Thus, the surface characteristics are visible, while the sensor images targets of higher temperatures and radiation. The examination of Kelley Hot Springs with the indium antimonide detector provided a better view of the hot spring than with the mercury-cadmium-telluride detector. The indium arsenide sensed less of the vapor plume and thus presented a clearer image.

This research was not conclusive in determining which sensor or sensor combination was best suited for locating hydro-geothermal sources. Equipment malfunction, weather conditions, and general uncontrollable problems prohibited the acquisition of significant imagery combinations for analysis. However, through the analysis of the imagery, of the sensor characteristics, and of the hot spring temperatures, this research suggests that the indium antimonide detector be utilized when a single channel sensor is to be used. Both geographic location and the warmer targets are identifiable from this sensor. To achieve the best possible analysis of the imaged radiation

levels, a two channel system utilizing the indium antimonide and indium arsenide detectors is suggested by this research. The indium antimonide can be used for geographic location and the indium arsenide detects the hotter hydro-geothermal anomalies. Confirmation of these suggestions must occur through further research with ample sample combinations.

From the ground truthing data obtained at the moment of overflight, the most ideal time to obtain thermal infrared imagery is in the pre-dawn hours. Just as concluded by Hodder (1970), Moxham (1969), and Valle, Friedman, Gawarecki, and Banwell (1970), the decline in soil surface temperature and mixing ratio, as dawn approaches, in conjunction with constant hydro-geothermal temperatures, produced optimum conditions for data acquisition.

Thermal infrared sensors depict variations in temperatures (emitted radiation) of the water body surface. Since the sensors do not penetrate the water surface, the evaluation of the number and location of individual hot spring sources within a pool is not feasible, except as those locations affect the surface temperature. The use of a dual channel system including the indium arsenide detector gave the most accurate TIR surveying technique for locating hotter hydro-geothermal surface expression. The shorter peak wavelength sensitivity of the indium arsenide detector did not allow for the detection of surface steam and thus produced sharper resolution of the imaged

surface. The indium antimonide and mercury-cadmium-telluride detectors, peaking at longer wavelength values, did not produce this clarity in resolution.

The fusee road flares were helpful to the pilots in verifying their ground track. However, the flares did not always show up on the imagery as a result of the sensor configuration and the flare's variable emitted radiation levels. The flares were imaged most often on the indium arsenide, sporadically on the indium antimonide, and rarely on the mercury-cadmium-telluride. Therefore, the use of the imaged flares for evaluating scale and temperature was ineffective.

Temperature Estimation Via Density

The attempt to analyze the imagery according to its various gray scale levels, i.e., density, was inconclusive. The instrumentation utilized in the research proved to be the limiting factor. The Welch Densichron Photometer required manual operation and possessed a large diameter aperture. The one millimeter diameter aperture did not produce instrument sensitivity conducive to the proper evaluation of the density of the TIR imagery.

Pre-flight calibration of the aircraft's sensors became useless when the detector's gain and contrast settings were re-adjusted manually in-flight. The resulting temperature-density distribution

(Figure 48) of an individual detector was inconclusive. The figure did, however, graphically depict the detector's response sensitivity to the emitted energy. The mercury-cadmium-telluride (8-14 μm) detector sensing in wavelengths more closely aligned to the wavelengths of the emitted energy (7.89-8.57 μm) consistently produced larger density values than the indium arsenide (1-3.4 μm) which senses at a shorter wavelength.

The objective of relating density to temperature was not achieved. Further research in which the re-adjustment of pre-calibrated sensors be forbidden in-flight and the use of a highly sensitive scanning type microdensitometer should produce the desired results.

Ground Truthing

The evaluation of SLAR and TIR imagery identified the potential hydro-geothermal surface expressions and structural lineaments. The hydro-geothermal sources were more readily identifiable through the use of a dual channel combination of indium arsenide and either the indium antimonide or mercury-cadmium-telluride sensors. Single channel sensors either failed to separate higher radiation sources from the cooler, lower radiation sources, or they failed to provide necessary terrain information for adequately relating to geographic location.

Ground truthing of the hydro-geothermal sites was required after imagery analysis. The on-site examination was required in order to verify that the site of high IR radiation was actually a hydro-geothermal surface expression, and not just a campfire or other similar heat source. More ground truthing was required when using a single sensor than when using the dual channel combination.

The complementary use of the SLAR and dual channel TIR imagery proved useful in locating the potential hydro-geothermal sites. However, the need for ground truthing for site and temperature determination was not eliminated by the use of that imagery.

Map Product

The map produced from the SLAR and TIR imagery analysis graphically depicts the relationship of the hydro-geothermal hot springs and geysers, found along the TIR flightlines, to the geologic structure implied by the lineaments. The sub-surface fault and fracture traces serve as transport routes to the surface for the geothermal waters.

The initial selection of TIR flightlines should be made along the major lineaments analyzed from SLAR or Landsat imagery or from topographic maps. The majority of hydro-geothermal sites were found to lie in close proximity to the lineaments of large vertical displacement.

The selection of TIR flightlines, however, should not be made strictly from the SLAR analysis. Prior knowledge of the area is useful in establishing the TIR flightlines. The known location of an existing hot spring is beneficial in determining which lineament should be flown. A clustering of hot springs was observed in the study area. Rarely was a single isolated hot spring found. Almost always, other hot springs existed along the same or adjacent lineament.

Three of the four major hot spring clusters (Lakeview, Crump Lake, and Middle Alkali Lake) were found to exist along the periphery of deeply filled grabens. Not always were the lineaments observable in the grabens, a result of the fault trace being covered by the valley sediment. Whenever the grabens lie adjacent to major lineaments, they should be considered for TIR overflights. The hot springs in the study area were found to lie relatively close to the major fault scarps, as well as directly on them.

Utilizing an estimated temperature decay function, isothermal rings were established. Within the isotherms, water of consistent temperature could be supplied via insulated pipes. The land area that could be supplied with 70^{o} C temperature water or hotter has great potential for utilizing the geothermal resource. Except for the extreme northern end of the study area and the land between Abert Rim and Poker Jim Ridge, all of the study area can potentially receive 70^{o} C temperature water. The area within the 80^{o} C isotherm

can be supplied with water with a temperature ideal for space heating and other uses. This research suggests the principle use of the hydro-geothermal resource in the study area is for space heating of homes and other structures, as well as for space heating and soil warming for year around agricultural production in greenhouses.

No hydro-geothermal source temperatures above 94° C were found in the study area. The lower water surface temperatures indicate that the geothermal sites are of the Hot-Water dominated system. Renner, White, and Williams (1975) and Nathenson and Muffler (1975) report potential electrical production from the reservoir storage near Surprise Valley, Lakeview, and Crump Spring. However, the surface water temperatures recorded in this research suggest the hydro-geothermal sites fall in the middle (90-150° C) to lower (less than 90° C) divisions of the Hot-Water System. These lower surface temperatures indicate that the hot springs and geysers located by the complementary use of SLAR and TIR imagery do not represent surface anomalies that indicate geothermal electrical potential in this portion of the Great Basin. However, through the use of the reservoir potential, electrical production by a binary means is feasible. The heated geothermal water may be utilized in conjunction with other forms of electrical generation.

Although the remote sensing survey of surface hydro-geothermal sites failed to show heat potential for near surface direct

electrical production, the thermo-structural relationship mapped may serve along with other geophysical techniques to direct subsurface exploration of the resource. Structural lineaments and hydrogeothermal source locations can be determined through the complementary use of SLAR and TIR. Once potential locations are determined, limited ground truthing would be required to verify the remotely sensed data. Such a reconnaissance tool may be of greatest value in a less developed area with similar geologic structure and geothermal promise.

BIBLIOGRAPHY

Alexander, Larry et al. 1974. "Remote Sensing Environmental and Geotechnical Applications: The State of the Art." Dames and Moore Engineering Bulletin. Los Angeles.

Allison, Ira S. 1949. "Fault Patterns of South-Central Oregon." Geological Society of American Bulletin 60:1935 (Abstract).

Anderson, David N. and L. H. Axtell (eds.) 1972. Compendium of First Day Papers Presented at the First Conference of the Geothermal Resource Council. El Centro, California.

Baker, Ralph N. 1975. "Landsat Data: A New Perspective for Geology." Photogrammetric Engineering 41(10):1233-1239.

Banwell, C. J. 1972. "Geophysical Techniques in Geothermal Exploration." Geothermics. Special Issue 2(1):52-57.

Barnea, J. 1972. "Geothermal Power." Scientific American 226(1): 70-77.

Barr, David J. and Robert D. Miles. 1970. "SLAR Imagery and Site Selection." Photogrammetric Engineering 36:1155-1170.

Bastuscheck, C. P. 1970. "Ground Temperature and Thermal Infrared." Photogrammetric Engineering 36:1064-1072.

Birdseye, H. S. 1969. "Geothermal Power Resources in the Southwest." Bureau of Mines and Mineral Resources, New Mexico. Circular 101:86-96.

Blackwell, David D. and Czang-go Baag. 1973. "Heat Flow in a 'Blind' Geothermal Area Near Marysville, Montana." Geophysics 38(5):941-956.

Blanchard, Maxwell B., Ronald Greeley and Robert Goettelman. 1974. "Use of Visible, Near-Infrared, and Thermal Infrared Remote Sensing to Study Soil Moisture." International Symposium on Remote Sensing of Environment, Ninth Proceedings: 693-700.

Blodget, H. W. and A. T. Anderson. 1973. "A Comparison of Gemini and ERTS Imagery Obtained Over Southern Moroco." Symposium of Significant Results Obtained from ERTS-1, Technical Presentations 1:265-272.

Bodvarsson, Gunnar. 1966. "Energy and Power of Geothermal Resources." Ore Bin. 28(7):117-124.

_____. 1970. "Evaluation of Geothermal Prospects and the Objectives of Geothermal Exploration." Geoexploration 8(1):7-17.

Bowen, R. G. 1971. "Electricity from Geothermal, Nuclear, Coal Sources: An Environmental Comparison." Ore Bin. 33(11): 197-209.

_____. 1972. "Geothermal Activity in 1971." Ore Bin. 34(1):12-14.

Bowen, R. G. and N. V. Peterson. 1970. Thermal Springs and Wells in Oregon. Portland: Dept. of Geology and Mineral Industries. Miscellaneous Paper 14.

Brennan, Peter A., Peter E. Chapman and Eddie R. Chipp. 1971. Remote Sensing Evaluation of the Klondike Mining District, Nevada. Reno: NASA Report 73-14371.

Broili, Christopher J. 1974. Technical Report on Geothermal Energy Development in South-Central Oregon, Northeastern California, and Northwestern Nevada. U. S. Dept. of Interior, Bureau of Lands Management.

Brooks, F. A. 1959. An Introduction to Physical Microclimatology. Davis: University of California Press.

Buckman, Harry O. and Nyle C. Brady. 1960. (6th ed.). The Nature and Properties of Soils. New York: The Macmillan Co.

Bunge, Brian. 1976. Personal interview with Mr. Bunge. He is a SLAR maintenance technician with the 1042 Military Intelligence Company of the Oregon Army National Guard.

Byers, Horace R. 1959. General Meteorology. New York: McGraw-Hill Book Co.

California Department of Water Resources. 1974. Water and Power from Geothermal Resources in California: An Overview. The Resources Agency. Bulletin No. 190.

Cameron, H. L. 1964. "Radar as a Surveying Instrument in Hydrology and Geology." International Symposium on Remote Sensing of Environment, Third Proceedings: 441-452.

Cannon, P. Jan. 1964. "Application of Radar Imagery to Environmental Geologic Mapping of Texas." International Symposium on Remote Sensing of Environment, Ninth Proceedings: 1981-1988.

Cantrell, J. L. 1964. "IR Geology." Photogrammetric Engineering 30:916-922, 941.

Cassinis, R., C. M. Marino and A. M. Tonelli. 1970. "Ground and Airborne Thermal Imagery on Italian Volcanic Areas." U. N. Symposium on the Development and Utilization of Geothermal Resources, Proceedings: 413-419.

Chang, Jen-Hu. 1958. Ground Temperature. Milton, Mass.: Harvard University, Blue Hill Meterological Observatory.

Colwell, Robert N. 1968. "Remote Sensing of Natural Resources." Scientific American 218(1):54-69.

Cook, Earl. 1976. Man, Energy, Society. San Francisco: W. H. Freeman and Co.

Coulson, Kinsell L. 1975. Solar and Terrestrial Radiation: Methods and Measurement. New York: Academic Press.

Crosby, J. W. 1971. "Geothermal Exploration." First NW Conference on Geothermal Power. Olympia, Washington.

Delwig, Louis F., Harold C. MacDonald and J. Norman Kirk. 1968. "The Potential of Radar in Geological Exploration." International Symposium on Remote Sensing of Environment, Fifth Proceedings: 747-763.

Denton, Jesse C. (ed.). 1972. Geothermal Energy. Washington, D. C.: U. S. Government Printing Office.

Donath, Fred A. 1962. "Analysis of Basin-Range Structure, South-Central Oregon." Geological Society of America, Bulletin 73: 1-16.

Donath, Fred A. and John T. Kuo. 1962. "Seismic Refraction Study of Block Faulting, South-Central Oregon." Geological Society of America, Bulletin 73:429-434.

Dragone, G. and O. Rumi. 1970. "Pilot Greenhouse for the Utilization of Low-Temperature Waters." U. N. Symposium on the Development and Utilization of Geothermal Resources, Proceedings: 918-920.

Duffield, Wendal A. and Robert O. Fournier. 1974. Reconnaissance Study of the Geothermal Resources of Modoc County, California. Menlo Lark: U.S.G.S. Open File Report.

Engineers Design Handbook: Infrared Military Systems: Part 1. 1971. AMC Pamphlet No. 706-127.

Estes, John E. 1966. "Some Geographic Applications of Aerial Infrared Imagery." International Symposium on Remote Sensing of Environment, Fourth Proceedings: 173-181.

Estes, John E. and Leslie W. Senger. 1974. Remote Sensing: Techniques for Environmental Analysis. Santa Barbara: Hamilton Publishing Co.

Facca, G. 1971. "The Status of World Geothermal Development." Geothermics. Special Issue 2:8-23.

Fischer, William. 1962. "An Application of Radar to Geological Interpretation." International Symposium on Remote Sensing of Environment, First Proceedings: 83-84.

Fleagle, Robert G. and Joost A. Businger. 1963. An Introduction to Atmospheric Physics. New York: Academic Press.

Freden, Stanley C. and Enrico P. Mercanti. 1973. Symposium on Significant Results Obtained from the Earth Resources Technology Satellite-1. Volume 1. Washington, D. C.: N.A.S.A.

Friedman, Jules D., David G. Frank, Duane Preble, and Earle J. Painter. 1973. "Thermal Surveillance of Cascade Range Volcanoes Using ERTS-1 Multispectral Scanner, Aircraft Imaging Systems, and Ground-Based Data Communication Platforms." Symposium on Significant Results Obtained from the Earth Technology Satellite-1. Volume 1:1549-1560.

Friedman, Jules D. and R. S. Williams. 1968. "Infrared Sensing of Active Geologic Processes." International Symposium on Remote Sensing of Environment, Fifth Proceedings: 787-815.

Fuller, Richard E. and Aaron Clement. 1929. "The Nature and Origin of the Horst and Graben Structure of Southern Oregon." Journal of Geology 37:204-238.

Geothermal Steam Act of 1970. Public Law 91-581.

Goetz, Alexander F. H. et al. 1973. "Preliminary Geologic Investigations in the Colorado Plateau Using Enhanced ERTS-1 Images." Symposium on Significant Results Obtained from the Earth Technology Satellite-1. Volume 1:403-411.

Goodwin, L. H., L. B. Haigler et al. 1971. Classification of Public Lands Valuable for Geothermal Steam and Associated Geothermal Resources. U.S.G.S. Circular 647.

Griggs, M. 1968. "Emissivities of Natural Surfaces in the 8-14 Micron Spectral Region." Journal of Geophysical Research 73(24):7545-7551.

Groh, Edward A. 1966. "Geothermal Energy Potential in Oregon." Ore Bin. 28(7):125-135.

Harris, E. E., C. O. Woodbridge and L. Casper. 1964. "Terraine Mapping by Use of IR Radiation." Photogrammetric Engineering 30:134-139.

Harthill, Norman. 1971. "Geophysical Prospecting for Geothermal Energy." Mines Magazine 60(6):13-18.

Hase, H. 1971. "Surface Heat-Flow Studies for Remote Sensing of Geothermal Resources." Japanese Society for Photogrammetry Journal 10(3):9-17.

Head, J. 1970. "Geothermal Energy for Greenhouse Heating." Ore Bin. 32(9):182-183.

Healy, J. 1970. "Pre-Investigation Geological Appraisal of Geothermal Fields." U. N. Symposium on the Development and Utilization of Geothermal Resources, Proceedings: 571-577.

Hewlett, John D. and Wade L. Nutter. 1969. An Outline of Forest Hydrology. Athens: University of Georgia Press.

Hodder, D. T. 1970. "Application of Remote Sensing to Geothermal Prospecting." U. N. Symposium on the Development and Utilization of Geothermal Resources, Proceedings: 368-380.

Hoppin, Richard A. 1973. "Structural Interpretations on ERTS-1 Imagery, Bighorn Region, Wyoming-Montana." Symposium on Significant Results Obtained from the Earth Technology Satellite-1: 531-538.

Jaeger, J. C. and C. H. Johnson. 1953. "Note on Diurnal Temperature Variation." Pure and Applied Geophysics 24:104-106.

Jenkins, Olaf P. (ed.). 1968. Geologic Map of California, Alturas Sheet. San Francisco: Dept. of Natural Resources, Division of Mines, State of California.

Kappelmeyer, O. and R. Haenel. 1974. "Geothermics with Special References to Application" in Geoexploration Monographs, Series 1(4). Berlin: Gebruder Borntraeger.

Karr, Don. 1976. "Uses of Geothermal Resources." Oral presentation given at Oregon State University on October 21, 1976.

Kiersch, G. A. and L. N. Chaturvedi. 1968. Geologic Structure and Its Effects on the Geothermal Hydrology of Southwestern Hreppar, Iceland. Cornell Water Resources and Marine Sciences Center.

Koenig, J. 1970. "Geothermal Exploration in the Western U.S." Geothermics. Special Issue 2, Vol. 2(1):1-13.

Kruger, Paul and Carel Otte (eds.). 1973. Geothermal Energy; Resources, Production, Stimulation. Stanford: Stanford University Press.

Kruse, Paul W., Laurence D. McGlauchlin and Richmond B. McQuistan. 1962. Elements of Infrared Techniques: Generation, Transmission, and Detection. New York: John Wiley and Sons.

LaPrade, George L. and Earl S. Leornado. 1969. "Elevations from Radar Imagery." Photogrammetric Engineering 35:366-371.

Lattau, Heinz. 1954. "Improved Models of Thermal Diffusion in the Soil." American Geophysical Union, Transactions 35(1):121-132.

Lattman, L. H. 1958. "Techniques of Mapping Geologic Fracture Traces and Lineaments on Aerial Photographs." Photogrammetric Engineering 24:568-576.

Lawrence, Robert D. 1974. Lineament Map of Oregon Using ERTS-1 Imagery. Portland: U.S.G.S. Open File Report.

_____. 1976. "Strike-slip Faulting Terminates the Basin and Range Province in Oregon." Geological Society of America, Bulletin 87:846-850.

Lawrence, Robert D. and James H. Herzon. 1975. "Geology and Forestry Classification from ERTS-1 Digital Data." Photogrammetric Engineering 41(10):1241-1251.

Lietzke, Keith R. 1974. The Economic Value of Remote Sensing of Earth Resources from Space: An ERTS Overview and the Value of Continuity of Service. Princeton: N.A.S.A. Report N75-14212.

Lowry, William P. 1969. Weather and Life. New York: Academic Press.

MacDonald, H. C. 1969. "Geologic Evaluation of Radar Imagery from Darien Province, Panama." Modern Geology 1:63.

MacDonald, H. C., J. N. Kirk, L. F. Delwig, and A. J. Lewis. 1969. "The Influence of Radar Look-Direction on the Detection of Geologic Features." International Symposium on Remote Sensing of Environment, Sixth Proceedings: 637-650.

MacDonald, W. J. P. and L. J. P. Muffler. 1972. "Recent Geophysical Exploration of the Kawerau Geothermal Field, North Island, New Zealand." New Zealand Journal of Geology and Geophysics 15(3):303-317.

Matsuno, K., H. Hase and K. Nishimura. 1969. "On IR Imagery and Its Applications to Mapping Geothermal Distributions." Photogrammetria 25(2/3):61-74.

Maul, George A., Robert Charnell and Robert H. Qualset. 1974. "Computer Enhancement of ERTS-1 Images for Ocean Radiances." Remote Sensing of Environment 3:237-253.

McAnerney, J. M. 1966. "Terraine Interpretation from Radar Imagery." International Symposium on Remote Sensing of Environment, Fourth Proceedings: 731-750.

McLerran, James H. and Joseph D. Morgan. 1964. "Thermal Mapping of Yellowstone National Park." International Symposium on Remote Sensing of Environment, Third Proceedings: 517-530.

McLerran, James H. 1967. "Infrared Thermal Sensing." Photogrammetric Engineering 33:507-512.

McNitt, J. R. 1970. "The Geologic Environment of Geothermal Fields as a Guide to Exploration." Geothermics. Special Issue 2:24-31.

Meadows, Katherine F. (ed.). 1972. Geothermal World Directory. Glendora, California.

Miller, Glen R. 1975. Vegetation and Land Use Map: Warner Valley, Oregon. Corvallis: Environmental Remote Sensing Applications Laboratory (ERSAL), Oregon State University.

Moore, Donald G. and Victor I. Myers. 1973. "Location of Flowing Artesian Wells and Natural Springs Using Thermal Infrared Imagery." American Society of Photogrammetry Symposium, Proceedings: 159-165.

Morgan, Joseph. 1962. "Infrared Technology." International Symposium on Remote Sensing of Environment, First Proceedings: 45-59.

Morgan, Joseph and V. L. Prentice. 1966. "Third Symposium on Remote Sensing." Photogrammetric Engineering 32(1):98-108.

Morrison, Roger B. 1965. "Quaternary Geology of the Great Basin." Found in: Wright, H. E., Jr. and David G. Frey (eds.). The Quaternary of the United States. Princeton: Princeton University Press. pp. 265-285.

Moxham, R. H. 1969. Aerial Infrared Surveys at the Geysers Geothermal Steam Field. U.S.G.S. Professional Paper 650-C.

_____. 1970. "Thermal Features at Volcanoes in the Cascade Range, as Observed by Aerial Infrared Surveys." Bulletin Volcanologique 34:77-106.

Moxham, R. H., G. W. Greene, J. D. Friedman, and S. J. Gawarecki. 1967. Infrared Imagery and Radiometry: Summary Report. N.A.S.A. Interagency Report, N.A.S.A.-105.

Mundorff, J. C. 1970. "Major Thermal Springs of Utah." Utah Geological and Mineralogical Survey Water Resources Bulletin 13.

Nathenson, M. and L. J. P. Muffler. 1975. "Geothermal Resources in Hydrothermal Convective Systems and Conduction-Dominated Areas." Found in: White, D. E. and D. L. Williams. Assessment of Geothermal Resources of the United States. pp. 104-121.

N.A.S.A. 1971. Data Users Handbook. Greenbelt, Maryland: Goddard Space Flight Center.

Norman, J. W. 1970. "Linear Geological Features as an Aid to Photogeological Research." Photogrammetrics 25(5/6):177-187.

Office of Arid Lands Studies. 1973. Exploration and Exploitation of Geothermal Resources in Arid and Semiarid Lands: A Literature Review and Selected Bibliography. Tucson: University of Arizona, Arid Lands Resource Information Paper Number 2.

ORNG. 1976. Personal interviews conducted with various personnel of the Oregon Army National Guard.

Pease, Robert W. and Claude W. Johnson. 1973. "A New Fault Lineament in Southern California." Symposium on Significant Results Obtained from the Earth Resources Technology Satellite-1: 547-552.

Peterson, Norman V. 1959a. "Preliminary Geology of the Lakeview Uranium Area, Oregon." Ore Bin. 21(2):11-16.

_____. 1959b. "Lake County's New Continuous Geyser." Ore Bin. 21(9):83-88.

Peterson, Norman and Edward Groh. 1969. "Geothermal Potential of Klamath Falls Area, Oregon." Ore Bin. 29(11):209-231.

Peterson, Norman V. and James R. McIntyre. 1970. The Reconnaissance Geology and Mineral Resources of Eastern Klamath County and Western Lake County, Oregon. Portland: Oregon Department of Geology and Mineral Industries, Bulletin 66.

Petterssen, Sverre. 1958. Introduction to Meteorology. (2nd ed.). New York: McGraw-Hill Book Co.

Phillips, Kenneth N. and A. S. VanDenburgh. 1971. Hydrology and Geochemistry of Abert, Summer, and Goose Lakes, and Other Closed-Basin Lakes in Southcentral Oregon. Portland: U.S.G.S. Professional Paper 502-B.

Raschen, Rory and William S. Cook. 1976. Exploration and Development of Geothermal Resources. Menlo Park: U.S.G.S., Conservation Division. (An Internal Working Document.)

Reeves, Robert G. (ed.). 1975. Manual of Remote Sensing. Falls Church: American Society of Photogrammetry.

Reifsnyder, William E. and Howard W. Lull. 1965. Radient Energy in Relation to Forests. U. S. Department of Agriculture, Technical Bulletin No. 1344. U. S. Forest Service.

Reistad, Gordon M. 1976. Personal interview conducted with Dr. Gordon M. Reistad, Assistant Professor, Mechanical Engineering, Oregon State University, Corvallis, Oregon.

Renner, J. L., D. E. White and D. L. Williams. 1975. "Hydrothermal Convective Systems." Found in: White, D. E. and D. L. Williams. Assessment of Geothermal Resources of the United States. pp. 5-57.

Rex, Robert W. 1974. "Economics of Geothermal Development." Ore Bin. 36(2):17-22.

Robinove, Charles J. 1968. "The Status of Remote Sensing Hydrology." International Symposium on Remote Sensing of Environment, Fifth Proceedings: 827-831.

Rose, C. W. 1966. Agricultural Physics. New York: Pergamon Press.

Rosenfeld, Charles L. and Thomas W. Hodler. 1976. "Hydro-Geothermal Reconnaissance Utilizing Remote Sensing Techniques." Pacific Northwest Meetings of American Geophysical Union, Proceedings. (Abstract).

Rosenfeld, Charles L. and H. G. Schlicker. 1976. "The Significance of Increased Fumarolic Activity at Mount Baker, Washington." Ore Bin. 38(2):23-35.

Rowan, L. C. 1973. "Near-Infrared Iron Absorption Bands: Applications to Geologic Mapping and Mineral Exploration." Fourth Annual Earth Resources Program Review. N.A.S.A. 3:60-1 to 60-12.

Rowan, L. C. and P. H. Wetlaufer. 1973. "Structural Geologic Analysis of Nevada Using ERTS-1 Images: A Preliminary Report." Symposium on Significant Results Obtained from the Earth Resources Technology Satellite-1. Volume 1:412-423.

Russell, I. C. 1884. "A Geologic Reconnaissance in Southern Oregon." U.S.G.S. Annual Report Number 4:431-464.

Russell, Richard Joel. 1927. "The Land Forms of Surprise Valley, Northwestern Great Basin." University of California Publications in Geography 2(11):323-358.

_____. 1928. "Basin and Range Structure and Stratigraphy of the Warner Range, Northeastern California." University of California Publications in Geological Sciences 17(11): 387-496.

Rydstrom, Hubert O. 1966. "Interpreting Local Geology from Radar Imagery." International Symposium on Remote Sensing of Environment, Fourth Proceedings: 193-201.

Sabins, F. F. 1967. "Infrared Imagery and Geology Aspects." Photogrammetric Engineering 33:743-750.

_____. 1969. "Thermal Infrared Mapping and Its Application to Structural Mapping in Southern California." Geological Society of America, Bulletin 80(3):397-404.

Scarpace, F. L., R. P. Madding and T. Green, III. 1974. "Scanning Thermal Plumes." International Symposium on Remote Sensing of Environment, Ninth Proceedings: 939-961.

Sellers, William D. 1965. Physical Climatology. Chicago: University of Chicago Press.

Skiles, J. J., T. A. Grzelak and R. S. Dixon. 1962. "An Airborne Instruction System for Microwave and Infrared Radiometry." International Symposium on Remote Sensing of Environment, Second Proceedings: 175-185.

Stearns, Norah D., Harold T. Stearns and Gerald A. Waring. 1937. "Thermal Springs in the United States." U.S.G.S. Water Supply Paper 679-B:55-206.

Steffenson, Roberto. 1973. "Structural Lineaments of Gaspe' from ERTS Imagery." Symposium on Significant Results Obtained from the Earth Resources Technology Satellite-1. Volume 1: 501-515.

Steiner, Dieter. 1974. "Digital Geometric Picture Correction Using a Piecewise Zero-Order Transformation." Remote Sensing of Environment 3:261-283.

Stewart, J. H. 1971. "Basin and Range Structure: A System of Horsts and Grabens Produced by Deep-Seated Extensions." Geological Society of America, Bulletin 82:1019-1044.

Stingelin, Ronald W. 1969. "Operational Airborne Thermal Imaging Surveys." Geophysics 34(5):760-771.

Stone, Kirk H. 1974. "Developing Geographical Remote Sensing." Found in: Estes, John E. and Leslie W. Senger. Remote Sensing: Techniques for Environmental Analysis: 1-13.

Strangway, D. W. and R. C. Holmer. 1964. "Infrared Geology." International Symposium on Remote Sensing of Environment, Third Proceedings: 293-319.

Summers, W. K. 1971. Annotated and Indexed Bibliography of Geothermal Phenomena. Socorro: State Bureau of Mines and Mineral Resources, New Mexico.

Summers, W. K. and S. H. Ross. 1971. "Geothermics in North America: Present and Future." Earth Science Bulletin 4(1): 7-22.

Suomi, V. E. and P. M. Kuhn. 1958. "An Economical Net Radiometer." Tellus X.1:160-163.

Thompson, F. J. and N. E. G. Roller. 1973. "Terrain Classification Maps of Yellowstone National Park." Symposium on Significant Results Obtained from the Earth Resources Technology Satellite-1. Volume 2: 1091-1096.

Thornbury, William D. 1965. Regional Geomorphology of the United States. New York: John Wiley and Sons, Inc.

United Nations Symposium on the Development and Utilization of Geothermal Resources, Proceedings. 1970. Piza, Italy.

U. S. Bureau of Lands Management. 1975. Environmental Analysis Record: Surprise, Warner, and Long Valleys (Proposed Geothermal Leasing). Department of the Interior.

_____. 1976. Summer Lake Basin Geothermal Leasing Environmental Analysis Record. Department of the Interior.

U. S. Department of Commerce. 1970. Census of Population, Number of Inhabitants. Bureau of the Census.

U. S. Department of Interior. 1973. Final Environmental Statement for the Geothermal Leasing Program. 4 Volumes. Washington, D.C.: U. S. Government Printing Office.

U. S. Forest Service. 1975. Geothermal Development-Breitenbush Area Environmental Statement, Draft. 2 Volumes. In-Service Use Only. Willamette National Forest and Mt. Hood National Forest.

U. S. Geological Survey. 1974. Geysers. Washington, D. C.: U. S. Government Printing Office, Department of Interior.

Valde, Gary. 1973. Resources Atlas: Lake County, Oregon. Corvallis: Oregon State University Extension Service.

Valle, R. Gomez, J. D. Friedman, S. J. Gawerecki, and C. J. Banwell. 1970. "Photogeologic and Thermal Infrared Reconnaissance Surveys of the Los Negritos-Ixtlan De Las Hervores Geothermal Area, Michoacan, Mexico." U. N. Symposium on the Development and Utilization of Geothermal Resources, Proceedings: 381-398.

VanDenburgh, A. S. 1975. Solute Balance at Abert and Summer Lakes, South-Central Oregon. U.S.G.S. Professional Paper 502-C.

Wagner, Thomas W. 1971. Processing of Thermal Remote Sensor Data from Geothermal Areas. Ann Arbor: Center for Remote Sensing Information and Analysis, University of Michigan.

Walker, G. W. 1963. Reconnaissance Geologic Map of the Eastern Half of Klamath Falls Quadrangle, Lake and Klamath Counties, Oregon. U.S.G.S. Map MF-260.

_____. 1967a. Contraction Jointing and Vermiculitic Alteration of an Andesite Flow Near Lakeview, Oregon. U.S.G.S. Professional Paper 565-D, Geological Survey Research 1967, Chapter D: 131-134.

_____. 1967b. Geologic Evaluation of Infrared Imagery of Highly Faulted Volcanic Terraine in Southeast Oregon. N.A.S.A. Technical Letter-77. Earth Resources Survey Program, Interagency Report.

_____. 1973. Preliminary Geologic and Tectonic Maps of Oregon, East of the 121st Meridian. U.S.G.S.

_____. 1974. "Some Implications of Late Cenozoic Volcanism to Geothermal Potential in the High Lava Plains of South-Central Oregon." Ore Bin. 36(7):109-119.

Walker, G. W. and C. A. Repenning. 1965. Reconnaissance Geologic Map of the Adel Quadrangle, Lake, Harney, and Malheur Counties, Oregon. U.S.G.S. Miscellaneous Geologic Investigations, Map I-446.

Waring, Gerald A. 1909. Geology and Water Resources of Harney Basin Region, Oregon. U.S.G.S. Water Supply Paper 231.

_____. 1965. Thermal Springs of the United States and Other Countries of the World--A Summary. U.S.G.S. Professional Paper 492.

Watson, Kenneth. 1974. "Geothermal Reconnaissance from Quantitative Analysis of Thermal Infrared Images." International Symposium on Remote Sensing of Environment, Ninth Proceedings: 1919-1932.

_____. 1975. "Geologic Applications of Thermal Infrared Images." IEEE, Proceedings 63(1):128-137.

Wendt, George E., Richard A. Thompson and Kermit N. Larson. 1975. Land Systems Inventory: Boise National Forest, Idaho. Ogden: U. S. Department of Agriculture, U. S. Forest Service.

White, D. E., L. J. P. Muffler and A. H. Truesdell. 1971. "Vapor-Dominated Hydrothermal Systems Compared with Hot-Water Systems." Economic Geology 66:75-97.

White, D. E. and D. L. Williams. 1975. Assessment of Geothermal Resources of the United States--1975. U.S.G.S. Circular 726. U. S. Department of Interior.

Wiedman, Robert M. et al. 1973. "Application of ERTS-1 to Lineament and Photogeologic Mapping in Montana--A Preliminary Report." Symposium on Significant Results Obtained from the Earth Resources Technology Satellite-1. Volume 1:539-546.

Williams, Richard S., Jr., and Thomas R. Ory. 1967. "Infrared Imagery Mosaics for Geologic Investigations." Photogrammetric Engineering 33:1377-1380.

Wing, R. S. 1971a. "Structural Analysis from Radar Imagery of the Eastern Panamian Isthmus." Modern Geology 2:1-21.

Wing, R. S. 1971b. "Structural Analysis from Radar Imagery of the Eastern Panamian Isthmus." Modern Geology 2:75-127.

Wise, D. U. 1967. "A Radar Geology and Pseudo-Geology Cross Section." Photogrammetric Engineering 33(7):752-761.

Wolfe, William L. (ed.). 1965. Handbook of Military Infrared Technology. Washington, D.C.: Office of Military Research.

Wright, J. J. 1971. "The Occurrence of Thermal Groundwater in the Basin and Range Province of Arizona." Hydrology and Water Resources in Arizona and the Southwest 1:269-290.